Alma Mater Studiorum – Università di Bologna

DOTTORATO DI RICERCA IN INGEGNERIA ELETTROTECNICA

Ciclo XXVII

Settore Concorsuale di afferenza: 09E2

Settore Scientifico disciplinare: ING-IND/33

MODELLING AND ANALYSIS OF NETWORKED CONTROL STRATEGIES IN SMART POWER DISTRIBUTION GRIDS: DEVELOPMENT OF CO-SIMULATION TOOLS

Presentata da: **RICCARDO BOTTURA**

Coordinatore Dottorato

Prof. Domenico Casadei

Relatore

Prof. Alberto Borghetti

Correlatore

Prof. Carlo Alberto Nucci

Esame finale anno 2015

INDEX

FIGURE INDEX

Chapter 1
INTRODUCTION

The technological progress of the last decade has facilitated the development of distributed generation (DG). Some of these DG technologies offer the possibility of co-generation or tri-generation.

DG, together with the use of distributed storage technologies, the integration of the hybrid electric cars, the widespread use of intermittent renewable energy sources and the development of demand response programs, can generate complex interactions among different energy systems and calls for the increased use of information and communication technologies (ICT) and requires a major reassessment of the function of the distribution network, which is transforming itself from a passive to an active network.

The concept of Smart Grid is recently used to describe the increased application of new ICT-based monitoring, control and protection approaches in electrical power grids. In its most encompassing form, implementation of a Smart Grid adds intelligence to all areas of the power system infrastructure that will interoperate with end-use applications and loads.

The main characteristics of a smart grid are the following: sensing and metering technologies, two-way communications infrastructure, control methods, software system architecture with improved interfaces, decision support, analytics, and advanced visualization. As illustrated in Figure 1.1 smart grid technologies span the entire electric grid.

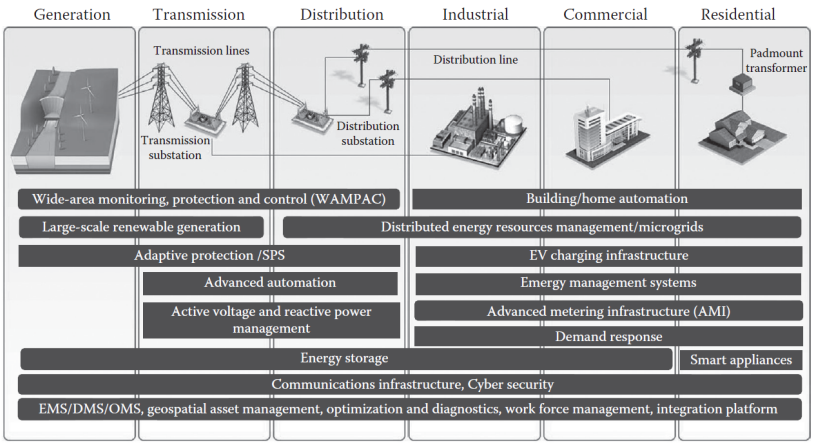

Figure 1.1 Smart grid technologies and applications [1]

This thesis is focused on the applications in medium voltage distribution networks. Figure 1.2 illustrates this scenario in which various types of communications links to the remote terminal

units (RTUs) are used. These communications links are now becoming more IP based using open protocols. The network is typically operated with the help of a SCADA (supervisory control and data acquisition) master hardware and software located at the control center.

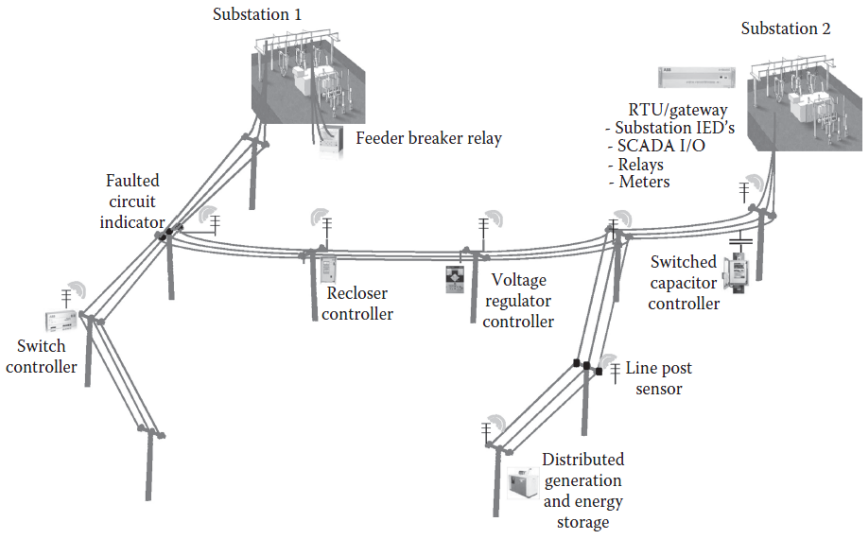

Figure 1.2 Illustrative figure of a distribution system with networked monitoring, control and protection devices. [1]

For the development of new applications it appears useful the availability of simulation tools able to model dynamic behavior of both the power system and the communication network. Such a co-simulation environment would allow the assessment of the feasibility of using a given network technology to support communication-based Smart Grid control schemes on an existing segment of the electrical grid, and, conversely, to determine the range of control schemes that different communications technologies can support.

This thesis presents a co-simulation platform that has been specifically built by linking the Electromagnetic Transients Program - Restructured Version Simulator (EMTP RV Works v3.0) with a Telecommunication Network Simulator: Optimized Network Engineering Tools (OPNET-Riverbed v18.0). The simulator is used to design and analyze a coordinate use of Distributed Energy Resources (DERs) for the voltage / var control (VVC) of the medium voltage distribution network.

The motivation of new solutions for the VVC problem is illustrated by Figure 1.3, that shows the GIS (geographic information system) scheme of the 15kV distribution network (in red) of a town with a population of 70,000 people with 3 substations (in blue) each equipped with two or three 30 MVA transformers. The total line length is about 200 km. Around 700 active clients (in yellow), with the power generation capability of 150 MW peak at medium voltage (MV) and 13 MW at low voltage (LV), mostly with photovoltaic units (PV) have been installed mainly in the last 10 years.

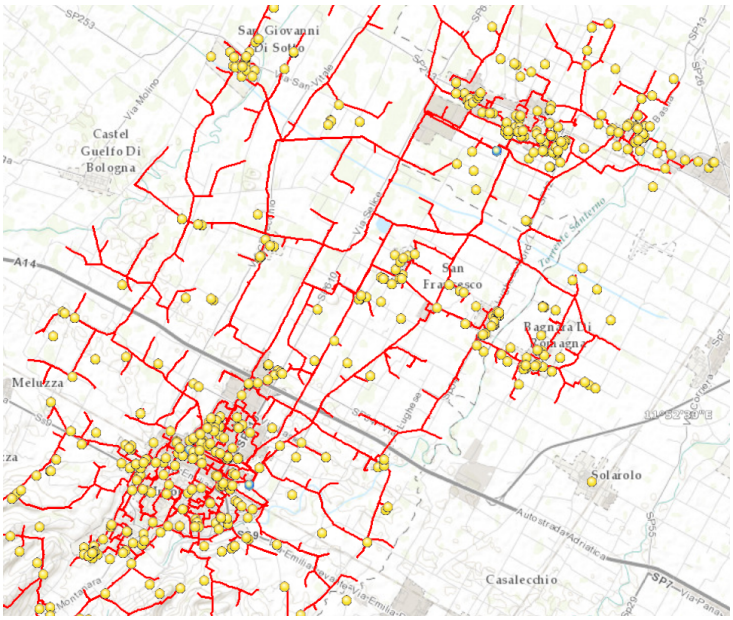

Figure 1.3 Scheme of the medium voltage distribution network of Imola with the indication of clients with generation capability (data curtesy of Hera Multiutility Company).

Three possible approaches to address the issue of coordinating the outputs of the various energy resources (and loads) with the action of available control means, such as transformers equipped with on-load tap changers (OLTC), mechanical switched, shunt capacitors, static var compensators (SVC), inverters, batteries, etc. are

- local: local regulators for each distributed generator and control mean that use only local measurements;
- centralized: Active Network Management (ANM) functions in the central Distribution Management System (DMS) coupled with the SCADA;
- distributed: networked Multi-Agent System (MAS) [2] composed by numerous localized controllers with the ability to communicate with each other.

Both the centralized ANM scheme and the MAS approach are based on the exchange of information using a shared communication network ([3],[4],[5]) that is in general characterized by stronger limitations than the communication links adopted for the operation of high voltage transmission networks.

This thesis is focused on a distributed and networked control structure based on the use phase measurement units (PMUs). In order to limit the required reinforcements of the communication infrastructures currently adopted by Distribution Network Operators (DNOs), the study is focused on leader-less MAS, i.e. MAS schemes that do not assign special coordinating rules to specific agents. Leader-less MAS are expected to produce a more uniform traffic in the communication links than both centralized DMS and MAS approaches that include a moderator agent. Moreover, leader-less MAS are expected to be less affected by limitations and constraint of some communication links due for example to high levels of the background traffic.

The developed co-simulator has allowed the definition of specific countermeasures against the limitations of the communication network, with particular reference to the latency and loss and information, for both the case of wired and wireless communication networks.

Moreover, the co-simulation platform has bee also coupled with a mobility simulator () in order to study specific countermeasures against the negative effects on the medium voltage distribution network caused by the concurrent connection of electric vehicles to fast charging systems.

The thesis is organized as follows:

Chapter 2 presents the developed ICT and power distribution network co-simulation platform.

Chapter 3 describes and analyses the conceived multi agent system for the VVC in the medium voltage distribution network.

Chapter 4 presents the integration of the co-simulation platform with the mobility electric vehicles simulator and describes the obtained results.

Chapter 5 is devoted to the conclusions.

Chapter 2
ICT AND POWER SYSTEM CO-SIMULATION PLATFORM

In both transmission or distribution networks, the adoption of generation that make also use of renewable resources and storage systems, together with electricity market mechanisms and the expected use of the electric vehicles, lead to complex interactions among different system components. Power system operation is therefore expected to need advanced information and communication technology (ICT) to ensure the required reliability level and performances. This need has stimulated the concept of Smart Grid - a broad term used to include the application of two-way secure communication links as well as computer based monitoring, management and protection systems to electrical power grids [6]. In this framework, there is a significant interest on the modeling of the interaction between communication networks and power systems by means the development of an offline test bed. This approach, which is called ITC-power system co-simulation in the literature, can represent the characteristics of both ICT components and the power system operation.

The key requirements that an ICT-power systems co-simulation platform is expected to meet are:

- easy configuration and operating system compatibility;
- ability to interconnect with external thirty-party program/system;
- hardware-in-the-loop (HIL) capability;
- time resolution of simulation steps;
- time synchronization;
- level of detail of modeling (both in power and communication modeling);
- interoperability to import models;
- scalability.

In the literature, several approaches have been presented in order to develop ITC-power systems co-simulation platforms. They are generally related to transmission networks (e.g. [7],[8],[9],[10],[11]), although some approaches have been also proposed for distribution networks [12],[13],[14]. One of the pioneering efforts to design a co-simulation platform including communication network and power system simulators is the EPOCHS framework [9]. Three off-the-shelf simulators are federated in this integrated platform: PSCAD/EMTDC for power system transients, Positive Sequence Load Flow (PSLF) for power system modeling, and Network Simulator 2 (ns-2) for communication network modeling. The same type of simulators are also included the GECO platform presented in [11] that uses a global event-driven mechanism in order to improve the synchronization. In [15] a hybrid simulation design based on HLA (High-Level Architecture), IEC 61850, OLE for Process Control (OPC) and the Common Information Model (CIM) is proposed with a focus on the evaluation of the real-time performance of wide-area monitoring, protection and control (WAMPAC) applications. In [15] a hardware/software co-design approach is presented that applies the discrete event system specification (DEVS) model of computation. In [16] a general co-simulation platform for cyber-physical systems is also applied to a small power grid.

The simulation environments are of both static and dynamic type. Static tools allow the analysis of the power system under varying load conditions, taking into account the communication system characteristics and performance. Dynamic tools allow the analysis of the power system transients and the assessment of the adequacy of both security and communication times for advanced control strategies and rapid back-up protections. In dynamic approaches, the synchronization between a continuous–time power system simulator and an event-based communication simulator requires the application of specific techniques.

Among the dynamic tools, real-time co-simulation platforms are capable to perform fine-grained analysis of power systems, e.g. at millisecond level, and allow for the interfacing of HIL (Hardware In the Loop) devices. Real time simulators have been already presented in the literature for the same purposes, e.g. GridSim [17] and SmartTS Lab [18]. GridSim is a comprehensive platform combining power system, communication network, sensor system, data concentration and monitoring/control applications. It is designed to study the impact of the IT system supporting the phase measurement unit (PMU) based monitoring and control applications and it uses the communication framework GridStat [19]. SmartTS Lab uses OPAL-RT [20] as a real-time simulator for the electrical power process and interfaces it with industrial grade hardware by using the HIL method.

This chapter introduces the main characteristics of the developed co-simulation platform and illustrate the type of analysis that can be performed by using the simulator through a simple example. Other specific functions and details are provided in the subsequent chapters.

This simulator has been developed also through a collaboration with the research group of the Professor Lars Nordström of the KTH of Stockholm. In [21], the architecture and configuration of this simulator have been compared with that of a different simulator built at KTH in order to create an environment where real time hardwire-in-the-loop (HIL) tests are performed.

2.1 Architecture

This co-simulation platform is based on the link between the communication network simulator OPNET-Riverbed Modeler Wireless suite v18.0 [22] and the time-domain power system simulation environment EMTP-RV v3.0 [23]. This platform is devoted to the analysis of ICT infrastructures that could facilitate the deployment of embedded energy resources in distribution networks.

As show in Figure 2.1, both the communication and power system simulators communicate with the outside environment through specific dynamic link libraries (DLLs). All the DLLs are compiled and implemented in C/C++. They communicate with each other through socket application programming interfaces (APIs) provided by the operating system. The socket API allows the developed DLL to control and use the network sockets that are the endpoints of the inter-process communication (IPC) flow.

In the socket communication, OPNET controller works as a server (Execution controller), whilst EMTP controller acts as a client. At the simulation startup, OPNET enables the communication in the Execution Controller, opens a socket channel, sets the parameters and starts to listening/waiting for a possible connection from the external environment. The co-simulation begins when the EMTP sends the connection request as a client to the specific port and IP address provided by the server.

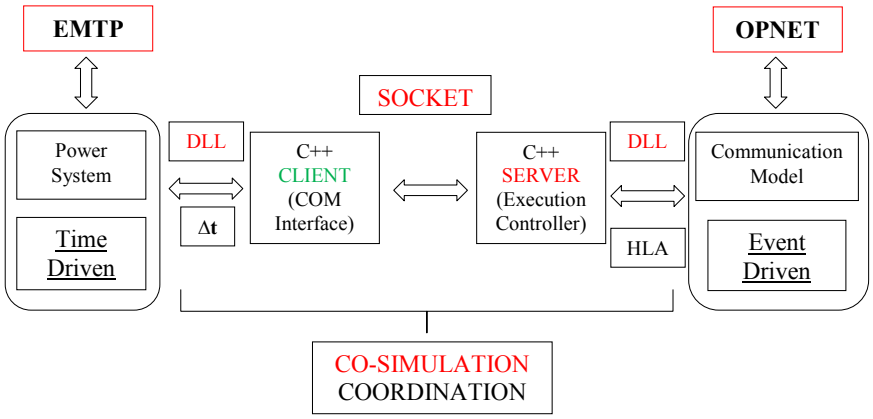

Figure 2.1. Architecture of the HLA co-simulation platform.

The synchronization mechanism is based on the typical waiting order of a communication through sockets. Simulation interval Δt defines the sampling period of the differential algebraic equations solved by EMTP. As illustrated in Figure 2.1, Δt is communicated to OPNET that, in turn, executes the simulation until the subsequent sampling time.

The integration time-step Δt is defined in EMTP so to be smaller than the shortest electromagnetic propagation delay in the network lines. As distribution network lines are short (typically hundreds of meters or less), Δt needs in general to be very small (in the order of microseconds).

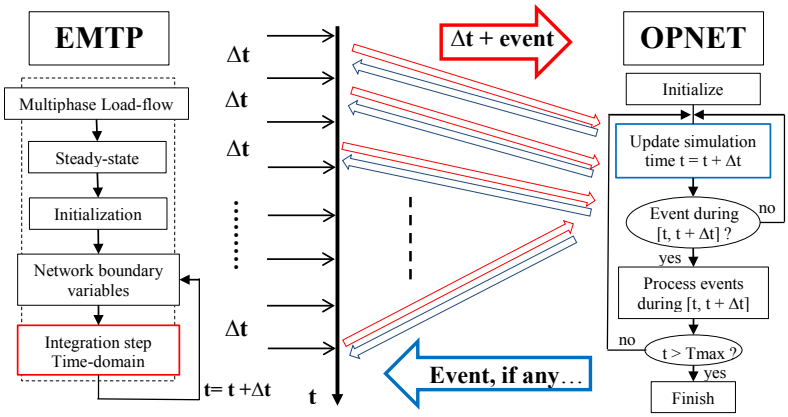

Figure 2.2 Synchronization mechanism

2.2 EMTP-RV model

In EMTP the DLL co-simulation interface is defined by two components [24]:

1. DLL symbol, with the adequate number of pins and attributes
2. user-defined DLL with a specific structure and calls to variables used by the EMTP solution code.

Figure 2.3 shows an example of the DLL symbol developed by using the Symbol Editor. It contains the pins for the connection to the power system components. The attributes of the symbol are used to define the path of the associated DLL and other information data that could be useful at the interface such as the number of inputs (*Ncontrol_signals*) and the number of outputs (*Nobserve_signals*).

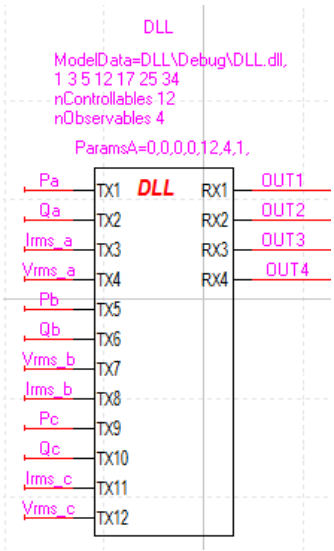

Figure 2.3 - Example of a symbol for a user- defined DLL

2.3 OPNET Riverbed programming

As described in [25][26], the OPNET interface through HLA DLLs permits to use the OPNET GUI interfaces during the simulation and reduces the so-called memory swapping as the different functions of the simulator are loaded only when they are actually needed.

An OPNET DLL interface is defined by five main components:

1. External System (esys) module and the corresponding process model;
2. External System Definition / Domain (ESD) model;
3. Simulation Description (SD) file;
4. Esys API package;
5. External Simulation Access (ESA) API package DLL.

Esys module: it enables the management and the delivery of the communication packets. As illustrated in Figure 2.4-(a) the TCP client-server model is extended by one additional module called “cosim_client_server”. Figure 2.4-(b) shows the logic as a Finite State Machine (FSM) of the “cosim_client_server” module that performs the data exchange with the external code and communicates with the “tcp” module that represents the standard TCP layer.

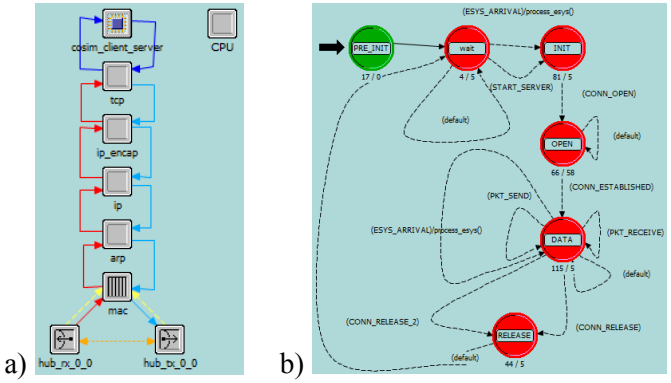

Figure 2.4. a) Extended TCP client-server model; b) esys module associated to the “cosim_client_server” module.

ESD model: it is an attribute of the “cosim_client_server” module that defines the "esys interfaces" (Figure 2.5) for each agent. These interfaces can be written and read by both the external code and within the OPNET program through specific DLL APIs. In the same “cosim_client_server” module, it is possible to define an arbitrary number of "esys interfaces", each one characterized by data of different type (integer, floating point, bit, pointer, string, etc.) and direction.

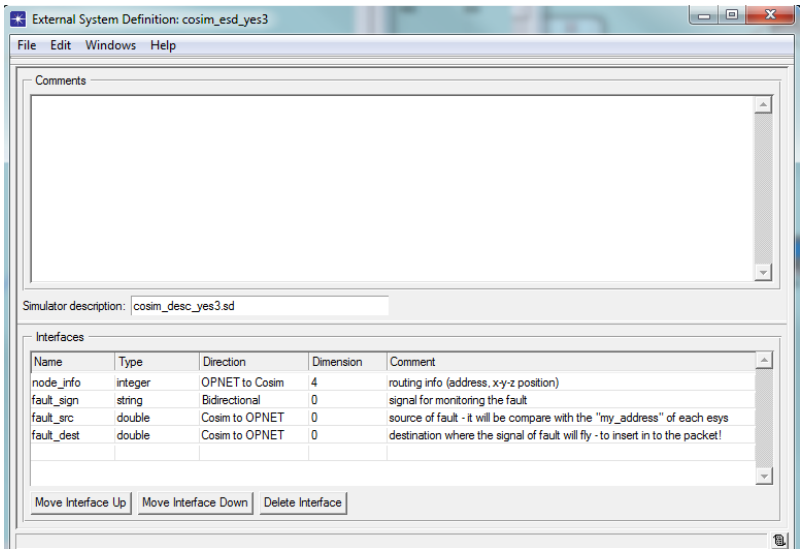

Figure 2.5 ESD Model

SD file: a text file for the definition of the main characteristics of the external interface. Figure 2.6 shows the adopted SD file, in which the "platform" is Windows, the co-simulation method is "use_esa_main", namely the use of the external program in OPNET external DLL; "bitness" is 32bit; "kernel" is "development" (useful for debugging); "dll_lib" specifies the path of the external DLL.

```
# Simulation Description
start_definition
        platform:           windows
        use_esa_main:       yes
        bitness:            32bit
        kernel:             development
        dll_lib:            C:\\myOPNET\\HLA_dll\\ … \\Debug\\cosim_tcp5.dll
end_definition
```

Figure 2.6. Example of a SD file.

Esys API Package: it contains specific C/C++ function (listed in the header file "esa.h") for the initialization and the application flow control of each interface identified by a specific number as defined by the order in the ESD model.

ESA API package – DLL: this component is used for the control of the external DLL, by means of the command '*extern "C" DLLEXPORT*' located before the body of the ESA API package_main function (called "esa_main"). In addition, "esa_main" contains the initialization of the sockets for the communication over the physical network with EMTP. At the end, the command "Esa_Execute_Until" is passes control back to OPNET and starts the simulation for time interval Δt set by EMTP.

2.4 Illustrative test case

In order to illustrate the functionalities of the co-simulation platform, a simple communication-based protection scheme has been modeled. Figure 2.7 shows both the distribution feeder represented in the EMTP and the communication network model implemented in OPNET. The monitoring of currents and voltages governs the operation of the three installed protection relays. Each relay operation causes the opening of the corresponding circuit breaker located at the beginning of a line and therefore the disconnection of all the loads connected to the subsequent nodes.

When a fault occurs (in this case a solid three phase fault at bus 1), it is identified by all the protection relays located ahead of the faulted node due to the large value of the current. In order to ensure that only the relay closest to the fault trips, the operation of both relays 1 and 2 is delayed. For illustrative purposes, a fixed time delay equal to 0.3 s has been selected. However, the relays are allowed to trip immediately if they receive a consensus message from the relays located at a subsequent position in the feeder. Relay 2 and Relay 3 send the consensus message that accelerates the trip of the preceding relays in the feeder when the node voltage where they are located is unusually low, but at the same time the current at their location is not so high as to cause their operation. The consensus message is sent through the communication network represented in OPNET. For each transmission, only 4 bytes of information are encapsulated into the TCP packet payload.

A client-server communication model has been implemented for each interface. The message generated by the EMTP model is transferred to the client through the “esys interfaces”. In the client side, the message is built into the TCP (Transmission Data Protocol) datagram and sent to the corresponding server. The server processes the datagram received, extrapolates the information from the payload, and returns the consensus message to the associated EMTP interface.

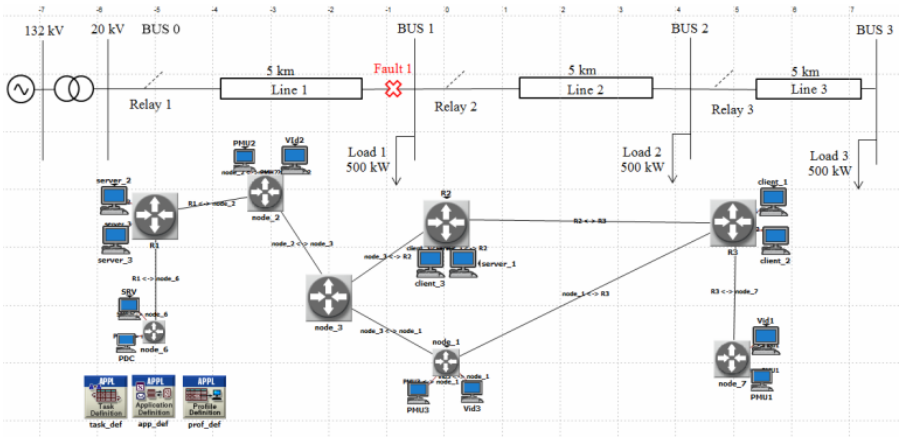

Figure 2.7. Electrical and corresponding Communication system

As shown in Figure 2.7, the simulated communication network consists of the three main routers corresponding to the protection relays of the feeder. These routers are connected to each other via a 2Mbit link. Background communication traffic in the communication links is

represented and its effects are analyzed by the end-to-end delay metric, which affect the performance of intervention of the relays.

Four different experiments were run by setting the background traffics level in the communication links equal to 0%, 50%, 75% and 100% respectively. The results of end-end delay for all the four scenarios are shown in Table 2.I.

Table 2.I. End-to-End delay of HLA data stream

BACKGROUND TRAFFIC	RELAY 2 → RELAY 1 DELAY [MS]	RELAY 3 → RELAY 1 DELAY [MS]
0%	1,258	0,859
50%	61,759	49,959
75%	87,154	80,430
100%	107,536	101,623

Figure 2.8 shows the behavior of the root mean square (rms) value of the current measured at relay 1 in the occasion of the considered balanced fault at bus 1 for three scenarios of communication traffic.

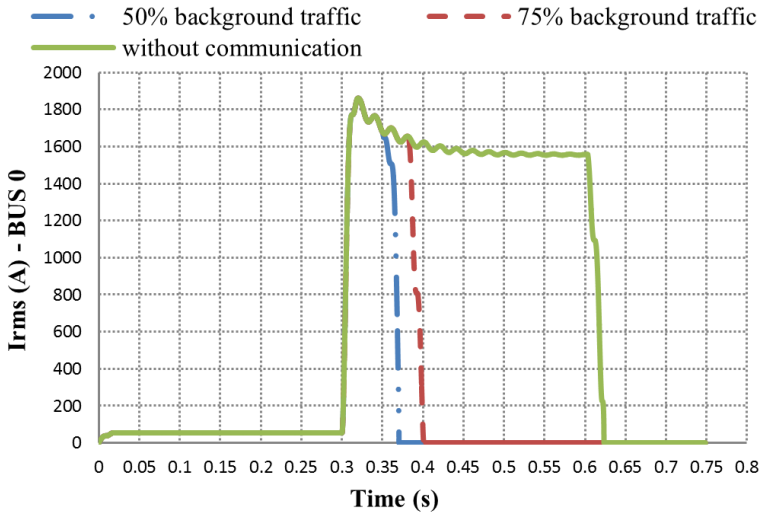

Figure 2.8. Comparison between the behavior of the current at relay 1 for the three scenarios of communication traffic of Table 2.I.

Chapter 3
ANALYSIS OF COMMUNICATION-BASED VOLT/VAR OPTIMIZATION IN DISTRIBUTION FEEDERS

The adoption of networked multiagent systems (MAS) has been recently proposed for the solution of the volt/var control (VVC) problem in distribution feeders. However, constraints and limitations due to the communication network, to the dynamic behavior of power system components and regulators, as well as to the measurement uncertainties of the adopted sensors need to be specifically analyzed for the design of the MAS. For this purpose, the co-simulation platform described in Chapter 2 has been developed for modelling and simulation of an asynchronous leaderless MAS-based approach that coordinates the reactive power outputs of a set of power compensators equipped with phasor measurement units (PMUs) via a shared band-limited packet-switched digital communication network. The effects of communication network latency and packet loss on the VVC performances are analyzed for two unbalanced IEEE Test feeders equipped with on-load tap changer transformers. The chapter compares the results obtained by using a transmission control protocol (TCP) and a user datagram protocol (UDP), for different levels of background traffic (BT) and different packet discard ratios (PDRs) in the communication links.

3.1 Aim of the study

Co-simulation environments that integrate a simulator of the communication network with a power system simulator are very useful for the design and analysis of improved monitoring, control, and protection techniques in modern electric power systems, as all these functions rely on the exchange of information using a shared communication network [27]. This approach appears particularly suitable for the development of active network management (ANM) functions of medium voltage (MV) networks that need to coordinate an increasing number of various type of spatially distributed energy resources and control devices by using communication networks characterized by more stringent limitations than those adopted for the operation of high voltage transmission networks [28]. As analyzed in [3], the implementation of all ANM functions in a central distribution management system (DMS) is expected to require significant reinforcements of the communication infrastructures currently adopted by distribution network operators (DNOs). A reduction of the communication requirements can be obtained by using distributed approaches

based on networked multiagent systems (MAS) composed by multiple local controllers interacting through the communication network. A general review of the applications of MAS in power systems, not limited to distributed control purposes, has been the object of a specific IEEE Power and Energy Society (PES) Working Group [29]. Control theory aspects, specifically consensus and cooperation topics, have been recently reviewed in [4]. These approaches avoid that all the information and decisions are concentrated in a specific node of the communication network connected to the centralized processor with demanding computational tasks. However, specific techniques of control over communication network are needed in order to minimize the effects of finite bandwidth, transmission delays, and packet loss, as well as to limit the cyber-attacks risk. These constraints due to the use of a shared communication network are common to all networked control systems (NCS) approaches as recently reviewed in [5] and [30].

3.2 Volt – Var Optimization (VVO) of distribution feeders

Among the ANM functions, this chapter focuses on the volt/var control (VVC), defined as the online coordination of reactive power resources and transformers equipped with on-load tap changers (OLTCs), in order to achieve an efficient and feasible operating condition of the power feeder. This chapter does not directly deal with conservative voltage reduction (CVR). However, VVC tries to achieve flat voltage profiles along the feeder and, therefore, it facilitates the implementation of CVR projects. Modern VVC approaches exploit the presence of distributed generators (DGs), especially of those connected to the power distribution feeder through power electronic converters, in addition to the classical control means such as OLTCs, mechanical switched capacitors, and static var compensators. Real power outputs of DGs are assumed to be defined by the availability of the energy resources and by market conditions. VVC can be formalized as a single optimization problem as recently described, e.g., in [31] and [32], which also review previous contributions on the subject. Nevertheless, various distributed approaches have been also proposed in the literature for the solution of the VVC problem.

3.2.1 Multi agent system approaches for VVO

In [33], a decomposition method of the inverse of the Jacobian of the power flow problem is proposed in order to decompose VVC in smaller size optimization problems that could be implemented in MAS. There is also an increasing literature relevant to the application of distributed optimization procedures to VVC, with particular reference to power networks with radial structure (e.g., [34],[35],[36],[37]). In some MAS schemes, special coordinating roles are assigned to specific agents. As an example, in the scheme proposed in [38], a moderator collects all the sensitivity factors from the agents and sends backward the contracts to them stating that the amount of reactive power support is needed from each controlled DG. In [39], a similar coordinating role is attributed to a top feeder relay which has the additional role to provide the coordination with the central energy management system of the bulk transmission network. In other approaches, the sequence of agent actions should follow a specific order, based, as in, e.g., [40], on the location of the controlled DG in the feeder. Moreover, leader-less MAS approaches

have been recently proposed in [41] and [42]. These approaches are based on gossip-like algorithms that use the measurement of bus voltage synchrophasors and exchange the information between two randomly-chosen neighboring agents at a time. A related strategy has been presented in [43]. In [44] an algorithm is proposed in which each agent sets a target voltage value on the basis of the voltage measurements collected from all the neighbors. The action of each agent is cyclically activated by a token ring control strategy so to ensure that the output of only one DG or of few DGs at a time are adjusted depending on the number of circulating tokens. In [45] the solution of a fuzzy-based algorithm is achieved by means of an average consensus procedure between agent state vectors. The results shows that a large number of iterations and therefore a large number of exchanged messages are needed to achieve a consensus on the mean value of the bus voltages that is used by the fuzzy algorithm.

This chapter aims at showing the application of the ICT-power system co-simulation platform presented in the Chapter 2 to the analysis of the effects of the limitations of the communication links on the performances of a MAS approach and for the design of the relevant countermeasures.

As described in the following section, the chapter focus on a leader-less asynchronous gossip like approach given by subsequent repetition of the execution of simple rules between different couple of agents. The procedure, based on the one proposed in [41],[42],[43], is enriched by several countermeasures against communication latency and packet loss. Moreover the procedure incorporates additional heuristic rules that improve the coordination with OLTCs, as described in the step-by-step description provided in Section 3.2.3. Section 3.4 is devoted to the performance analysis of the procedure for the case of the IEEE 37-bus test feeder and of the IEEE 123-bus test feeder [46] with several agents, each controlling a reactive power compensator. The statistical results obtained by applying both a Transmission Control Protocol (TCP) model and User Datagram Protocol (UDP) model are compared for different levels of background data traffic and packet discard ratios.

3.2.2 Implemented Gossip-like VVO Procedure

Consensus algorithms in MAS can be described as rules that periodically update the column vector of the agent states $\mathbf{x}(t+\Delta t)$ at time step $t+\Delta t$ by an exchange of information between the agent relevant to their present state:

$$\mathbf{x}(t+\Delta t) = \mathbf{P}(t)\,\mathbf{x}(t) \tag{3.1}$$

Element P_{ij} of matrix **P** represents the influence of the present state of agent j on the future state of agent i at each time step. Therefore matrix **P** incorporates the available communication links between different agents.

In the described VVC application, the state of agent i represents reactive power Q_i injected in a bus of the feeder by the reactive power compensator (based on a power electronic converter) supervised by the agent. As the objective of VVC is the achievement of a feasible and efficient operating condition, the updated value of the reactive power depends also on the state of the

electrical network represented by the vector of bus voltage phasors **V**. Therefore, the consensus mechanism may be described by

$$\begin{aligned} \mathbf{Q}(t+\Delta t) &= \mathbf{Q}(t) + \Delta\mathbf{Q}(\mathbf{P}(t)\mathbf{V}) \\ \mathbf{V}(t) &= f(\mathbf{Q}(t), \mathbf{u}(t)) \end{aligned} \tag{3.2}$$

where ΔQ_i is the adjustment function of reactive power output of the compensator associate with agent *i*. It is a nonlinear function of the voltage phasors, the values of which are communicated to agent *i* by the available communication links represented by the nonzero elements of matrix **P**(*t*). Nonlinear function *f* represents the nonlinear relationship between the bus voltage phasors and the reactive power output of the compensators. It incorporates the power network equations, the voltage dependence of loads and generators as well as the effects of disturbances (switching, sudden load and generation changes, etc.) indicated by vector **u**(*t*).

Among the various approaches that could be represented with the mechanism described by (3.2), this chapter focuses to a gossip-like approach that avoids the synchronization of the action of the agents.

Although distributed optimization approaches, such as those presented in [34]–[37] are characterized in general by improved convergence behavior and quality of the results with respect to gossip-like algorithms, they entail stronger synchronization constraints between the actions of all the agents of the network, as well as more communication requirements. The analysis of the effects of the limits of the communication network and the design of countermeasures against latency and packet loss in distributed optimization approaches is outside the scope of this chapter.

The aspects that mainly characterize the implemented procedure are:

a) repetition of reactive power compensations between a couple of compensators, evaluated by using only the measurements available at the buses where the two compensators are connected;

b) activation of different couples of compensators at each time, so to limit the interference of concurrent action of multiple compensators connected to the same feeder;

c) robustness against communication latency and packet loss (at the limit, it is expected to continue also in the presence of the complete failure of a communication link).

3.2.2.1 Evaluation for the reactive power compensation

Each agent updates the reactive power injected by its three phase compensator in a bus of the electric power feeder on the basis of the information received from the other agent, as well as local information provided by a phasor measurement unit (PMU).

PMU applications for transmission system operation and control could be considered mature [47]. There is a growing interest to develop PMU-based applications also for distribution

networks and PMUs are foreseen to be more commonly installed in future distribution equipment, as reviewed in [48] and references therein. The different characteristics of distribution feeders with respect to transmission grids justify the development of specific PMU algorithms. For example, in [49], [50] a PMU prototype is described that addresses the issue of small phase shifts between different buses in distribution networks due to short line lengths and reduced power flows.

The principal aim of the action of each couple of agents that operates at each step of the procedure is the minimization of reactive power flows in the network. The minimization of the reactive power flows reduces the currents into the overhead lines and cables, resulting in a reduction of losses and voltage drops. For this purpose, each couple of active agents tries to compensate the reactive power flow between them, i.e. each agent tries to supply the reactive power needed by the nearby loads.

In order to evaluate the amount of this reactive power counterflow to be generated by the two compensators, we assume the feeder as a balanced three phase system. The single phase equivalent positive circuit is replaced by a reduced network, the nodes of which are the bus of the substation (at the low voltage side of the transformer) and the N busses at which the compensators are connected. The reduced N+1 bus network is obtained by using the Kron's technique [51], [52].

As the feeder is unbalanced, the positive sequence admittance matrix $\mathbf{Y}$ is calculated by averaging the diagonal and off-diagonal values of the impedances matrices of unbalanced lines, by neglecting shunt capacitances.

According to the Kron's reduction technique [51],[52], the relationships between node current phasors $\mathbf{I}$ and voltage phasors $\mathbf{V}$ though matrix $\mathbf{Y}$ (assumed symmetrical) can be written as

$$\begin{bmatrix} \mathbf{I}_\alpha \\ \mathbf{I}_\beta \end{bmatrix} = \begin{bmatrix} \mathbf{Y}_{\alpha\alpha} & \mathbf{Y}_{\alpha\beta} \\ \mathbf{Y}_{\alpha\beta}^T & \mathbf{Y}_{\beta\beta} \end{bmatrix} \begin{bmatrix} \mathbf{V}_\alpha \\ \mathbf{V}_\beta \end{bmatrix} \tag{3.3}$$

where subscript α indicates the set of N+1 nodes to be maintained in the reduced network whilst subscript β denotes the other nodes. By applying the Gaussian elimination of the voltage phasors $\mathbf{V}_\beta$ in equation (3.3) gives an electrically-equivalent reduced network with α nodes obeying the reduced current-balances:

$$\begin{cases} \mathbf{I}_\alpha = \mathbf{Y}_{\alpha\alpha}\mathbf{V}_\alpha + \mathbf{Y}_{\alpha\beta}\mathbf{V}_\beta \\ \mathbf{I}_\beta = \mathbf{Y}_{\alpha\beta}^{\mathrm{T}}\mathbf{V}_\alpha + \mathbf{Y}_{\beta\beta}\mathbf{V}_\beta \end{cases}$$
$$\Rightarrow \mathbf{V}_\beta = \mathbf{Y}_{\beta\beta}^{-1}\mathbf{I}_\beta - \mathbf{Y}_{\alpha\beta}^{\mathrm{T}}\mathbf{Y}_{\beta\beta}^{-1}\mathbf{V}_\alpha \tag{3.4}$$
$$\Rightarrow \mathbf{I}_\alpha - \mathbf{Y}_{\alpha\beta}\mathbf{Y}_{\beta\beta}^{-1}\mathbf{I}_\beta = \left(\mathbf{Y}_{\alpha\alpha} - \mathbf{Y}_{\alpha\beta}\mathbf{Y}_{\beta\beta}^{-1}\mathbf{Y}_{\alpha\beta}^{\mathrm{T}}\right)\mathbf{V}_\alpha$$

$$\mathbf{I}_\alpha + \mathbf{Y}_{ac}\mathbf{I}_\beta = \mathbf{Y}_{red}\mathbf{V}_\alpha \tag{3.5}$$

with $\mathbf{Y}_{ac} = -\mathbf{Y}_{\alpha\beta}\mathbf{Y}_{\beta\beta}^{-1}$ and $\mathbf{Y}_{\text{red}} = \mathbf{Y}_{\alpha\alpha} - \mathbf{Y}_{\alpha\beta}\mathbf{Y}_{\beta\beta}^{-1}\mathbf{Y}_{\alpha\beta}^{T}$, being $\mathbf{Y}_{\beta\beta}$ not singular as there exist at least one connection between a β-bus and a α-bus of the feeder. In case that the variation of the current in the nodes β is almost equal to zero:

$$\begin{bmatrix} \Delta\mathbf{I}_{\alpha} \\ \Delta\mathbf{I}_{\beta} \simeq \mathbf{0} \end{bmatrix} = \begin{bmatrix} \mathbf{Y}_{\alpha\alpha} & \mathbf{Y}_{\alpha\beta} \\ \mathbf{Y}_{\alpha\beta}^{\mathrm{T}} & \mathbf{Y}_{\beta\beta} \end{bmatrix} \begin{bmatrix} \Delta\mathbf{V}_{\alpha} \\ \Delta\mathbf{V}_{\beta} \end{bmatrix} \Rightarrow \cdots \Rightarrow \Delta\mathbf{I}_{\alpha} = \mathbf{Y}_{\text{red.}}\Delta\mathbf{V}_{\alpha} \qquad (3.6)$$

Where the equivalent reduced impedance matrix obtained from the Kron's reduction technique is the following:

$$\mathbf{Z}_{\mathbf{hk}}^{\text{Kron}} = \begin{cases} -\mathbf{1}/\mathbf{Y}_{\text{red.}} & \text{if } \mathbf{Y}_{\text{red,hk}} \neq \mathbf{0} \\ -\infty & \text{if } \mathbf{Y}_{\text{red,hk}} = \mathbf{0} \end{cases} \Leftarrow \text{Transadmittance} \qquad (3.7)$$

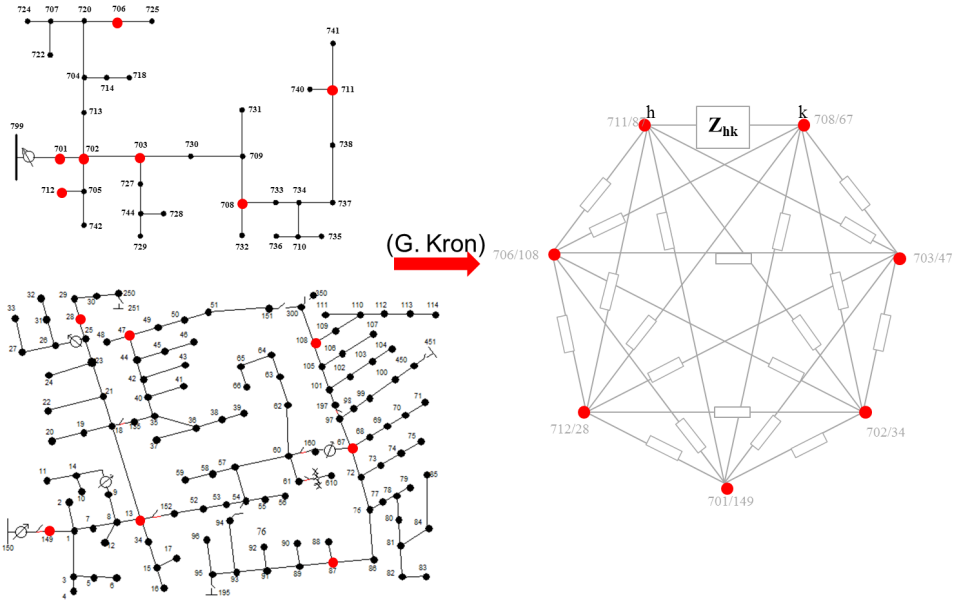

Figure 3.1 Equivalent network obtained through the Kron's reduction technique

The reduced network described by equation (3.6) and shows in Figure 3.1 exchange the same real and reactive power with the external components through the α-nodes as the original system does. As far as $\mathbf{I}_{\beta}$ is independent on voltages, if $\mathbf{I}_{\alpha}$ could be modified so to obtain a power loss drop in the reduced network, the same loss drop is achieved also in the original system. A power loss reduction is reasonably expected also in unbalanced feeders with loads that do not exactly maintain the same current phasor, in view of the limited bus voltage deviations expected in power distribution feeders (namely few percentage points for the amplitude deviation and very few degrees for phase deviation). This is supported by the simulation results presented in section 3.4 that are obtained for two unbalanced test systems with loads with different voltage dependence: constant impedance, constant current and constant power.

Indeed, as shown in [32], Cartesian coordinates variations $\Delta I_{\mathrm{L},k}^{re}$ and $\Delta I_{\mathrm{L},k}^{im}$ (in pu) of load current phasor at node *k* can be written as linear combination of bus voltage variations ΔV_k^{re} and ΔV_k^{im} with respect an initial voltage phasor equal to 1 e^{j0} pu:

$$\begin{cases} \Delta I_{\mathrm{L},k}^{re} = G_{\mathrm{L},k}\ \Delta V_k^{re} - B_{\mathrm{L},k}\ \Delta V_k^{im} \\ I_{\mathrm{L},k}^{im} = G_{\mathrm{L},k}\ \Delta V_k^{im} + B_{\mathrm{L},k}\ \Delta V_k^{re} \end{cases} \tag{3.8}$$

for a load with constant admittance $Y_{\mathrm{L},k} = G_{\mathrm{L},k} + jB_{\mathrm{L},k}$;

$$\begin{cases} \Delta I_{\mathrm{L},k}^{re} = \left|In_k\right| \Delta V_k^{im} \sin\varphi \\ \Delta I_{\mathrm{L},k}^{im} = \left|In_k\right| \Delta V_k^{im} \cos\varphi \end{cases} \tag{3.9}$$

for a constant current with $\left|In_k\right|$ RMS value and $\cos\varphi$ power factor;

$$\begin{cases} \Delta I_{\mathrm{L},k}^{re} = -In_k^{re} \Delta V_k^{re} - In_k^{im} \Delta V_k^{im} \\ \Delta I_{\mathrm{L},k}^{im} = In_k^{re} \Delta V_k^{im} - In_k^{im} \Delta V_k^{re} \end{cases} \tag{3.10}$$

for a constant power load, where In_k^{re} and In_k^{im} correspond to the load real and reactive power requests in pu at 1 e^{j0}. Assuming a load with rated apparent power of 1 pu and 0.75 power factor, a voltage deviation of 5% for the amplitude and of 2° for the phase corresponds to a 6.2% maximum variation of the load current Cartesian coordinates.

In general, even if the feeder has a radial topology (as those considered in Section 3.4) that is usually preferred by DNOs, the reduced network may contain loops. However, if we consider two *α*-buses *h* and *k* so that there is not any other *α*-bus connected close to the path between them in the feeder (from now on buses *h* and *k* will be indicated as adjacent), the impedance between the corresponding two nodes of the reduced network is equal or very similar to the effective positive-sequence impedance of the path by assuming the substation serving as slack bus. The positive sequence matrix is calculated by averaging the diagonal and off-diagonal values of the impedances matrices of unbalanced lines and neglecting shunt capacitances. The approximation method proposed in [42] for the analysis of the micro-grid power flow is based on the fact that the grid operating point, in its regular regime, is characterized by a relatively high nominal voltage compared to the voltage drops across the power lines, and by relatively small power distribution losses, compared to the power delivered to the loads.

$$Y = A^T Z^{-1} A = L \tag{3.11}$$

$$\begin{cases} XL = I - \mathbf{1}\mathbf{1}_0^T \\ X1_0 = 0 \end{cases} \tag{3.12}$$

$$
\begin{aligned}
&(X = X^T)\\
&XL = I - \mathbf{1}\mathbf{1}_0^T \\
&X = L_{reduced}^{-1} = Y_{red.}^{-1}
\end{aligned}
\tag{3.13}
$$

$$
Y = \begin{bmatrix} y_{11} & y_{12} & \cdots & y_{1n} \\ y_{21} & & & \\ \vdots & & Y_{red.} & \\ y_{n1} & & & \end{bmatrix} \Rightarrow Y_{red.}^{-1} = X_{red.} \Rightarrow X = \begin{bmatrix} 0 & 0 & \cdots & 0 \\ 0 & & & \\ \vdots & & X_{red.} & \\ 0 & & & \end{bmatrix} \tag{3.14}
$$

$$
\begin{aligned}
Z_{\text{eff},hk} &= R_{\text{eff},hk} + jX_{\text{eff},hk} = \\
&= (1_h - 1_k)^T X (1_k - 1_h) = X_{hh} - X_{kh} - X_{hk} + X_{kk} = \\
&= Z_{hh} + Z_{kk} - 2Z_{hk}
\end{aligned}
\tag{3.15}
$$

where Z_{hh}, Z_{kk} and Z_{hk} are the *(h,h)*th, *(k,k)*th, and *(h,k)*th elements of impedance matrix $\mathbf{Z}$, obtained as the inverse of admittance matrix **Y** by assuming the substation as slack bus.

We assume that bus *h* and bus *k* are adjacent buses and each of them is equipped with a reactive power compensator. In order to estimate the adequate reactive power counter-flow, the two agents calculate the following values of reactive power transfer both positive in the direction from *h* to *k*

$$
\begin{aligned}
&S_{hk} = P_{hk} + jQ_{hk}^{'} = V_h I_{hk}^{*} = V_h \left(V_h - V_k \middle/ Z_{hk}\right)^{*} = \frac{V_h^2}{Z_{hk}^{*}} - \frac{V_h V_k^{*}}{Z_{hk}^{*}} = \\
&= \frac{V_h^2}{Z_{hk}} \frac{(R_{hk} + jX_{hk})}{(R_{hk} + jX_{hk})} - \frac{V_h V_k^{*}}{Z_{hk}^{*}} \frac{(R_{hk} + jX_{hk})}{(R_{hk} + jX_{hk})} = \\
&= \frac{V_h^2}{|Z_{hk}|^2}(R_{hk} + jX_{hk}) - \frac{V_h V_k^{*}}{|Z_{hk}|^2}(R_{hk} + jX_{hk}) = \\
&= \frac{V_h^2}{|Z_{hk}|^2}(R_{hk} + jX_{hk}) - \frac{|V_h||V_k| e^{i(\theta_h - \theta_k)}}{|Z_{hk}|^2}(R_{hk} + jX_{hk}) = \\
&\Rightarrow Q_{hk}^{'} = \frac{V_h^2}{|Z_{hk}|^2} X_{hk} - \frac{|V_h||V_k|}{|Z_{hk}|^2}\cos(\theta_h - \theta_k) X_{hk} - \frac{|V_h||V_k|}{|Z_{hk}|^2}\sin(\theta_h - \theta_k) R_{hk}
\end{aligned}
\tag{3.16}
$$

$$
\begin{aligned}
&S_{hk} = P_{hk} + jQ^{"}_{hk} = -V_k I^{*}_{hk} = -V_k \left(\left.V_k - V_h \right/ Z_{hk}\right)^{*} = -\frac{V_k^2}{Z^{*}_{hk}} + \frac{V_k V_h^{*}}{Z^{*}_{hk}} = \\
&= -\frac{V_k^2}{Z_{hk}} \frac{(R_{hk} + jX_{hk})}{(R_{hk} + jX_{hk})} + \frac{V_k V_h^{*}}{Z^{*}_{hk}} \frac{(R_{hk} + jX_{hk})}{(R_{hk} + jX_{hk})} = \\
&= -\frac{V_k^2}{|Z_{hk}|^2}(R_{hk} + jX_{hk}) + \frac{V_k V_h^{*}}{|Z_{hk}|^2}(R_{hk} + jX_{hk}) = \\
&= -\frac{V_k^2}{|Z_{hk}|^2}(R_{hk} + jX_{hk}) + \frac{|V_k||V_h| e^{i(\theta_k - \theta_h)}}{|Z_{hk}|^2}(R_{hk} + jX_{hk}) = \\
&\Rightarrow Q^{"}_{hk} = -\frac{V_k^2}{|Z_{hk}|^2} X_{hk} + \frac{|V_k||V_h|}{|Z_{hk}|^2}\cos(\theta_k - \theta_h) X_{hk} + \frac{|V_k||V_h|}{|Z_{hk}|^2}\sin(\theta_k - \theta_h) R_{hk}
\end{aligned}
\tag{3.17}
$$

where $|V_h|$, $|V_k|$ are the RMS values and θ_h, θ_k are the phases of the positive-sequence voltage synchrophasors V_h and V_k, respectively, measured by the two agents and exchanged between them through the communication network.

Each agent is assumed to know the values of the effective impedances between the bus where its compensator is connected and the adjacent α-buses where the compensators of the neighboring agents are connected.

In [41]–[43] it is shown that a sequence of repeated compensations of the mean value of (3.16) and (3.17) is globally convergent to the minimum network loss operating condition under some simplifying assumptions, namely that all the loads consumptions and the DG power outputs are balanced and independent of voltage variations, all line impedances are balanced and have the same inductance/resistance ratio, voltage drops and phase variations between neighboring buses are limited, communication between agents is free from delays and information losses, and the behavior of power electronic converters is almost ideal.

3.2.2.2 Subsequent activation of couples of agents

The environment to be controlled is characterized by scarcely predictable changes and unreliable exchange of information. The subsequent activation of couples of agents based on a random choice makes easier the overcoming of communication problems and the unavailability of a specific compensator. The activation of each updating process in the gossip asynchronous algorithm is typically represented by a Poisson process (e.g. [53]), i.e. by a random activation so that the time interval between consecutive activations has an exponential probability distribution and it is independent of previous time intervals. The activated agent randomly choses another neighboring agent, exchange the information, both apply the updating rules and change their state.

If the updating procedure is very fast, the probability of a concurrent activation of different couple of compensators is negligible. As both the communication and the action of the reactive power compensators requires some time, in the implemented procedure each couple of active

agents choses the following couple to be activated. The implemented procedure limits the probability that an agent will be never activated as the following couple is chosen so to avoid, if possible, those agents already involved in the procedure.

Only after a predefined long time (e.g., tens of minutes) in which an agent is never activated (e.g., due to the failure of a critical communication link), a spontaneous activation governed by a Poisson process with a large rate parameter is allowed.

In order to guarantee the persistence of the procedure also in the presence of packet losses, the algorithm includes the possibility of concurrent multiple reactive compensation processes. However, the convergence of the algorithm may be hindered by the presence of concurrent compensation processes. Therefore such a possibility is limited by the introduction of priority indexes so that concurrent compensation processes with priority indexes lower than the others are progressively stopped by the agents.

The analysis presented in [43] shows the advantages of a multi-hop random selection of the agents on the convergence of the algorithm to the optimal operating point. However, the multi-hop procedure appears more vulnerable in presence of latency and packet loss than the implemented single-hop procedure in which the compensation is performed by neighboring agents.

3.2.2.3 Countermeasures against the loss of packets and communication latency

As a countermeasure against the loss of packets, a priority index is associated to each compensation process. When there is packet loss during the procedure of choice of the next couple of active agents, multiple concurrent processes might be initiated in order to avoid the block of the procedure for the loss of packets carrying this critical information. Each new process is characterized by an increased priority index. Whenever an agent is involved in a process with a lower priority index than that of a previous process to which the same agent has participated, it stops the lower-priority-index process. This mechanism avoids the long permanence of multiple concurrent compensation processes.

The countermeasure against communication latency is based on the availability of a memory buffer at each agent. The memory buffer stores the PMU-provided phasor data with the relevant time tag. This memory allows each couple of agents to estimate the reactive power flow by using synchronous values of voltage phasors. Another countermeasure against excessive communication latency is provided by the definition of a maximum delay t_{wait} after which the procedure carries on with the choice of a new active agent, as described in the next section.

3.2.3 Algorithm

Summarizing, *N* reactive power compensators are assumed to be connected to different buses of the power distribution feeder with the capability to inject a controllable value of reactive power between minimum limit $Q_{\min}$ and maximum limit $Q_{\max}$. The reactive power injection level is adjusted by an agent of the MAS connected to a node of the communication network. Each agent is equipped with a bus voltage sensor that incorporates the PMU function (Figure 3.2) and with a memory buffer where it cyclically stores both the measured phasors and the corresponding measurement times for a predefined time interval equal to t_{wait}.

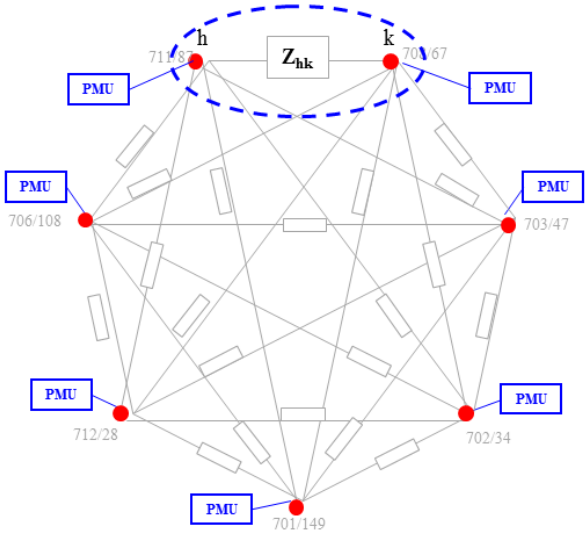

Figure 3.2 Agents (red dotted) of the equivalent reduced network equipped with a bus voltage sensor that incorporates the PMU function

The algorithm corresponds to the repeated execution of the following steps (indicated as a compensation cycle).

3.2.3.1 Measurement, information exchange and calculation of ΔQ

1. An agent, which we denote as agent *h,* is assumed to be activated by another agent that also provides its updated priority index p_h as explained in the last steps.

2. Agent *h* randomly chooses a neighboring agent in the communication network, identified as agent *k* (by avoiding the agent that has activated him, if there is another one available).

3. Agent *h* sends to agent *k* both the most updated values (present in the memory buffer) of $|V_h|$ and θ_h of the positive sequence voltage phasor of the bus to which its compensator is connected and the indication of corresponding measurement time t_{meas}. Moreover it sends the identifier of bus *h*, value p_h equal to its priority index and the values of the margins between the current reactive output Q_h of its compensator and the relevant minimum and maximum limits, i.e. $\delta_h^{\max} = Q_{h,\max} - Q_h$ and $\delta_h^{\min} = Q_{h,\min} - Q_h$. (Figure 3.3)

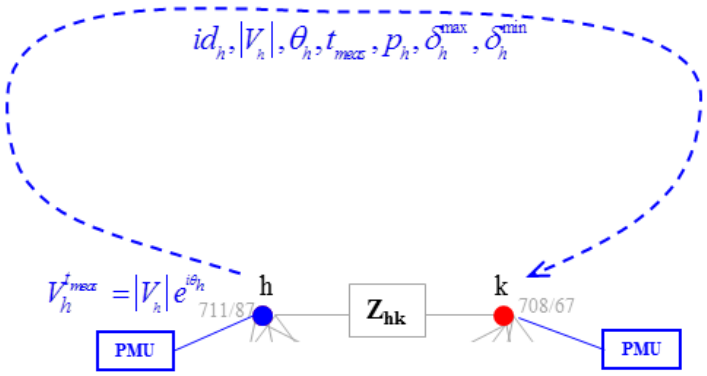

Figure 3.3 Measurement, information exchange from node *h* to node *k* – step 3

4. When agent *k* receives the information from agent *h*, it accepts the assignment only if p_h is not lower than its priority index, otherwise it denies the assignment by sending the relevant message to agent *h* that concludes the compensation process with priority p_h.

5. If agent *k* accepts the assignment, it updates its priority index, if necessary, and it finds the bus voltage phasor V_k measured at t_{meas} stored in his memory buffer. It calculates Q'_{hk} and Q''_{hk}, by using (3.16) and (3.17). Moreover, analogously to agent *h*, it calculates reactive power margins δ_k^{max} and δ_k^{min} relevant to its compensator connected to bus *k*.

6. In order to define adjustment ΔQ of the compensator set point, agent *k* compares the value $\overline{Q_{hk}} = \min(|Q'_{hk}|, |Q''_{hk}|) \cdot \mathrm{sgn}(Q'_{hk})$ with the maximum allowed variations of the reactive output of both compensators, i.e., δ_k^{max}, δ_k^{min} and $\delta_h^{max}, \delta_h^{min}$:

$$\Delta Q = \max\left(\min\left(\overline{Q_{hk}}, \delta_k^{max}, -\delta_h^{min}\right), \delta_k^{min}, -\delta_h^{max}\right) \tag{3.18}$$

If Q'_{hk} and Q''_{hk} have different signs, then ΔQ is set equal to 0.

3.2.3.2 Implementation of ΔQ

7. Agent *k* changes the output of its compensator by adding ΔQ only if at least one of the following two conditions is met:

$$\begin{aligned} &\Delta Q > 0 \text{ and } |V_k| < V_{max} \\ &\Delta Q < 0 \text{ and } |V_k| > V_{min} \end{aligned} \tag{3.19}$$

where V_{max} and V_{min} are two values a few percent higher and lower than bus voltage rated value, respectively, so to define the voltage interval of the normal operating state. If none of (3.19) is met, the reactive power output is not changed.

8. Agent *k* sends back value ΔQ to agent *h*.

9. If agent h does not receive the message from agent k before t_{wait} after t_{meas}, it randomly selects another agent k (step 2). Priority index p_h remains unchanged.

10. If agent h receive the message from agent k, it changes the reactive output reference of its compensator by subtracting ΔQ only if at least one of the following two conditions is met:

$$\begin{aligned} \Delta Q < 0 \text{ and } |V_h| < V_{\max} \\ \Delta Q > 0 \text{ and } |V_h| > V_{\min} \end{aligned} \tag{3.20}$$

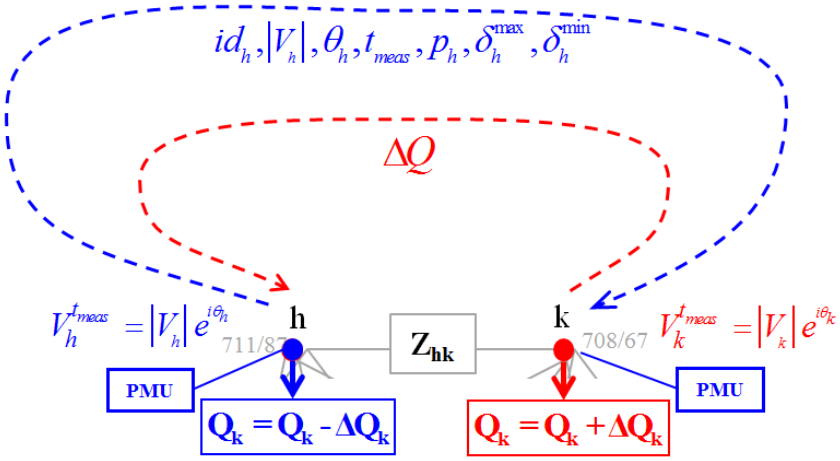

Figure 3.4 Measurement, information exchange, calculation and injection of ΔQ

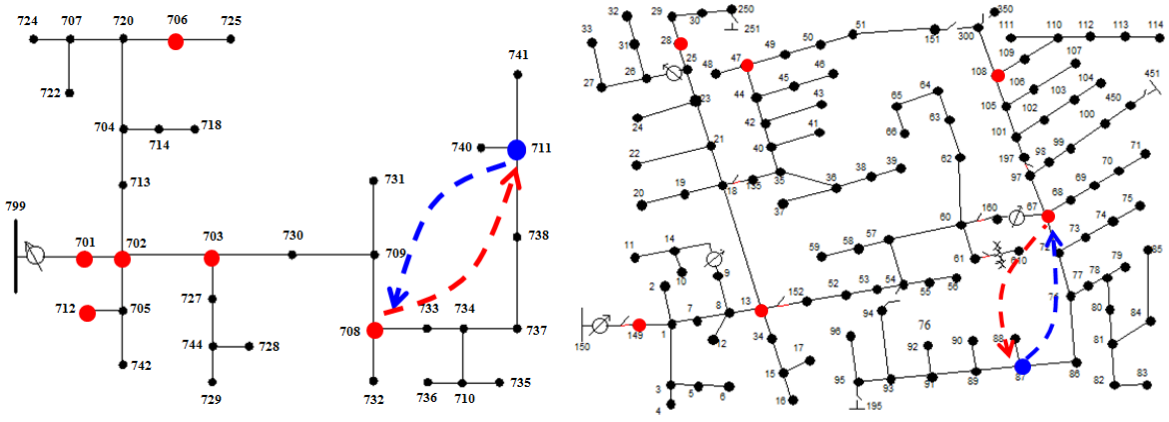

Figure 3.5 Correspondent example of bi-directional information exchange in the IEEE 37 and 123 node test feeders

3.2.3.3 Selection of the new couple of agents

11. Agent h randomly choses another agent to be activated as new agent h. (Figure 3.6)

12. When the chosen agent receives the relevant message from agent h with the priority p_h, it checks whether p_h is greater or lower than its priority index. If it is equal or greater, the receiving agent becomes the new agent h. If necessary, it updates its priority index to p_h and sends the relevant acknowledgment message back to the old agent h, which then

returns in the idle state. If p_h is lower than the priority index of the receiving agent, it denies the assignment by sending the relevant message to agent h that concludes the compensation process with priority p_h.

13. The new agent h starts again the procedure from step 1, waiting at least t_{wait} after t_{meas} so to allow the stabilization of both compensators in the new operating conditions.

14. If old agent h does not receive the acknowledgment message from the new one by t_{wait} after t_{meas}, it increments its priority index p_h and randomly selects another agent to be activated (step 11).

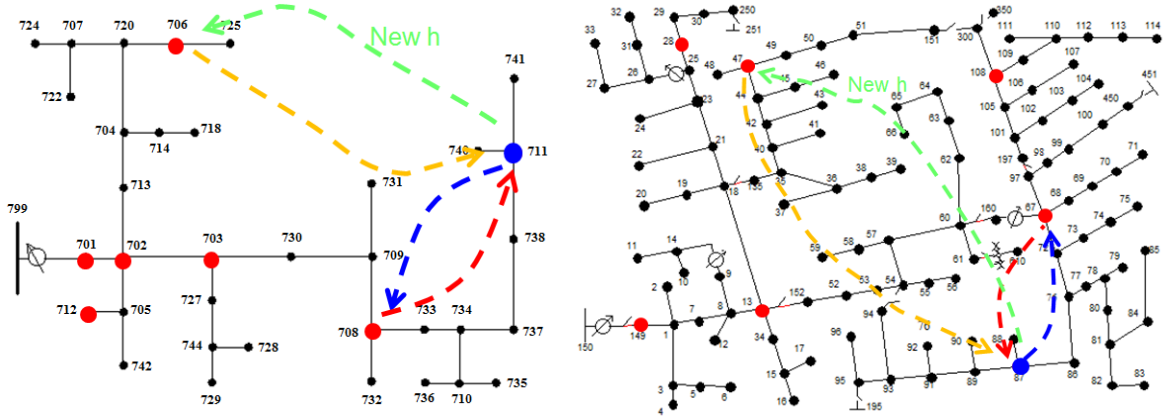

Figure 3.6 Selection of the new couple of agents

Conditions (3.19) and (3.20) exploits the fact that the connection to the transmission network through the substation guarantees the reactive power balance in the feeder.

3.3 Extended simulation platform

As already mentioned in Chapter 2, the developed platform is based on the interface between the communication simulator Riverbed-OPNET v18.0 [22] and the power system simulation environment EMTP-rv [23].

3.3.1 Communication model

A client-server communication model has been implemented for each OPNET-EMTP interface between a node of the communication network and the relevant agent that regulates a reactive power compensator implemented in the EMTP-rv model.

As illustrated in Figure 3.3, both the TCP and UDP node models are extended by an Esys module that as already explained in section 2.3 enables the management and the delivery of the communication packets. Each agent model in OPNET is composed by a client and a server in order to establish a point-to-point communication link.

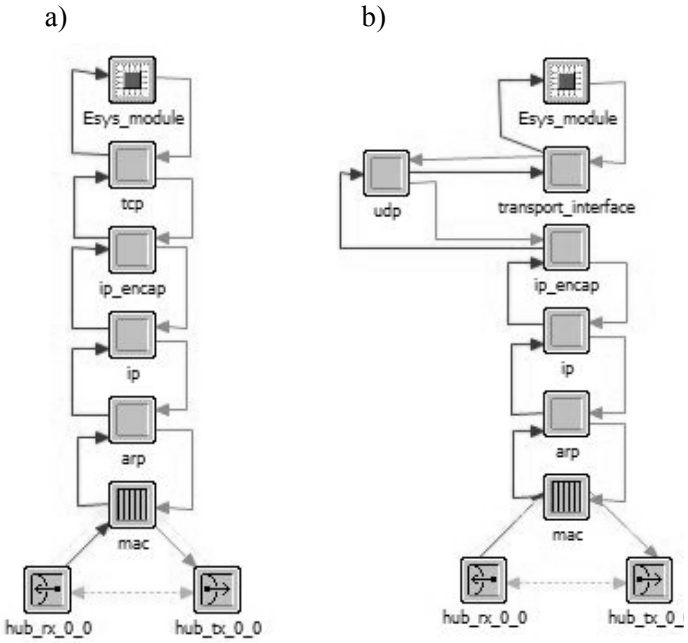

Figure 3.7. a) TCP and b) UDP extended node models. hub_rx and hub_tx: physical layer; mac (Media Access Control) and arp (Address Resolution Protocol): link layer; ip (Internet Protocol) and ip_encap (which encapsulates packets into IP datagrams): internet layer; tcp or udp and transport_interface: transport layer.

A message generated by the EMTP-rv model of the agents, implemented by using a specific DLL, is transferred at first to the socket communication and then to the relevant Esys interface of the client in the OPNET agent model. The message is built into the TCP or UDP datagram and sent to the server of the destination agent through the communication network. The destination server processes the received datagram, extrapolates the information from the payload, and returns the message to the associated EMTP-rv interface.

The TCP model establishes a connection-oriented point-to-point communication link and includes connection set-up, data exchange, acknowledgment, retransmission, and connection termination functionalities. In the UDP model, the communication is connectionless, i.e. a message is sent from one end-point to another without prior arrangement or control. In our application, the dimension of TCP packets is 408 bits for data exchange and 376 bits for set-up, acknowledgment and connection termination. The dimension of UDP packets is 312 bits.

In OPNET, each agent node is connected to an IP-based gateways and a background data traffic generator. As illustrated in Figure 3.4 the IP-based gateways are connected to each other by a communication network with 64 kilobits per second (kbps) serial twisted-pair links and characterized by topology that follows the same tree configuration of the power distribution feeder. Each agent node is connected to the own router via a 10BaseT Ethernet link.

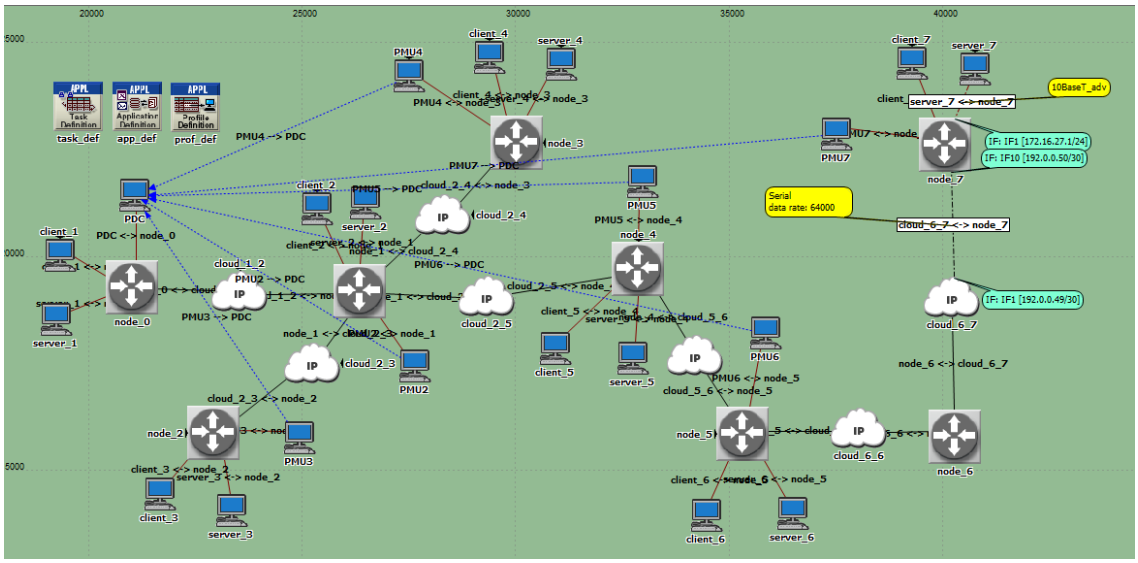

Figure 3.8 Correspondent Internet based communication network of the IEEE 37 node Test Feeder

The background traffic (BT) in the communication links is represented by an IP layer traffic flow from each node towards the router located at the substation. Each communication link is also characterized by a packet discard ratio (PDR), representing the probability of a packet to be lost in the link.

3.3.2 Power distribution feeder model

The EMTP-rv model of the network is mainly composed by the three-phase constant-parameters PI models for the representation of the unbalanced lines a three-phase OLTC transformer model at the substation fed by a positive sequence constant voltage generator (Figure 3.5), the models of reactive power compensator, loads and other cascaded OLTC transformers.. As EMTP-rv converts all the load models in RLC branches in time domain simulations, constant PQ and constant current three-phase unbalanced load models are represented by adopting the same two-triplets current-generators structure used for the compensators, with the difference that a per-phase control of active and reactive power (negative) injections has been implemented.

3.3.2.1 Control of the OLTC transformers

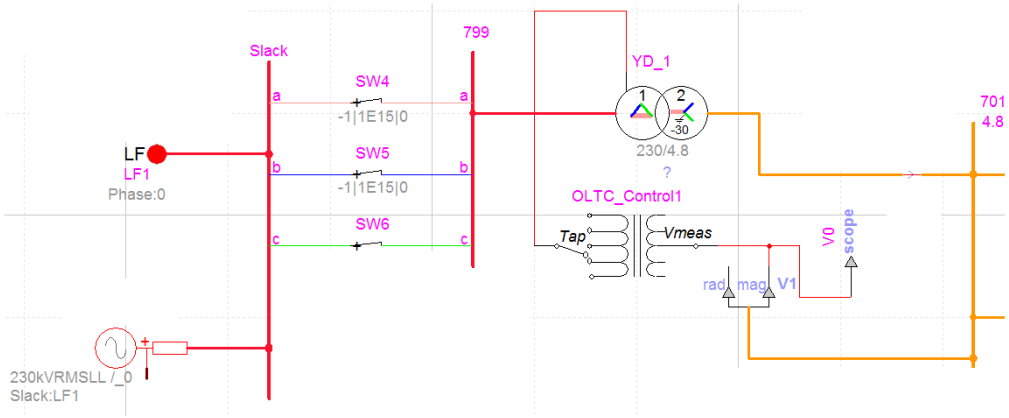

Figure 3.9 EMTP-rv model design of the substation fed by a three-phase voltage generator and control by an OLTC transformer

The OLTC model is adapted from [54]. The OLTC regulator (Figure 3.6) changes the tap when the RMS value of voltage at the secondary side differs from the reference value more than a predefined dead band for at least 0.5 s. The first tap change of each control action is postponed by a fixed delay, whilst subsequent changes are applied after a delay time fixed or with an inverse law.

In order to coordinate the action of the OLTC regulators within the MAS, an additional agent, i.e. a communication networked controller, is associated to the secondary side of each OLTC transformer. Also this agent participates to the gossip-like procedure by providing the PMU measurements to the other agents for the estimation of the reactive power flows, but it does not directly adjust the output of any converter. Then, in order to avoid unnecessary operations and wear of the OLTCs of a series of cascaded transformers, the upstream transformer sends a message to downstream transformers in order to delay their actions if those actions are of the same type of the one that the upstream transformer is applying [55]. Once the upstream transformer terminates its action, after t_{wait} it sends another message to downstream transformers in order to release their actions. In case of an OLTC transformer located in the middle of the radial power feeder, the set of networked controllers relevant to downstream feeder nodes (with respect to the transformer secondary side) do not communicate with networked controllers connected to upstream nodes.

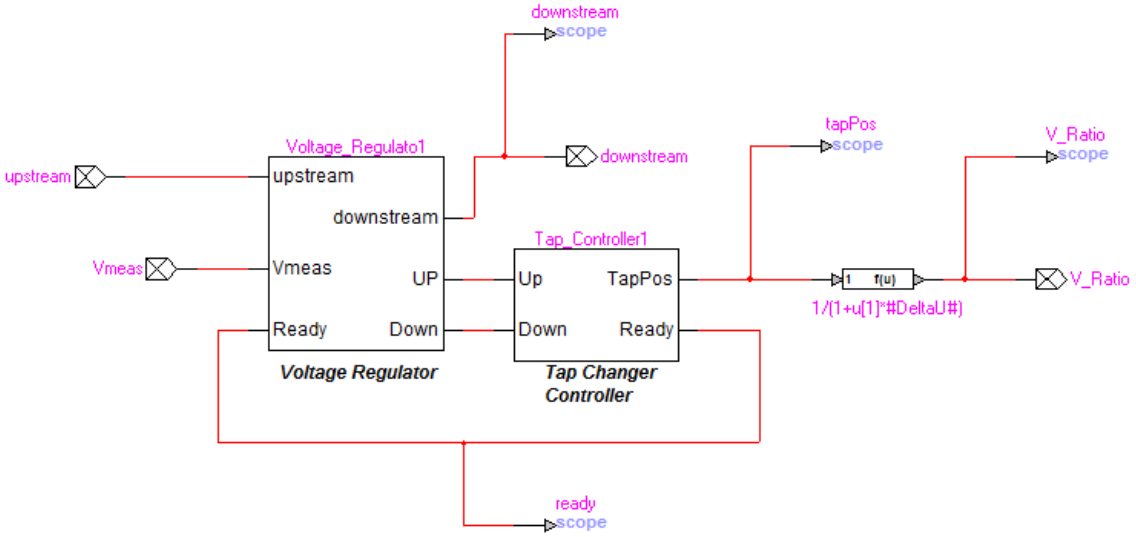

Figure 3.10 OLTC model

3.3.2.2 Reactive power compensators

The compensators are represented by components able to inject assigned and adjustable three-phase active and reactive powers. A first approximation of the quasi-steady-state behavior of both synchronous generators and power electronic interfaced sources connected to an unbalanced network is provided by a three positive-sequence current sources in parallel with a 3×3 Y matrix (e.g. [56],[57]). The DG model implemented in EMTP-rv is composed by two positive-sequence triplets of current generators. As it can be seen in Figure 3.7 the amplitude of one triplet is controlled by a feed-back regulator in order to inject or absorb the requested value of three-phase active power, whilst the phase angle between current and bus voltage is regulated so to achieve a zero value of reactive power. The regulators of the second triplets have a reverse function, i.e. amplitude is controlled in order to inject the requested reactive power and phase angle is controlled in order to cancel out active injection. Reference value Q_i of the reactive power injection of compensator i is dynamically changed by the associated agent. A smooth transition between different power levels in a short time window of few hundreds of milliseconds is represented. The agent of each compensator includes also the model of a PMU that provides a sampling time of 10 estimates per second ($t_{sampling}$ = 100ms). The accuracy of PMUs is also represented by the Normal distribution of the measurement errors. In the simulations, the corresponding standard deviation values are assumed equal to 8.1 μrad for phase error and 9.3×10^{-6} p.u. for RMS error, respectively [50]. Also the accuracy associated with a capacitive voltage divider is included by means a Normal distribution with standard deviation equal to 7 μrad for the phase error and 58×10^{-6} p.u. for RMS error, respectively.

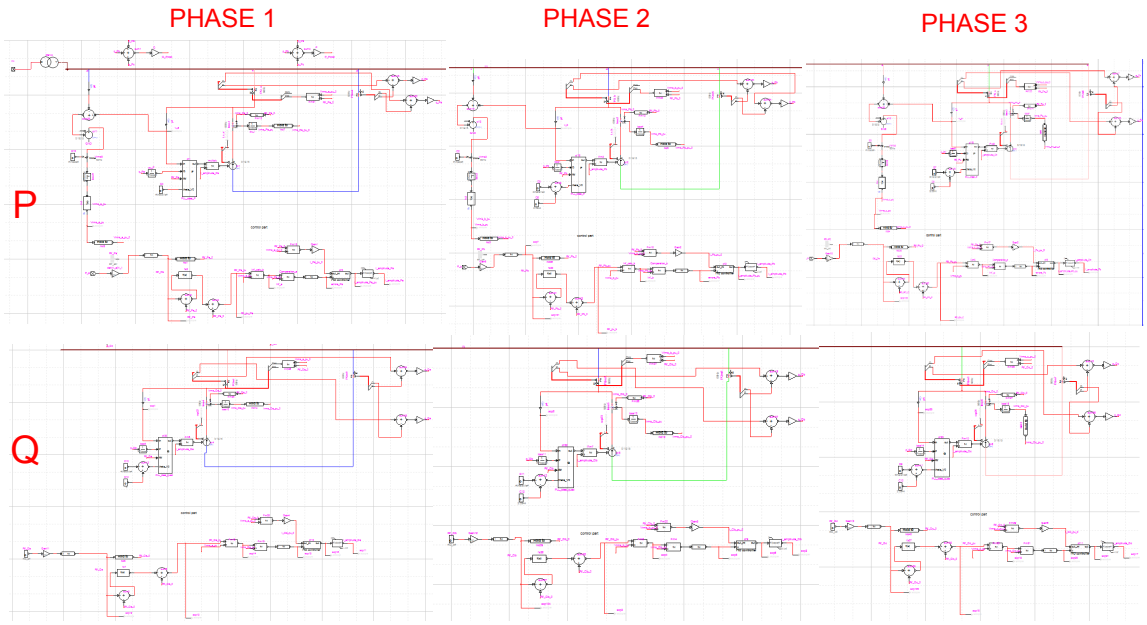

Figure 3.11 EMTP-rv model design of the compensators

3.3.2.3 Local voltage control function

The above-described gossip-like VVC algorithm is coordinated with a faster local voltage control function. Each compensator *i* is equipped with a fast local controller [58] and we assume that the local voltage control function on the i-th inverter adjusts reactive power level Q_i defined by th agent of the gossip-like algorithm by a quantity $\Delta Q_{\text{local},i}$ in the RMS value of the local voltage $|V_i|$ significantly differ from the rated value. The voltage interval of the normal operating state is defined by two values, V^+ and V^-, a few percent higher and lower than bus voltage rated value (in the simulations, they are equal to 1.03 pu and 0.97 pu, respectively). Q_i is reduced if $|V_i| > V^+$ and to increase Q_i if $|V_i| < V^-$:

$$\begin{aligned} \Delta Q_{\text{local},i} &= -\left(|V_i| - V_{\max}\right)\frac{\left(-Q_{\min} + Q_i\right)}{\Delta V_{\max}} \quad \text{if} \quad |V_i| > V^+ \\ \Delta Q_{\text{local},i} &= \left(V_{\min} - |V_i|\right)\frac{\left(Q_{\max} - Q_i\right)}{\Delta V_{\max}} \quad \text{if} \quad |V_i| < V^- \end{aligned} \tag{3.21}$$

where $\Delta V_{\max}$ indicates the transient voltage deviation that causes a complete utilization of the available reactive power margin and $Q_{\min/\max}$ are the size limit of the compensators (e.g.: inverters, capacitor banks, batteries, etc.). In order to avoid oscillations, $\Delta Q_{\text{local},i}$ is added to Q_i through a transfer function (chosen with a single pole equal to -5 in these simulations) [58].

In order to avoid a conflict between the action of the local voltage regulator and that of the distributed MAS compensation process, the gossip-like algorithm sets ΔQ=0 if $|V_i|$ is outside the normal operating interval and the sign of ΔQ would be different than that of the local voltage regulator as defined by (3.21).

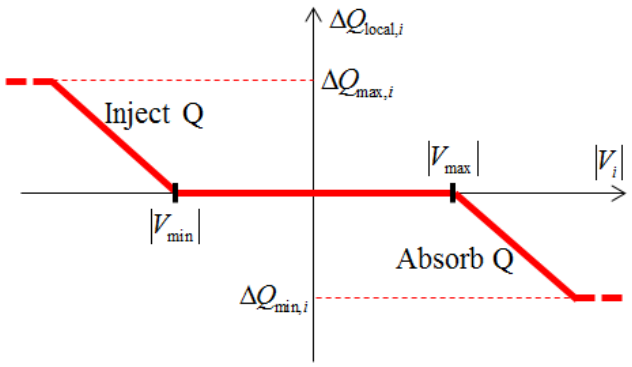

Figure 3.12 Local voltage regulator [58]

3.4 Simulation results

Numerical tests have been carried out for the two following test feeders adapted from [46] with 6 additional three-phase reactive power compensators, indicated with Q1 … Q6:

TF1: IEEE 37 Node Test Feeder, with the 6 reactive power compensators connected to buses 702, 712, 706, 703, 708 and 711, respectively (Figure 3.9).

TF2: IEEE 123 Node Test Feeder, with the 6 reactive power compensators connected to buses 13, 28, 47, 67, 87, and 108, respectively (Figure 3.10).

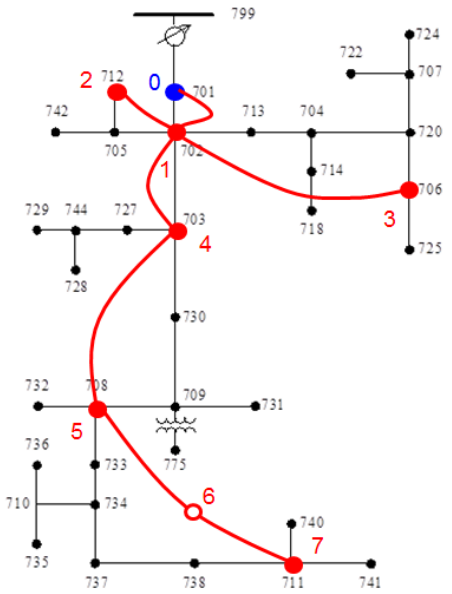

Figure 3.13 TF1: power feeder in black and communication network in red. Red dots indicate the agents associated to compensators whilst the blue one indicates an agent that does not directly adjust the output of any compensator.

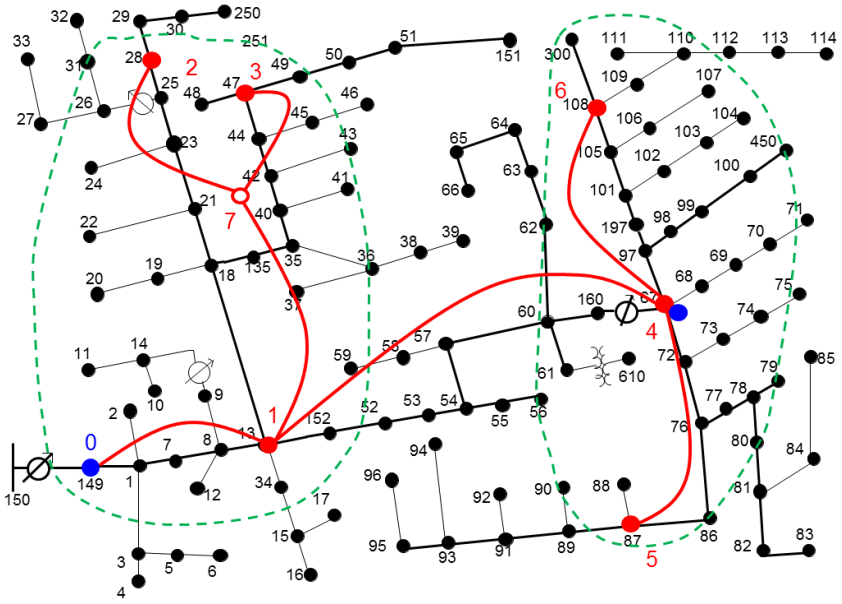

Figure 3.14 TF2: power feeder in black and communication network in red. Red dots indicate the agents associated to compensators whilst the blue ones indicate agents that do not directly adjust the output of any compensator.

As a base case, limits $Q_{\max}$ and $Q_{\min}$ are set equal to 500 kvar and -500 kvar, respectively, for all the compensators. The influence of more stringent limits (namely ±250 and ±150 kvar) has been also analyzed. Initially the reactive power output of all the compensators is null.

The characteristics of unbalanced lines and loads have been defined as in [46]. In order to speed up the simulations, the constant power and constant current load models described in

Section 3.3.2 have been applied only to the loads larger than 100 kW in TF1 and to the loads larger or equal than 40 kW in TF2, whilst the other loads are represented as constant impedances.

The procedure has been also applied to both the case of a higher load level and a lower load level than that indicated in [46]. The former (high load) is obtained by multiplying both the original active and reactive power values at each load bus (normal load) by a different number obtained by a uniformed distribution between 1.3 and 1.7. The latter (low load) is obtained by using multipliers uniformly distributed between 0.3 and 0.7.

Substation transformers are equipped with OLTC with ±8 tap increments of 1.875%. The tap mechanical delay is 2s, the time to first tap change is 20 s and the maximum delay time of the subsequent tap changes is 15 s with an inverse law.

Three different BT levels are analyzed, identified as BT0, BT1 and BT2, which correspond respectively to 0, 4.75, and 9.5 kbps that each BT generator sends towards node 0. Each BT level is analyzed both without PDR (case identified as PDR0) and by assuming a 5% PDR (case identified as PDR5) for each communication link. For BT levels 0 and 1 we assume t_{wait}=1 s. For BT level 2, we have compared the results obtained for two t_{wait} values, namely a) t_{wait}=1 s (BT2a) and b) t_{wait}=10 s (BT2b). For the simulations with t_{wait}=1 s the final time is t_f = 80 s, whilst when t_{wait} =10 s t_f is extended to 100 s. In order to compare the promptness of the procedure in the various scenarios characterized by different BT levels, we define settling time t_{set} as the time to enter and remain within a 500 W band for at least 30 s. V_{max} and V_{min} are chosen equal to 1.03 and 0.97 respectively (±3%).

3.4.1 IEEE 37 Node Test Feeder

An ideal positive-sequence three-phase source is connected to the primary side of the substation transformer with line-to-line RMS value voltage equal to 230 kV. The rated ratio of the 2.5 MVA substation transformer is 230/4.8 kV with resistance r=2% and reactance x=8%.

An additional agent is associated with bus 701, at the secondary side of the substation transformer (blue dot in Figure 3.13). This agent participates to the regulation cycles of the VVC procedure but it does not directly adjust the output of any compensator.

As shown by Figure 3.13, the wired communication network has 8 nodes with a tree topology that follows the same configuration of the power feeder: node 0 is located at the feeder substation (bus 701), nodes 1, 2, 3, 4, 5, and 7 connect the agents associated with the reactive power compensators, respectively, and node 6 is located in the path between node 5 and node 7. The communication network is therefore composed by 7 links: link 0 (nodes 0–1), link 1 (nodes 1–2), link 2 (nodes 1–3), link 3 (nodes 1–4), link 4 (node 4–5), link 5 (nodes 5–6), link 6 (nodes 6-7). Table 3.I shows the BT percentage values in all the links for the considered three BT levels. Link 0 is the most affected by the traffic caused by the BT data flow concentration. The BT percentage value in link 0 produced by each BT generator is: 8.4% with 4.75 kbps and 16.7% with 9.5 kbps.

Table 3.I BT levels and corresponding BT percentage values for each of the links of the communication network of TF1.

BT LEVELS	BT (%)					
	LINK 0	LINK 1	LINK 2	LINK 3	LINK 4	LINK 5&6
BT0	0	0	0	0	0	0
BT1	49.7	8.4	8.4	25	16.8	8.4
BT2	98.7	16.7	16.7	49.5	33.1	16.7

Table 3.II Mean and standard deviation values of the number of compensation cycles, percentage of incomplete compensations, power loss decrease and settling time for TF1.

BT PDR LEVEL	NO OF COMPENSATION CYCLES MEAN (STDEV)		% OF INCOMPLETE COMPENSATIONS MEAN (STDEV)		POWER LOSS DECREASE (KW) MEAN (STDEV)		SETTLING TIME (S) MEAN (STDEV)	
	TCP	UDP	TCP	UDP	TCP	UDP	TCP	UDP
BT0 PDR0	70.5 (0.5)	75.8 (0.4)	0 (0)	0 (0)	13.4 (0.1)	13.5 (0.1)	26.0 (13.0)	28.3 (10.9)
BT1 PDR0	68.2 (0.5)	74.5 (0.5)	0 (0)	0 (0)	13.4 (0.2)	13.5 (0.1)	26.0 (10.6)	23.1 (13.5)
BT2A PDR0	59.2 (1.9)	63.4 (1.9)	0 (0)	0 (0)	8.2 (3.1)	7.9 (3.0)	32.8 (19.3)	31.6 (23.5)
BT2B PDR0	9.5 (0.6)	10.0 (0.1)	0 (0)	0 (0)	10.6 (2.5)	11.5 (1.4)	-	-
BT0 PDR5	30.6 (11.8)	67.9 (5.3)	32.3 (11.5)	6.1 (2.7)	12.1 (1.9)	13.0 (2.1)	33.5 (21.9)	28.1 (12.9)
BT2A PDR5	35.4 (5.1)	58.3 (3.8)	29.0 (10.3)	7.3 (3.8)	10.9 (3.3)	10.7 (3.1)	33.3 (15.3)	33.8 (19.3)
BT2B PDR5	7.4 (1.3)	9.2 (1.6)	11.8 (14.8)	5.0 (6.4)	9.8 (2.4)	10.7 (2.8)	-	-

Table 3.III Mean and standard deviation values of the number of packets, percentage of ignored and lost packets, packet delay and number of stopped processes for TF1.

BT (PDR) LEVEL	NO. OF PACKETS MEAN (STDEV)		% OF PACKETS IGNORED OR LOST MEAN (STDEV)		% OF PACKET LOST MEAN (STDEV)	PACKET DELAY (MS) MEAN (STDEV)		NO. OF STOPPED PROCESSES MEAN (STDEV)	
	TCP	**UDP**	**TCP**	**UDP**	**UDP**	**TCP**	**UDP**	**TCP**	**UDP**
BT0 PDR0	282.0 (1.9)	303.2 (1.5)	0 (0)	0 (0)	0 (0)	49 (14)	11 (3)	0 (0)	0 (0)
BT1 PDR0	272.7 (1.7)	297.9 (1.9)	0 (0)	0 (0)	0 (0)	66 (33)	18 (16)	0 (0)	0 (0)
BT2A PDR0	245.9 (4.9)	264.4 (5.6)	4.2 (1.2)	4.2 (0.8)	0 (0)	76 (39)	22 (21)	0 (0)	0 (0)
BT2B PDR0	37.8 (2.5)	39.9 (0.5)	0 (0)	0 (0)	0 (0)	462 (918)	194 (523)	0 (0)	0 (0)
BT0 PDR5	188.6 (15.1)	276.1 (18.8)	47.2 (18.6)	5.7 (1.5)	5.7 (1.5)	52 (36)	12 (3)	2.6 (1.5)	1.8 (1.3)
BT2A PDR5	186.8 (7.3)	247.9 (10.6)	34.4 (6.6)	9.8 (1.5)	6.3 (1.4)	93 (88)	24 (33)	4.3 (1.8)	1.7 (1.3)
BT2B PDR5	30.7 (4.2)	37.7 (6.1)	11.2 (11.0)	4.5 (4.1)	4.5 (4.1)	890 (1509)	241 (561)	0.3 (0.6)	0.3 (0.6)

Table 3.II and Table 3.III compare the results obtained for the 7 scenarios characterized by different values of BT and PDR by using TCP and UDP with both OLTC and local controllers blocked. Since the gossip-like procedure is based on the random choice of the active agents, the Tables report the results of the statistical analysis carried out by performing 30 simulations for the

same case. For each simulation, the pseudorandom number generator is initialized by a different seed state associated with the computer system time. In Table 3.II, the number of compensation cycles is the number of cycles in which at least one compensator changes its reactive power and the percentage of incomplete compensations indicates the percentage of cycles that do not complete regularly; the power loss decrease indicates the difference between the values of power losses at the starting time and at t_{set}. In Table 3.III, the number of packets takes into account only the packets carrying the compensation data sent by the agents; the percentage of ignored or lost packets refers to those that arrive at destination after t_{wait} or do not arrive at all (for UDP the specific percentage of the lost packets is also provided); packets delay indicates the travelling time of the packets that regularly arrive at destination before t_{wait}; the number of stopped process is the number of stopping actions on the basis of the priority index value. The packet delay values indicated in Table III are the mean values of the statistical parameters obtained for each of the 30 simulations.

For BT0-PDR0, the mean value (standard deviation) in kvar of the final reactive power outputs of the 6 compensators is: 146.5 (25.6), 63.1 (2.2), 148.2 (1.4), 144.7 (7.6), 169.8 (4.0), 164.7 (1.6). The limited values of the standard deviations show that the reactive output scheduling at the end of different compensation cycles is almost the same. The significant value of the first standard deviation is due to the location of compensator Q1 close to the slack bus. The low value of the standard deviation relevant to the loss decrease (fractions of a kW) also indicates that an analogous power flow conditions is achieved at the end of different sequence of compensations. The procedure converges in less than 30 s to a mean value of the final power losses of about 76.3 kW. The reduction of nearly 13.5 kW is in agreement with the results shown in [43]. Despite the significant differences between the two approaches, the results are also in reasonable agreement with those obtained by applying the three-phase version of the mixed integer linear programming (MILP) model proposed in [32] to the same distribution system. The solution of the MILP model provides the following reactive power scheduling (in kvar): 140, 75, 150, 140, 170, 170 (in the implemented MILP model the reactive power outputs can be changed in steps of 5 kvar). The minimum power loss calculated by the MILP model is 76.27 kW, only some tens of watts lower than that achieved by the gossip procedure.

As shown in Table 3.II and Table 3.III similar results are obtained also for case BT1-PDR0.

For the cases without packet loss (PDR0), as expected, the results show larger delays for increasing BT levels from 0 to 2. Even without PDR, in scenario BT2a, due to the congestion of the communication links, several packets do not reach the expected receiver within t_{wait}=1 s and, therefore, they are ignored. Table 3.III shows that in BT2b this problem is solved as t_{wait} is extended to 10 seconds. Whilst for t_{wait}=1 s the compensation procedure is fast enough so that t_{set} could be considered the time at which the procedure converges, this is no longer true for BT2b. Therefore for BT2b the power loss decrease is evaluated at t_f = 100 s, although the convergence is not yet reached due to the insufficient number of compensation cycles.

For the cases with PDR=5% (PDR5), the number of compensation cycles reduces in particular for TCP. The PDR causes an incomplete cycle when there is the loss of the packet that

carries the information from agent *k*, which compensates first, to agent *h*. Moreover, the loss of the return packet from the new agent *h* and the old one causes the start of a process with increased priority index, as described in Section 3.2.2.3. The presence of concurrent processes is then eliminated by the stop of the process with lower priority index.

We could distinguish between packets lost because of PDR5 from those ignored due to excessive delay only by using UDP, whilst this classification is not possible with the implemented TCP model because it closes the communication after t_{wait}.

The comparison between BT2-PDR0 and BT2-PDR5 cases shows that packet loss due to PDR5 partially attenuates the effect of the high BT level, especially in link 0. As a consequence, Table 3.II shows that the mean power loss decrease value is higher in BT2-PDR5 than in BT2-PDR0.

As already described in Section 3.4, two other load levels have been analyzed, one higher and one lower than the normal one. The results have been obtained by using the same seed state for the random number generation, i.e. by the same sequence of active agent pairs. The convergence of the procedure is similar for all the load levels and the obtained reductions of power losses are shown in Table 3.IV for both BT0-PDR0 and BT0-PDR5.

Table 3.IV Power loss reductions obtained for TF1 and different load levels.

LOAD LEVEL	INITIAL POWER LOSS (KW)	POWER LOSS DECREASE (KW)			
		BT0-PDR0		BT2-PDR5	
		TCP	UDP	TCP	UDP
NORMAL LOAD	89.8	13.5	13.5	11.8	12.9
LOW LOAD	25.2	3.9	3.9	3.4	3.8
HIGH LOAD	211.8	31.1	31.1	24.6	28.0

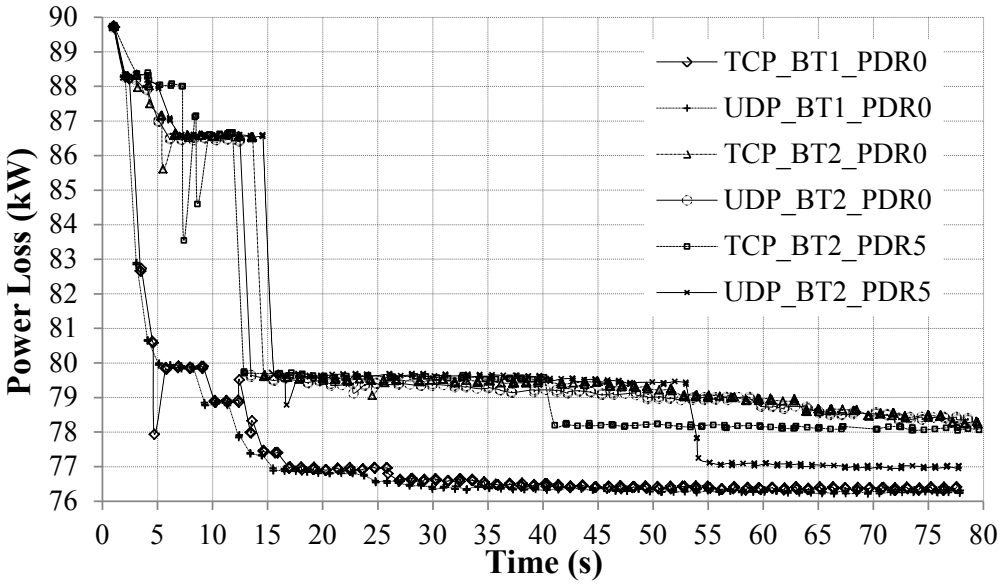

Figure 3.15 Power loss variation in TF1 for different BT levels and PDR by using TCP and UDP.

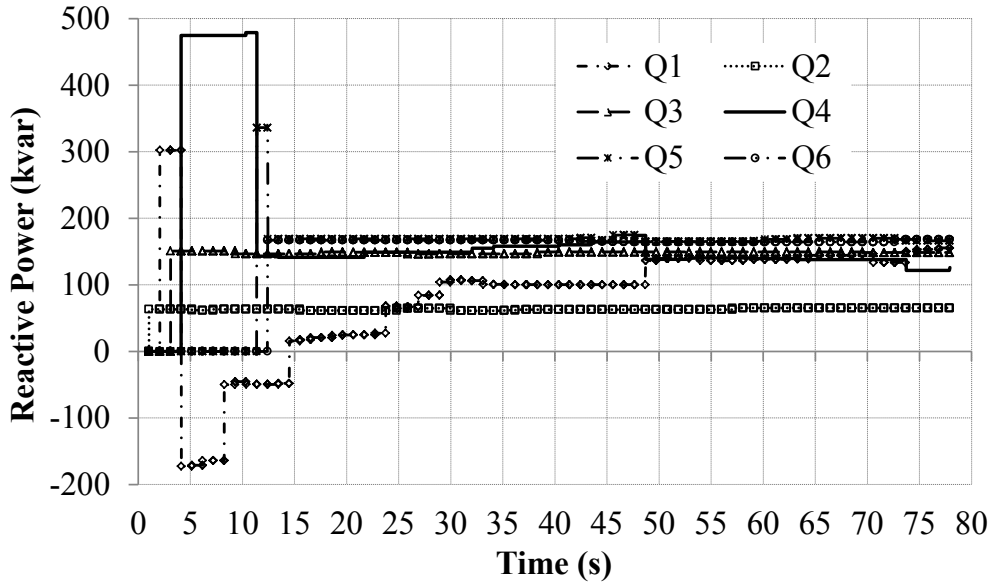

Figure 3.16 Variations of reactive power outputs of the compensators in TF1 for BT1-PDR0 case with UDP.

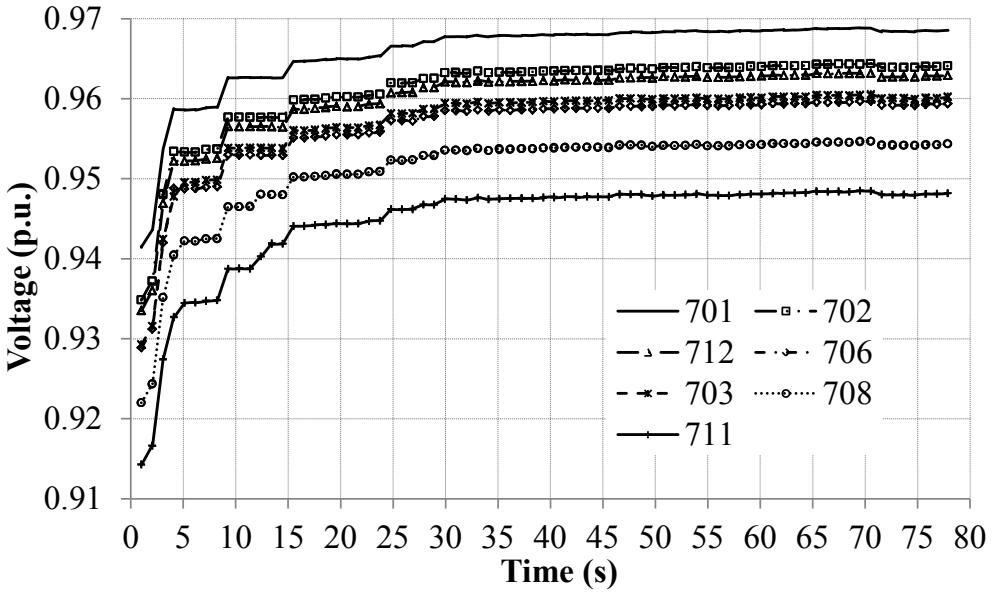

Figure 3.17 Bus voltage variations in TF1 for BT1-PDR0 case with UDP.

Figures from Figure 3.15 to Figure 3.17 illustrate the time behavior obtained by the same sequence of active agents (i.e. determined by the same initial seed of random number generation) for the two different communication protocols and different networks conditions. The feeder has normal load level and the OLTC at the substation is blocked at tap position 0. Figure 3.15 compares the feeder power loss for cases BT1-PDR0, BT2-PDR0 and BT2-PDR5, by using TCP and UDP. Figure 3.15 shows that the VVC action with TCP is slightly delayed with respect to the one obtained by using UDP. Moreover, whilst for the case BT1-PDR0 (which represents a medium utilization level of the communication links without PDR) all the compensation cycles are completed, for BT2-PDR0 and BT2-PDR5 some cycles cannot be completed. This justifies the reduced level of obtained efficiency. Figure 3.16 shows the reactive power outputs of the various

compensators during the process and Figure 3.17 shows the positive-sequence voltage RMS values measured by the agents for a case with efficient communication.

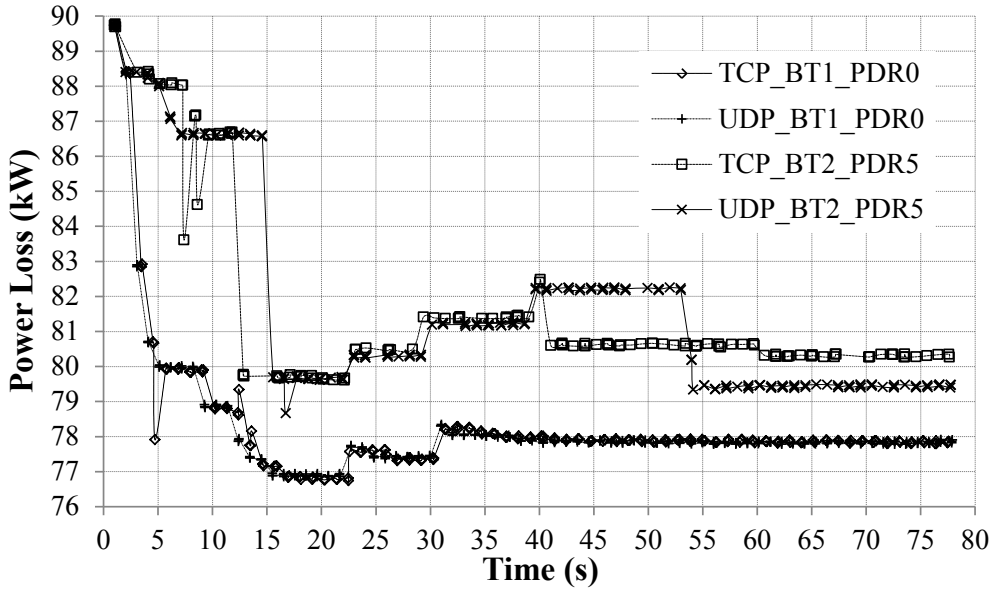

Figure 3.18 Power loss variation in TF1 with active OLTC for different BT levels and PDR by using TCP and UDP.

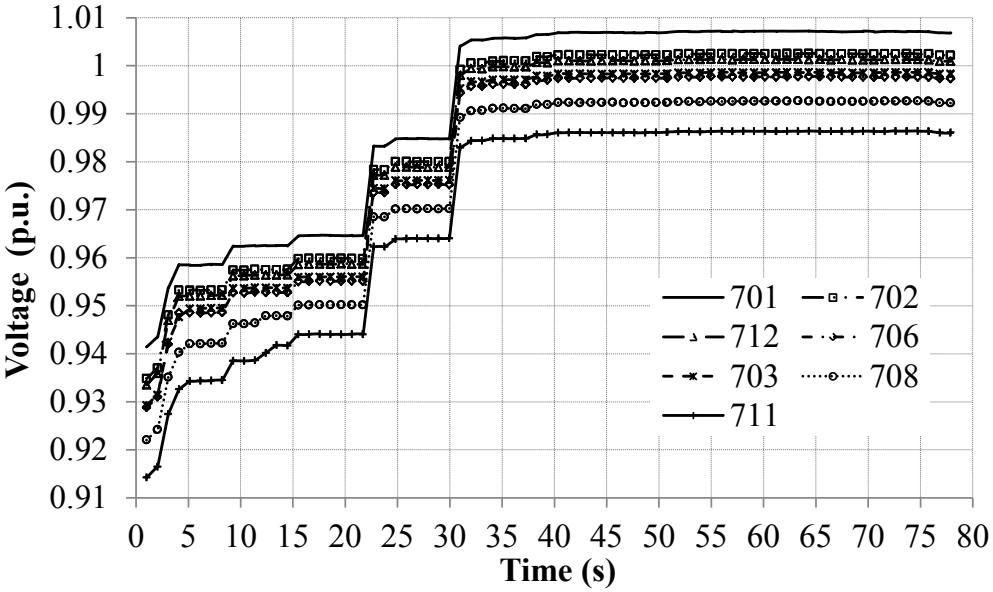

Figure 3.19 Bus voltage variations in TF1 with active OLTC for case BT1-PDR0 with UDP.

The coordination between the VVC procedure and the action of the OLTC at the substation is illustrated in Figure 3.18 and Figure 3.19. The value of the desired regulated voltage at the secondary side is 1.02 pu with a dead band limit of ±0.015 pu. The results show that in BT2-PDR5 cases the OLTC starts in tap position 0, operates a first tap change at 22 s and, after other 2 changes, reaches a final tap equal to -3 at 40 s. In BT1-PDR0 cases, the OLTC operates the first tap change at the same time and after one additional change reaches a steady state condition at tap -2 at 30 s. The improved action by the agents with efficient communication results in a lower

OLTC regulation. The increase of the power losses after each tap change is due to the increased consumption of voltage dependent loads.

Figure 3.20 and Figure 3.21 compare the results obtained by using the MAS procedure with those obtained by using the local controllers of the compensators described by (3.21) with ΔV_{max} = 0.3 pu. Figure 3.20 compares the power loss decrease and Figure 3.21 compares the voltage behavior at buses 701 and 711 calculated:

a) by using the MAS procedure without local controllers,

b) by using only the local controllers,

c) by using the MAS procedure with the local controllers activated.

The local controllers provide a first and fast action after a sudden perturbation whilst the MAS procedure acts as a secondary regulation with the aim to achieve a more efficient utilization of the available resources.

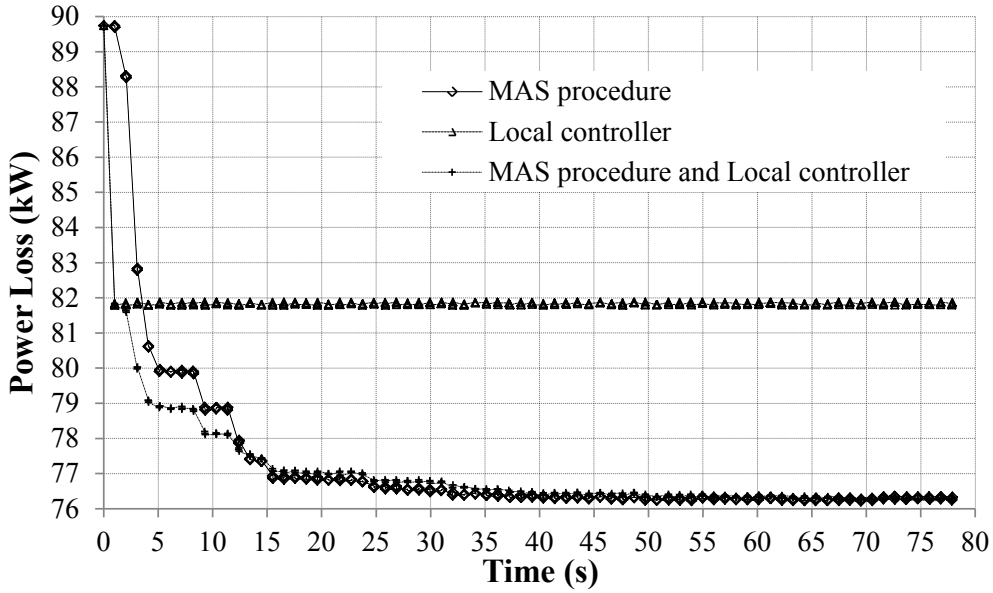

Figure 3.20 Comparison of power loss variation in TF1 with blocked OLTC by using the MAS procedure, by using only the local controllers and by using both regulations (case BT1-PDR0 with UDP).

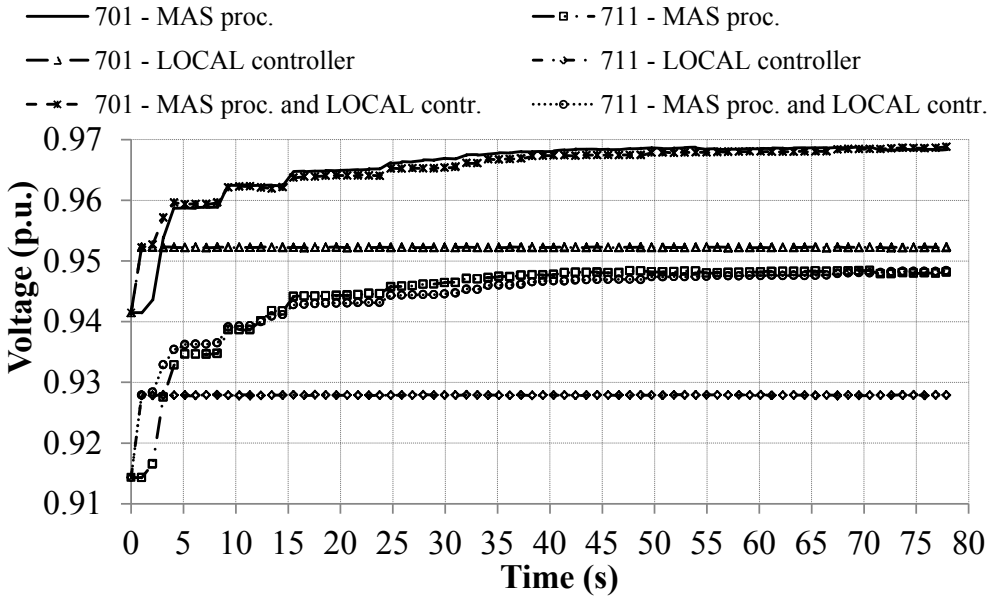

Figure 3.21 Comparison of bus voltage variations in TF1 with blocked OLTC by using the MAS procedure, by using only the local controllers and by using both regulations (case BT1-PDR0 with UDP).

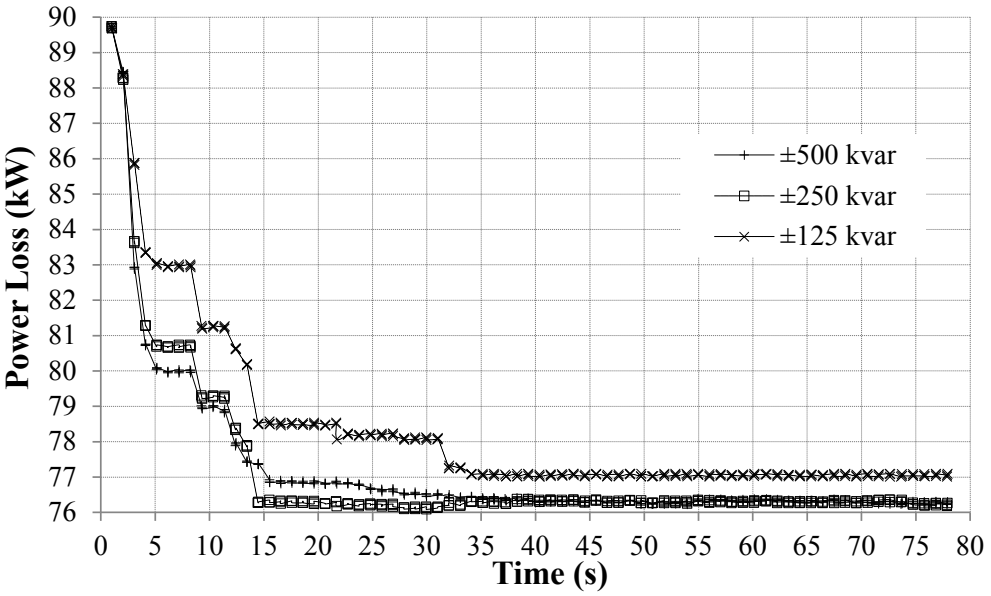

Figure 3.22 Comparison of power loss variation in TF1 with blocked OLTC by using compensators of different size (case BT1-PDR0 with UDP).

Figure 3.22 compares the power loss decrease obtained by using the ±500 kvar compensators with the results obtained by using smaller-size compensators: ±250 kvar and ±125 kvar. The final reactive power scheduling in kvar of the 6 compensators is: 136.19, 64.74, 146.84, 147.55, 168.89, 164.71 (±500 kvar); 131.53, 66.15, 148.62, 165.65, 170.44, 165.85 (±250 kvar) and 125, 65.39, 125, 125, 125, 125 (±125 kvar). Both the ±500 and ±250 limits are not binding; therefore the same 13.5 kW final loss reduction is achieved. The ±125 limits bind the optimal solution of 5 compensators causing a reduction of the power loss decrease to 12.7 kW.

3.4.2 IEEE 123 Node Test Feeder

The ideal positive-sequence three-phase source connected to the primary side of the substation transformer has line-to-line RMS value voltage equal to 115 kV. The rated ratio of the 5 MVA substation transformer is 115/4.16 kV with r=1% and x=8%. Agent 0, associated with bus 701 at the secondary side of the substation transformer, participates to the regulation cycles of the VVC procedure but it does not directly adjust the output of any compensator.

The transformer located between bus 160 and 67 has an OLTC with ±16 tap increments of 0.625%. The time to first change and the maximum time of subsequent-changes inverse-law delay of are both 10 s and the mechanical delay is 2 s.

As shown in Figure 3.14, the communication network has 8 nodes with a tree topology: node 0 is located at the feeder substation (bus 149), nodes 1, 2, 3, 4, 5, and 6 connect the agents associated with the reactive power compensators, respectively, and node 7 is located in the path between nodes 1, 2 and 3. The communication network is therefore composed by 7 links: link 0 (nodes 0–1), link 1 (nodes 1–7), link 2 (nodes 7–2), link 3 (nodes 7–3), link 4 (node 1–4), link 5 (nodes 4–5), link 6 (nodes 4-6). Table 3.V shows the BT percentage values in all the links for the considered three BT levels. The BT percentage value in link 0 produced by each BT generator is: 8.4% with 4.75 kbps and 16.5% with 9.5 kbps.

Agent 4 controls the reactive power compensator connected to bus 67 only when the OLTC between bus 160 and 67 is not operating. When the OLTCs are in operation, the agent set is divided into two groups, namely {0,1,2,3} and {4,5,6} as shown in Figure 3.14, so that at each compensation cycle both agent h and agent k must belong to the same group. Moreover, agent 0 sends a message to agent 4 when the voltage at the secondary side of the substation transformer leaves the dead band. This message increases the tap delay of the downstream OLTC of 120 s. Once the voltage returns inside the dead band, after t_{wait} agent 0 sends a reset message to agent 4.

Table 3.V BT levels and corresponding BT percentage values for each of the links of the communication network of TF2.

BT	**BT (%)**				
LEVEL	**LINK 0**	**LINK 1**	**LINK 2&3**	**LINK 4**	**LINK 5&6**
BT 0	0	0	0	0	0
BT 4.75	49.0	16.5	8.4	24.8	8.4
BT 9.5	98.2	33.0	16.5	49.3	16.5

Table 3.VI Mean and standard deviation values of the number of compensation cycles, percentage of incomplete compensations, power loss decrease and settling time for TF2.

BT (PDR) LEVEL	NO OF COMPENSATIONS CYCLES MEAN (STDEV)		% NO. OF INCOMPLETE COMPENSATIONS MEAN (STDEV)		POWER LOSS DECREASE (KW) MEAN (STDEV)		SETTLING TIME (S) MEAN (STDEV)	
	TCP	UDP	TCP	UDP	TCP	UDP	TCP	UDP
BT0 PDR0	70.7 (0.7)	77 (0.0)	0 (0)	0 (0)	11.4 (0.2)	11.4 (0.1)	24.7 (13.5)	21.0 (11.6)
BT1 PDR0	68.1 (0.8)	75.9 (0.4)	0 (0)	0 (0)	11.4 (0.2)	11.4 (0.2)	26.2 (12.6)	18.9 (12.9)
BT2A PDR0	59.1 (2.3)	65.5 (1.8)	0 (0)	0 (0)	8.9 (2.8)	8.9 (2.3)	30.3 (16.0)	34.8 (21.2)
BT2B PDR0	9.3 (0.7)	10.0 (0.2)	0 (0)	0 (0)	9.9 (2.2)	10.6 (1.4)	-	-
BT0 PDR5	32.6 (10.0)	65.7 (6.3)	34.8 (11.0)	7.2 (3.7)	10.8 (1.3)	11.3 (0.5)	31.7 (18.5)	26.4 (15.6)
BT2A PDR5	32.8 (5.1)	56.0 (10.4)	28.1 (8.3)	8.1 (4.1)	9.3 (2.2)	9.9 (2.0)	34.6 (20.0)	39.2
BT2B PDR5	7.3 (1.9)	8.6 (1.0)	11.4 (11.4)	5.1 (7.9)	8.1 (2.6)	9.3 (2.6)	-	-

Table 3.VII Mean and standard deviation values of the number of packets, percentage of ignored and lost packets, packet delay and number of stopped processes for TF2.

BT (PDR) LEVEL	NO. OF PACKETS MEAN (STDEV)		% OF PACKETS IGNORED OR LOST MEAN (STDEV)		% OF PACKET LOST MEAN (STDEV)	PACKET DELAY (MS) MEAN (STDEV)		NO. OF STOPPED PROCESSES MEAN (STDEV)	
	TCP	UDP	TCP	UDP	UDP	TCP	UDP	TCP	UDP
BT0 PDR0	282.5 (2.5)	308.0 (0.1)	0 (0)	0 (0)	0 (0)	61 (19)	15 (5)	0 (0)	0 (0)
BT1 PDR0	271.7 (2.9)	303.5 (1.7)	0 (0)	0 (0)	0 (0)	83 (33)	22 (17)	0 (0)	0 (0)
BT2A PDR0	244.6 (7.3)	271.7 (5.4)	3.6 (1.1)	3.5 (0.7)	0 (0)	98 (43)	29 (24)	0 (0)	0 (0)
BT2B PDR0	36.8 (2.9)	39.9 (0.7)	0 (0)	0 (0)	0 (0)	629 (1078)	184 (513)	0 (0)	0 (0)
BT0 PDR5	188.0 (14.9)	273.8 (25.3)	44.5 (17.0)	6.8 (1.4)	6.8 (1.4)	63 (35)	15 (5)	2.8 (1.8)	2.9 (1.7)
BT2A PDR5	185.0 (10.9)	240.2 (43.8)	38.7 (8.0)	10.2 (1.4)	7.2 (1.9)	99 (66)	30 (36)	3.7 (1.6)	2.6 (1.3)
BT2B PDR5	30.6 (4.5)	36.1 (3.0)	13.7 (15.4)	6.4 (4.1)	6.4 (4.1)	814 (1355)	162 (413)	0.2 (0.4)	0.4 (0.7)

Table 3.VIII Power loss reductions obtained for TF2 and different load levels.

LOAD PROFILE	INITIAL POWER LOSS (KW)	POWER LOSS DECREASE (KW)			
		BT0-PDR0		BT2B-PDR 5	
		TCP	UDP	TCP	UDP
NORMAL LOAD	125.8	11.4	11.4	11.2	11.3
LOW LOAD	33.0	1.05	1.06	1.03	1.03
HIGH LOAD	300.0	43.2	43.2	40.0	42.5

Table 3.VI and Table 3.VII compare the results of the statistical analysis relevant to 30 simulations for all the scenarios already defined for TF1. The random number generators are initialized by different seed states. Both OLTCs are blocked in tap position 0.

For BT0-PDR0 case, the mean value (standard deviation) in kvar of the final reactive power outputs of the 6 compensators is: 258.2 (67.7), 154.2 (2.3), 421.1 (2.3), 272.4 (56.2), -88.6 (17.0), 132.7 (5.9). As for TS1, also for TS2 a very small value of the standard deviation of loss decreases is obtained. It indicates that analogous power flow conditions are achieved at the end of different sequence of compensations.

Table VIII compares the loss reductions obtained for normal load, low load and high load conditions by assuming BT0-PDR0 and BT0-PDR5 communication conditions with both OLTCs blocked in tap position 0.

The sequence of compensations is illustrated by Figure 3.23 and Figure 3.24 with both OLTCs blocked in tap position 0 and by Figure 3.25 and Figure 3.26 with both OLTCs in operation. For the latter case, the reference values of the secondary side voltage are: 1.01 pu for the substation transformer and 1 pu for OLTC transformer at bus 67, respectively, both with a dead band of ±0.015 pu. In the simulation relevant to Figure 3.25 and Figure 3.26, the substation transformer changes the tap to -1 position at 22 s and reaches the steady state condition. For BT1-PDR0 case with both TCP and UDP, OLTC transformer at bus 67 changes the tap to -1 at 25.6 s and then at about 35.6 s, reaching the final tap -2. For BT2-PDR5 case with UDP, this OLTC after the first tap variation at 25.6 s changes again 2 other times, reaching the steady state condition to -3 at 44.8 s. For BT2-PDR5 case with TCP, the high BT level hinders the communication between agent 0 and agent 4. Therefore, the OLTC transformer at bus 67 anticipates the first change to nearly 12 s and it reaches the steady state condition with tap -4 at time 39.1 s after 3 other changes.

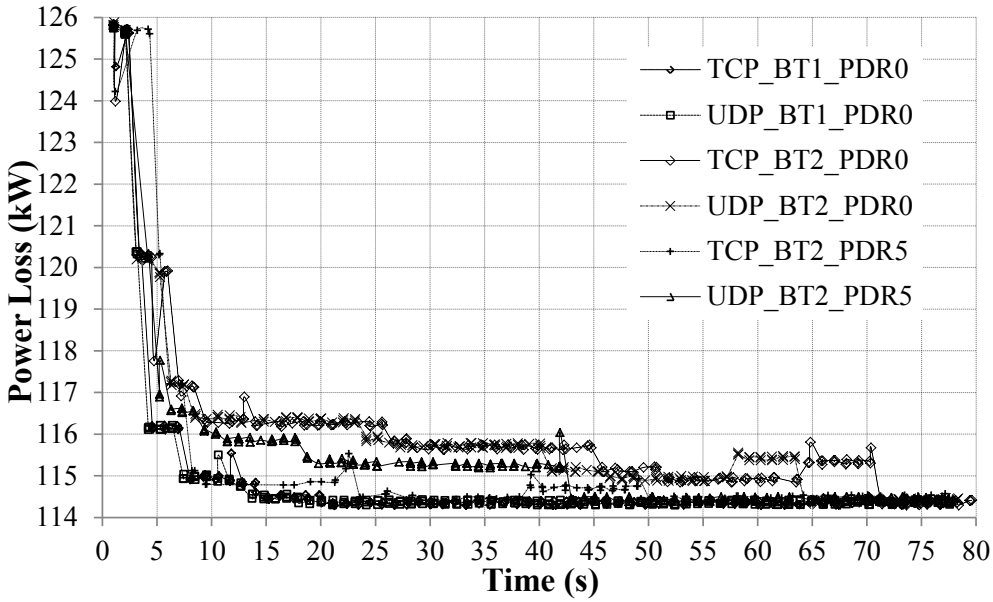

Figure 3.23 Power loss variation in TF2 with blocked OLTCs for two different BT and PDR levels by using TCP and UDP.

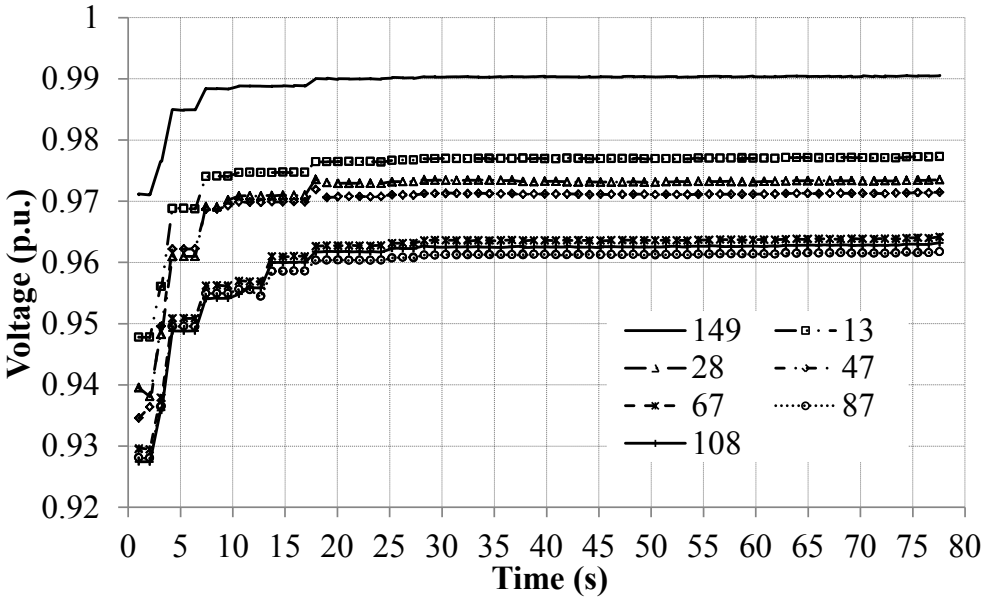

Figure 3.24 Voltage variations in TF2 with blocked OLTCs for BT2 by using UDP.

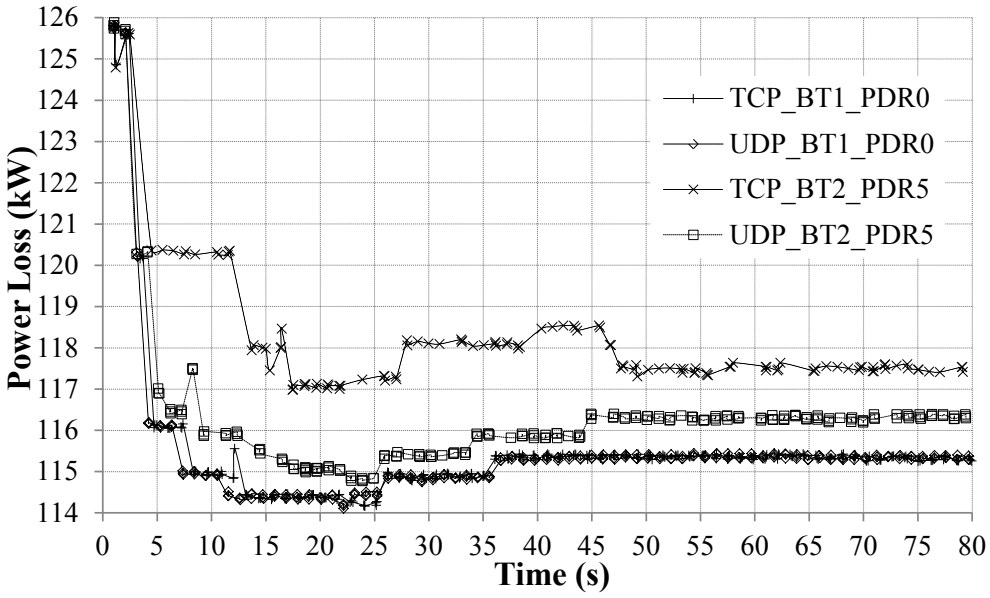

Figure 3.25 Power loss variation in TF2 with the OLTCs in operation for two different BT levels by using TCP and UDP.

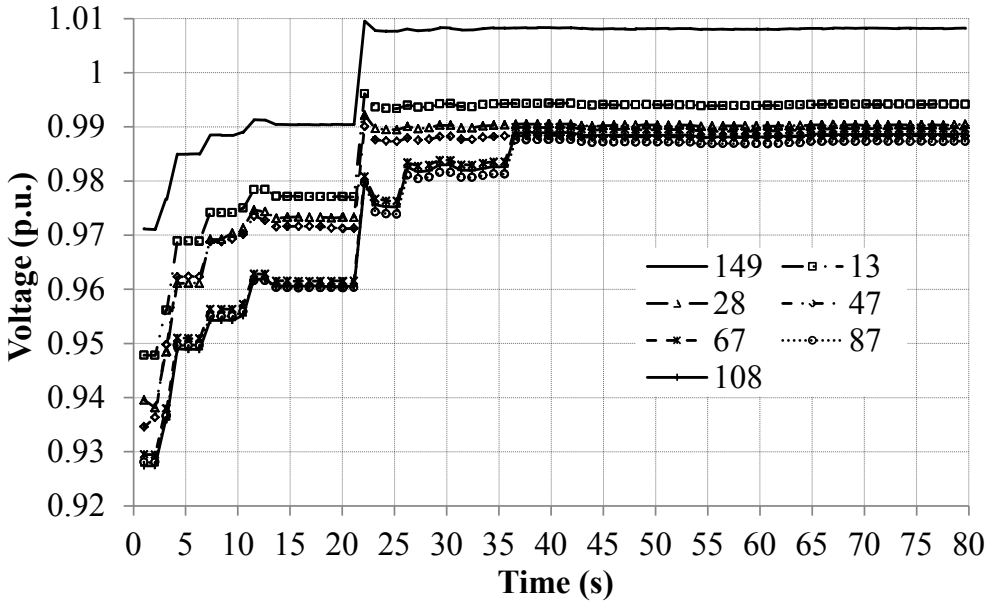

Figure 3.26 Voltage variations in TF2 with the OLTCs in operation for BT1 by using UDP.

3.5 Reactive power control of photovoltaic units over wireless UMTS cellular networks

The impact of the increasing connection of distributed generation to medium voltage (MV) distribution feeders, with particular reference to photovoltaic (PV) units, justifies the application of an adaptive control of voltages and reactive power flows.

This section describes the analysis of the voltage/var control (VVC) structure that includes the cooperative control of the reactive power regulators of the PV inverters over a third generation cellular network, namely a Universal Mobile Telecommunications System (UMTS). Also here, the control structure integrates the regulation of transformers equipped with OLTCs.

Due to the specific countermeasure already implemented against packet loss in section 3.2.2.3, the statistical analysis of the results shows the use of UDP is in general to be preferred for this application.

The high penetration of photovoltaic (PV) generation has an impact on the voltage profile along medium voltage (MV) feeders and may cause significant voltage variations during a cloud passage (e.g. [59]). Therefore the application of a voltage/var control (VVC) that exploits reactive power injection of distributed generators is justified [31]. Indeed, commercially available PV inverters have the capability to regulate their reactive power output and the usage of this capability to control the local voltage has been already described e.g. in [56],[58],[59]. Overvoltage correction may also be achieved by the curtailment on the active power output of PV units, as described in e.g. [62].

The choice of the most appropriate set-point values of the PV inverters may be determined by the solution of a global or distributed optimization problem (e.g. [61], [63]–[67] and references

therein). Moreover, various multi agent system (MAS) approaches have been proposed for the solution of the problem of interest, for example in [68], [40], [44].

Often a loss reduction could be achieved by the compensation of the reactive power flows in the feeder. This also helps in meeting the maximum current constraints in the feeder branches. In [43], [42] a gossip-like algorithm is proposed for a MAS that uses a communication network with a tree topology similar to that of the distribution feeder. In [69], [70] the gossip-like algorithm has been implemented in a ICT - power co-simulation platform in order to evaluate the effects of the limitations of a wired communication network on the performances of a MAS-based VVC and for the design of the relevant countermeasures.

In this final section of the Chapter 3 the gossip-like algorithm is applied for the case of a MAS that uses a third generation mobile cellular network, namely a Universal Mobile Telecommunications System (UMTS). The simulator implements an inverter model that takes into account the reactive limits of the PV inverters, which dynamically vary according to the variation of the real power output set point determined by the maximum power point tracking (MPPT) algorithm. The gossip-like algorithm is coordinated with the local voltage regulators of the PV inverters and of those of the transformers equipped with on-load tap changers (OLTCs).

3.5.1 Multi-agent PV inverter based voltage/var control

We envisage that the control system of the reactive power of each PV inverter, assumed to be three-phase and connected through a transformer to a MV bus of the power distribution feeder, is equipped with a UMTS communication module and with a phasor measurement unit (PMU). This PV networked control system is an agent of the MAS and it implements the gossip-like algorithm for the voltage and reactive power control of the power distribution feeder, already presented in Section 3.2.3, with some variants.

3.5.1.1 Gossip-Like VVC algorithm adapted for the PV units

At each control time step, the algorithm operates so that two PV units connected to different nodes of the power distribution systems change their reactive power outputs in coordinate way in order to compensate the reactive power flow between them, i.e. each agent tries to supply the reactive power needed by the nearby loads.

More in detail, at each control step, a couple of agents, each controlling a different PV inverter, is activated (by the previous active couple of agents). The two agents exchange the information relevant to their bus voltage phasor provided by the PMUs, evaluate the mean reactive power flow between them and change the reactive power output of their inverters in order to create a reactive power counterflow of the same magnitude. Then, after a time delay equal to twait, allowing the system to reach a new steady state condition (e.g.: equal to 1 s in the simulations) a different couple of agents is activated by the previous one.

In this scheme the successive compensation is expected to decrease branch currents and therefore both power network losses and voltage drops.

The basic steps of the gossip-like algorithm implemented in the ICT-power simulator are listed in [69]. The algorithm adopted for this case is characterized by the following specific aspects.

- Since each agent is a neighbor of all the others in the cellular network due to its star-topology, we apply the Kron's reduction technique to the power feeder in order to obtain a reduced equivalent, the nodes of which are the substation bus and the N busses at which the inverters are connected. Then, the impedance of the branch between two nodes, e.g., *h* and *k*, of the reduced network is used by the two agents, which control the PV inverters connected to node *h* and node *k* respectively, for the estimation of reactive power flow $\overline{Q_{hk}}$. Since the inductive characteristics of the feeder branches, the agents estimate the reactive power flows from *h* and *k* at both end of the branch Q'_{hk} and Q''_{hk}. If these values have different signs, $\overline{Q_{hk}} = 0$ otherwise

$$\overline{Q_{hk}} = \min(|Q'_{hk}|, |Q''_{hk}|) \cdot \mathrm{sgn}(Q'_{hk}) \tag{3.22}$$

- The countermeasure against communication latency is based on the availability of a memory buffer at each controller that stores the PMU data with the relevant time tag t_{meas}, so that reactive power flow values are calculated by using synchronous values of voltage phasors. Moreover, a maximum communication round-trip delay t_{wait} is defined, after which the procedure carries on with the choice of a new active controller.

- Since we assume that each converter *i* is the inverter of a PV plant connected to the MV feeder, the values of $Q_{max,i}$ and $Q_{min,i}$ are dynamically updated on the basis of the active power value P_i determined by the MPPT algorithm (Figure 3.27), so that both maximum inverter current $I_{max,i}$ and voltage $V_{max,i}$ limitations are met (e.g. [64], [71]):

$$\begin{aligned} Q_{\max,i}, Q_{\min,i} &= \pm\sqrt{\left(|V_i| I_{\max,i}\right)^2 - P_i^2} \\ Q_{\max,i} &= \sqrt{\left(\frac{|V_i| V_{\max,i}}{X_i}\right)^2 - P_i^2} - \frac{|V_i|^2}{X_i} \end{aligned} \tag{3.23}$$

where X_i represents the total reactance of the transformer and grid filters used for the connection of inverter i to the feeder.

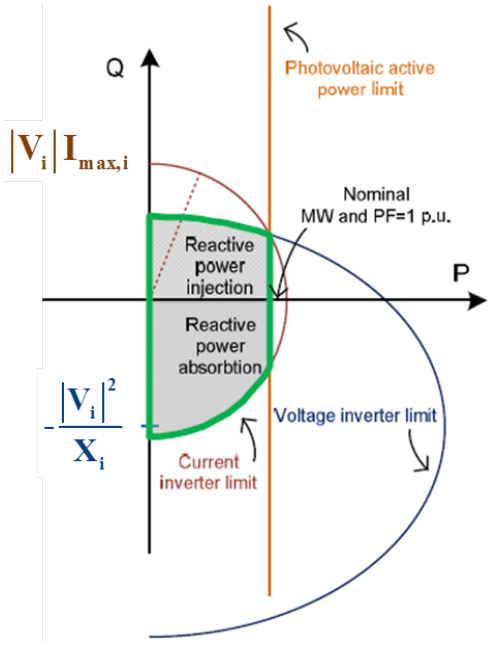

Figure 3.27 Active power value Pi determined by the MPPT algorithm [71]

- Each agent knows the communication addresses of all the other agents. After the var compensation, agent *h* randomly choses the next following couple of agents to be activated, by avoiding if possible, those controllers recently involved in the procedure. As a countermeasure against the complete failure of a critical communication links, a spontaneous activation is allowed after a predefined long time (e.g., several minutes) in which a controller is never activated.

- In order to guarantee the persistence of the procedure also in the presence of packet losses, the algorithm includes the possibility of concurrent multiple var compensation processes. In order to limit the possible negative effects of unwanted and unsynchronized multiple compensation process, such a possibility is limited by the association of an increasing priority index to each process. Concurrent compensation processes with priority indexes lower than the others are progressively stopped by the controllers.

Also in the PV inverters control systems the local voltage control function, explained in Section 3.3.2.3, is implemented with $Q_{min/max}$ of the equation (3.21) set as the size limit of the PV inverters.

3.5.2 Wireless cellular based ICT – Power System co-simulation platform

The architecture of the specifically developed ICT-power co-simulation platform has been described in [21], [69], [70]. It is based on the interface between the event-driven communication simulator Riverbed Modeler (formerly OPNET Modeler) and the time-driven power system simulation environment EMTP-rv. The synchronization mechanism between the two simulators is based on the typical waiting order of a communication through the use of the socket application programming interfaces (APIs). Simulation interval Δt is defined by the integration time-step

adopted in EMTP-rv (for this chapter Δt = 1 ms). As Δt is very small with respect to the analyzed transients, it is negligible the inaccuracy due the time shift of all Riverbed events that happen within a Δt interval to the end of the same interval.

3.5.2.1 UMTS network model

The Riverbed model represents the three basic components of the UMTS network (see Figure 3.28 and Figure 3.29): the user equipment (UE), i.e. the UMTS module of each agent, the UMTS Terrestrial Radio Access Network (UTRAN) and the Core Network (CN). UTRAN includes the Node B and the Radio Network Controller (RNC), which manages the Node B logical resources and also the UE-Node B interface resources. Each Node B controls the radio transmission and reception of a cell and performs the packet relay between UE and the corresponding RNC. CN contains the serving GPRS support node (SGSN) and the gateway GPRS support node (GGSN). SGSN maintains access controls, security functions and also keeps track of UE locations. The GGSN encapsulates the packets and routes them to the SGSN that are received from the external network or Internet.

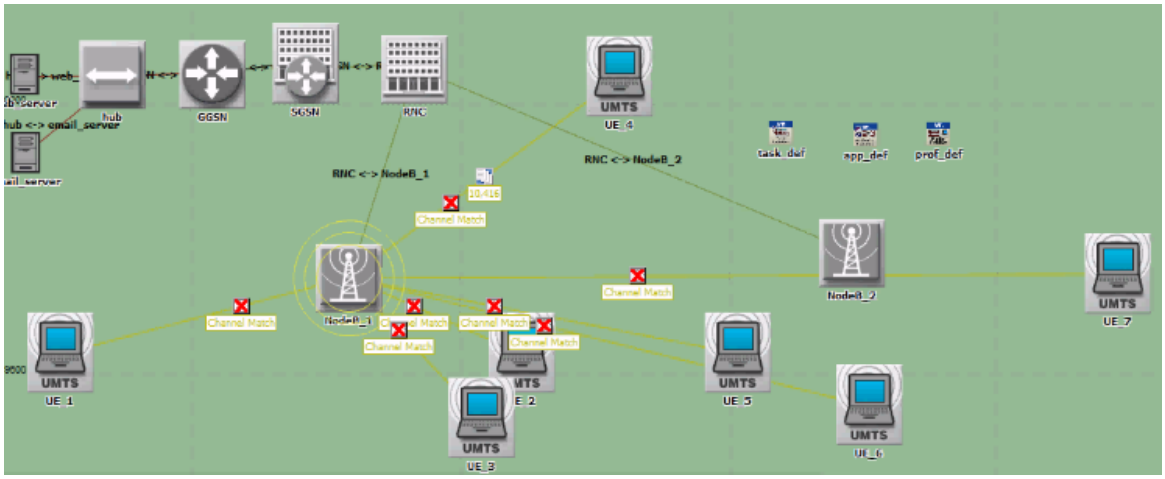

Figure 3.28 Screenshot during the simulation in debugging mode of the correspondent UMTS communication model of the IEEE 37 Node Test feeder

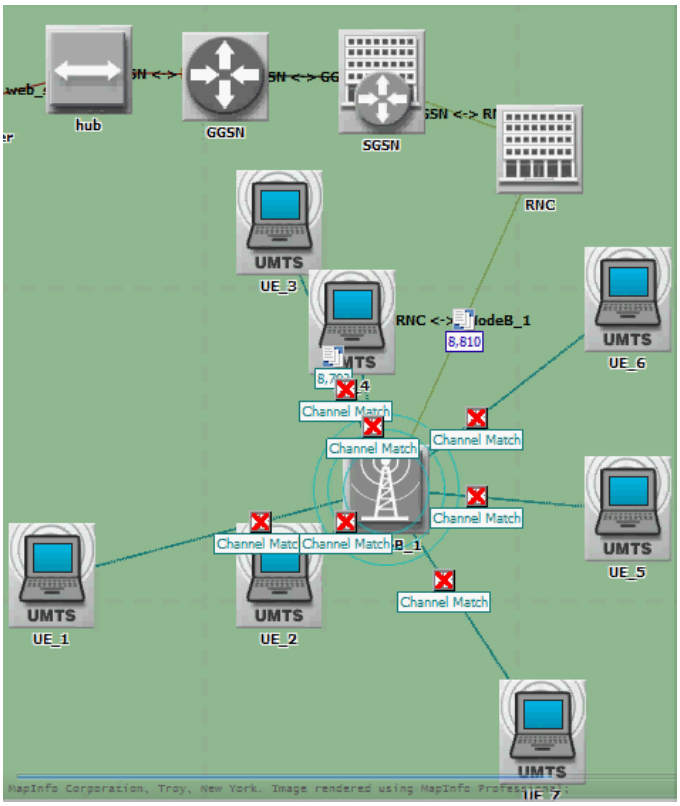

Figure 3.29 Screenshot during the simulation in debugging mode of the correspondent UMTS communication model of the IEEE 123 Node Test feeder

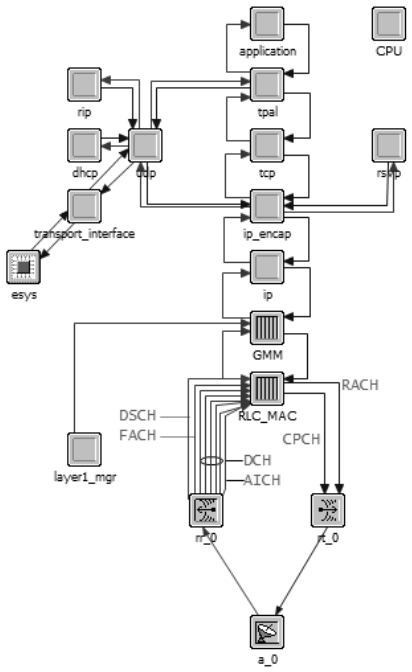

Figure 3.30 Extended UDP node model of UMTS UE.

Figure 3.30 shows the model of the UMTS UE. The GMM module (GPRS mobility/session management) manages GPRS attachment, PDP context establishment, service requests, and radio access bearer (RAB) activation and it handles the interface with the IP stack. The RLC_MAC module performs RLC and media access control (MAC) functionalities, both in UEs and router

control planes. The node model is extended by an external system (Esys) module that enables the Riverbed interface with the EMTP simulation environment as described in [21], [69], [70].

The air interface between each UE and the Node B is based on Wideband Code Division Multiple Access (W-CDMA) access scheme and uses a direct spread with a chip rate of 3.84 MHz and nominal bandwidth of 5 MHz. The model supports FDD (frequency division duplexing) duplex mode. The radio frame has a length of 10 ms and it is divided into 15 slots. Spreading factors vary from 256 to 4 for uplink and from 512 to 4 for downlink, which allow data rates of up to 2 Mbps. The model accounts for the block error rate (BLER) that is the percentage of transport blocks with errors over the total number of transport blocks. The communication channels between each Node B and RNC (and CN) are assumed wired with large data rate.

The Riverbed model supports four main types of quality of service (QoS) classes: background, interactive, streaming and conversational. These QoS attributes define the grade of service requested by the user. These attributes include the traffic class, maximum and guaranteed bit rates, delivery order, transfer delay, maximum size of the service data unit (SDU) and SDU error ratio [72]. The UE radio link control (RLC) interface could operate in either unacknowledged mode (UM) or acknowledged mode (AM). Retransmission decreases the effects of the BLER but increases the communication delay. In the simulations, the gossip-like procedure uses the interactive QoS class communication and operates in Acknowledge Mode (AM). The uplink and downlink dedicated signaling channels (DCHs) scheduling is adopted with the maximum bit rate of 64 kbps (as a default value for the interactive QoS traffic class).

In order to test the robustness of the gossip-like procedure with respect to delays generated in the communication network, some simulations includes a background traffic (BT), due to the presence of additional UEs, other than those associated with the agents. These new UEs and also the agents, generate the BT by using some default mobile user traffic profiles defined by Riverbed Modeler according to the 3GPP technical report TR 36.822 [73]. The analysis of the scheduling effects of the QoS for UMTS network is out of the scope of this thesis. For this reason also the mobile user traffic has been considered with the interactive QoS.

3.5.3 Power distribution feeder model

As described in [69],[70], the EMTP-rv model of the MV power feeder is mainly composed by the three-phase constant-parameters PI models for the representation of the unbalanced lines, the models of three-phase transformer with OLTCs (adapted from [54]), the models of the unbalanced voltage-dependent loads (constant impedance, constant current and constant active and reactive power) and the HV network is represented by an ideal positive sequence constant voltage generator. The accuracy of PMUs is represented by the Normal distribution of the measurement errors of the PMU prototype for MV systems described in [50].

Moreover, the model includes PV units, represented by components able to inject assigned and adjustable three-phase active and reactive powers. As a first approximation of the quasi-steady-state behavior of power electronic interfaced sources, the PV model is composed by two

positive-sequence triplets of current generators. The amplitude of one triplet is controlled by a feed-back regulator in order to inject the requested value of three-phase active power, whilst the phase angle between the injected current and bus voltage is regulated so to achieve a zero value of reactive power. The regulators of the second triplets have a reverse function, i.e. amplitude is controlled in order to inject the requested reactive power and phase angle is controlled in order to cancel out active injection. Reference value Q_i of the reactive power injection is dynamically changed by the associated networked controller and by the local voltage regulator taking into account the variable Q_{max} and Q_{min} limits, as described in Section 3.3.2.3. A smooth transition between different power levels in a short time window of few hundreds of milliseconds is represented.

3.5.4 Simulation results

Here is it presented the numerical results obtained for two test cases illustrated in Figure 3.31 (indicated as TF 1) and Figure 3.32 (TF2).

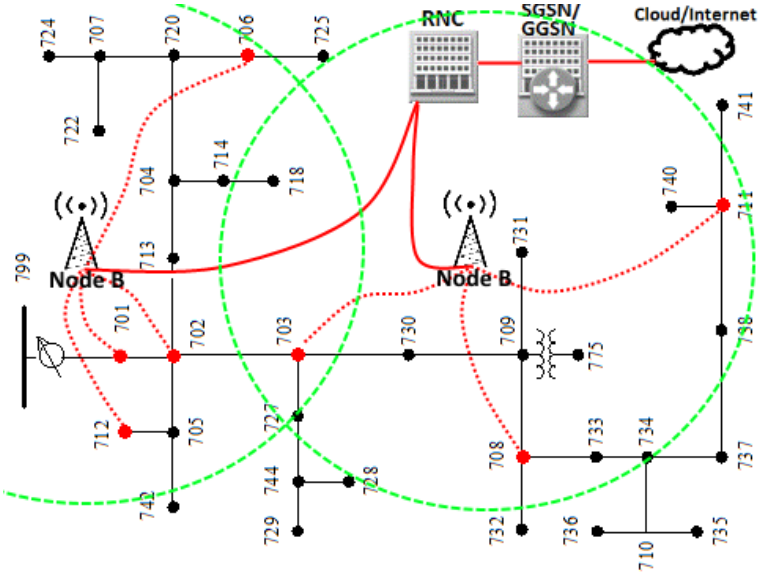

Figure 3.31 TF1: one-line diagram of power feeder (in black) and UMTS communication network (dotted red lines represent wireless channels, solid red lines represent wired channels). The dots represent 7 networked controllers (agents). The green circles indicate the estimated coverage areas of the Node B antennas.

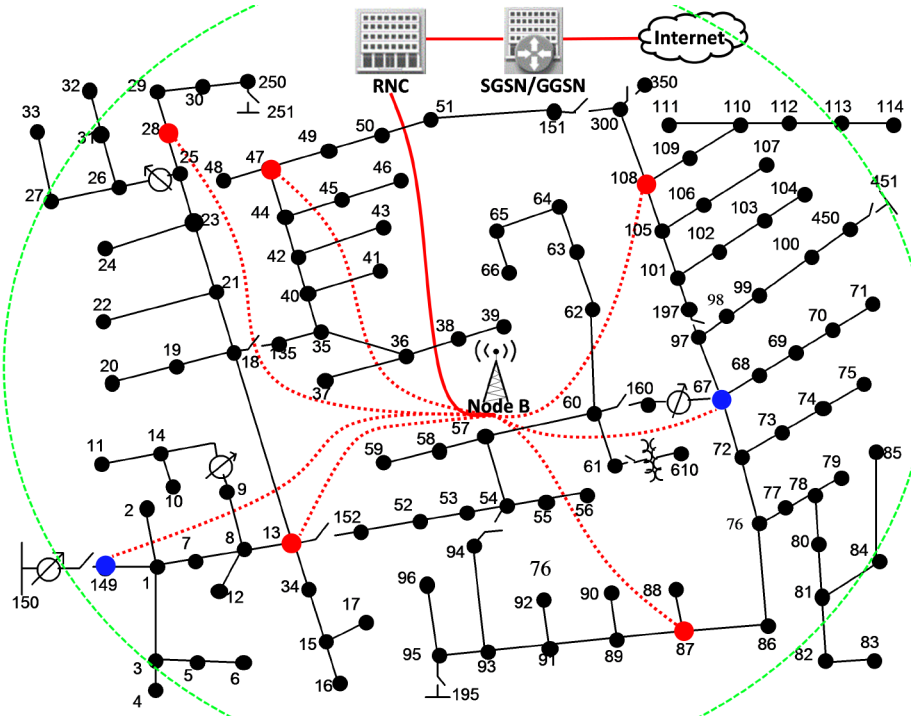

Figure 3.32 TF2: one-line diagram of power feeder, UMTS communication network and location of the agents.

TF1: IEEE 37-node Test Feeder [46] with 6 PV units (each equipped with a three-phase 500 kVA inverter) connected to nodes 702, 712, 706, 703, 708 and 711, respectively (red dots in Figure 3.31), and with an OLTC transformer at the substation (the secondary side node is 701 indicated with a blue dot). Two Node-Bs are needed to guarantee the coverage (the two cells include the UEs at nodes 701, 702, 712 and 706,703,708,711, respectively).

TF2: IEEE 123-node Test Feeder, with 5 PV units (each equipped with a three-phase 500 kVA inverter) connected to nodes 13, 28, 47, 87, and 108, respectively, and with two OLTC transformers (the secondary side are nodes 149 and 67). The two independent sets of agents are those relevant to nodes {149,13,28,47} and {67,87,108}, respectively.

The procedure has been applied to a constant normal load condition (as defined in [46]) and to a higher load level. For illustrative purposes, the high load condition has been obtained by multiplying both the active and reactive power normal values at each load node by a different coefficient (obtained as a uniformly-generated random number between 1.3 and 1.7). All the PV output is constant and equal to 400 kW and the initial reactive outputs are null. The OLTCs start in tap position 0.

The simulations are repeated for two different BLER values: $1E^{-5}$ (indicated as BLER0) and 0.1 (BLER1), which is a typical reference performance value (e.g. [74]).

Moreover the simulations are repeated with BT (case indicated as BT1) and without the BT (BT0). In order to obtain a significant value of the BT the UEs associated to the agents and 6 additional UEs are forced to generate the BT towards 2 additional UEs receivers belonging to the same RNC subnetwork. As it can be seen from Figure 3.33 and Figure 3.34, BT is generated by

the UEs associated to the agents (UE_1, …, UE_7) and by 6 additional UEs (UE_traffic_1, …, UE_traffic_6) and two traffic receivers (UE_RX1 and UE_RX2). The respective two adopted mobile users application models are characterized by a gamma distribution of the inter-arrival packet time (with parameters 0.0068, 5 s and 0.2, 0.5 s, respectively) and by an exponential distribution of packet size (with parameters 41.03 bytes and 62.97 bytes, respectively).

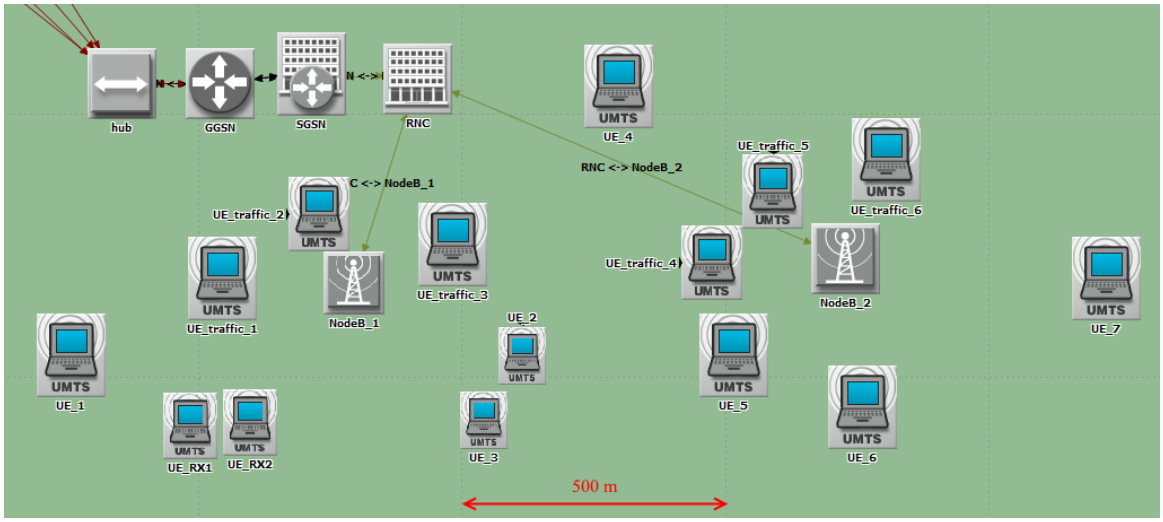

Figure 3.33 UMTS communication network of the IEEE 37 node test feeder with UEs that send "Mobile User traffic model" to the Interactive Content Receiver and the Gaming app Receiver

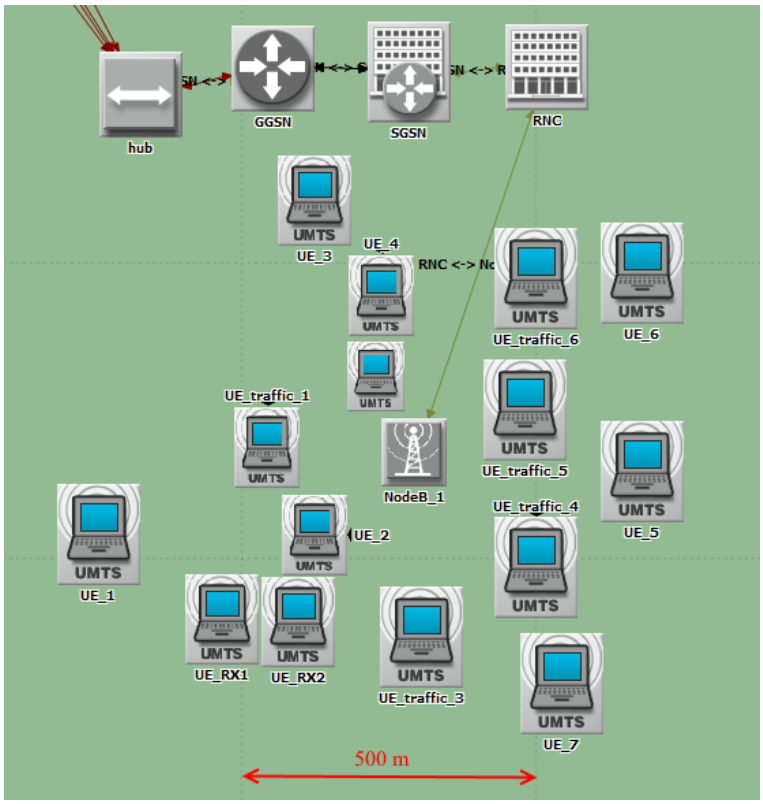

Figure 3.34 UMTS communication network of the IEEE 123 node test feeder with UEs that send "Mobile User traffic model" to the Interactive Content Receiver and the Gaming app Receiver

Table 3.IX number of compensation cycles, power loss decrease and settling time for tf1 and tf2

BLER BT (LOAD LEVEL)	NO OF COMPENSATION CYCLES MEAN (STDEV)		% OF INCOMPLETE COMPENSATIONS MEAN (STDEV)		POWER LOSS DECREASE (KW) MEAN (STDEV)		SETTLING TIME (S) MEAN (STDEV)	
	TF1	TF2	TF1	TF2	TF1	TF2	TF1	TF2
BLER0 BT0 (NORMAL)	154	154	0	0	15.8 (0.1)	5.5 (0.1)	62.4 (12.6)	31.5 (6.9)
BLER1 BT0 (NORMAL)	117.5 (32.5)	117.2 (24.2)	15.5 (3.2)	16.6 (4.0)	15.3 (1.4)	5.5 (0.1)	63.0 (17.0)	40.4 (11.8)
BLER0 BT1 (NORMAL)	119.5 (19.5)	122.9 (14.2)	16.0 (4.3)	11.6 (2.3)	15.3 (1.2)	5.4 (0.2)	71.0 (20.8)	43.6 (15.9)
BLER1 BT1 (NORMAL)	102.0 (18.9)	107.0 (15.1)	29.9 (5.0)	26.6 (5.4)	15.5 (0.9)	5.4 (0.5)	77.5 (20.3)	42.6 (18.0)
BLER0 BT0 (HIGH)	154	154	0	0	25.6 (0.05)	19.4 (0.5)	78.3 (11.5)	93.9 (36.4)
BLER1 BT0 (HIGH)	129.3 (12.6)	115.9 (30.7)	17.6 (3.3)	16.3 (2.8)	25.5 (0.9)	18.0 (3.4)	102.2 (29.8)	91.2 (27.0)
BLER0 BT1 (HIGH)	119.9 (18.8)	121.0 (23.1)	16.4 (3.9)	11.0 (3.3)	25.0 (2.3)	18.5 (3.3)	87.7 (16.3)	79.2 (17.5)
BLER1 BT1 (HIGH)	101.4 (22.3)	108.3 (11.2)	32.4 (7.2)	25.6 (4.9)	24.3 (3.8)	17.9 (1.4)	105.2 (39.2)	122.2 (21.2)

Table 3.X number of packets, packet delay and number of stopped process for tf1 and tf2

BLER BT (LOAD LEVEL)	NO. OF PACKETS MEAN (STDEV) TX MEAN (STDEV) RX		% OF PACKETS IGNORED MEAN (STDEV)		% OF PACKET LOST MEAN (STDEV)		PACKET DELAY (MS) MEAN (STDEV)		NO. OF STOPPED PROCESSES MEAN (STDEV)	
	TF1	TF2	TF1	TF2	TF1	TF2	TF1	TF2	TF1	TF2
BLER0 BT0 (NORMAL)	618.2(1.3)	618.8(1.4)	0	0	0	0	145.2 (10.2)	145.0 (10.1)	0	0
BLER1 BT0 (NORMAL)	542.6(125.8) 447.3(104.8)	526.5(104.4) 434.6(87.0)	5.5 (1.2)	6.0 (1.0)	11.9 (5.7)	11.5 (1.5)	147.2 (32.7)	146.2 (29.6)	11.1 (3.4)	11.1 (3.6)
BLER0 BT1 (NORMAL)	528.2(77.5) 443.9(68.7)	551.7(52.7) 478.2(50.6)	7.6 (1.3)	6.3 (1.1)	8.5 (1.3)	7.2 (1.0)	212.0 (154.1)	239.3 (173.5)	7.0 (2.6)	7.4 (2.7)
BLER1 BT1 (NORMAL)	527(91.0) 371.6(62.6)	510.1(68.7) 378.4(55.3)	13.0 (1.4)	12.2 (1.8)	16.2 (4.2)	13.8 (1.7)	244.6 (197.8)	259.0 (202.3)	13.0 (5.3)	9.6 (3.0)
BLER0 BT0 (HIGH)	618.5(1.3)	618.4(1.5)	0	0	0	0	145.1 (10.1)	145.4 (10.4)	0	0
BLER1 BT0 (HIGH)	569.9(56.6) 474.5(30.5)	520.0(139.1) 433.1(116.1)	5.3 (0.7)	5.7 (1.0)	11.5 (1.7)	10.9 (1.3)	146.2 (26.4)	147.0 (31.3)	11.5 (3.4)	11.5 (4.0)
BLER0 BT1 (HIGH)	548.6(49.1) 457.3(43.4)	543.5(102.9) 472.6(92.0)	7.2 (1.3)	6.1 (1.3)	9.3 (5.8)	7.3 (1.3)	213.0 (157.0)	239.0 (173.6)	6.9 (2.9)	7.9 (2.8)
BLER1 BT1 (HIGH)	488.7(104.7) 347.5(75.	524.2(37.3) 389.6(36.5)	13.4 (2.3)	12.0 (1.4)	15.3 (1.9)	13.8 (1.9)	244.5 (195.7)	260.3 (205.3)	10.5 (4.0)	12.0 (3.7)

Table 3.X and Table 3.XI compare the results obtained for the 8 scenarios characterized by different values of BLER, BT and load levels. The tables report the results of the statistical analysis carried out by performing 20 simulations for the same case. For each simulation, the pseudorandom number generator used for the choice of the active agents is initialized by a different seed state associated with the computer system time.

In Table 3.X, the number of var compensation cycles is the number of compensation between a couple of networked controllers in which at least one PV inverter changes its reactive power

output and the percentage of incomplete compensations indicates the percentage of cycles that do not complete regularly; the power loss decrease is the difference between power losses at the starting time and at t_{set} (time for the power loss value to enter and remain within a 500 W band for at least 30 s). In Table 3.X, the number of packets takes into account only those packets carrying data relevant to the gossip algorithm; the percentage of ignored or lost packets refers to those that arrive at destination after twait or do not arrive at all; packets delay indicates the travelling time of the packets that regularly arrive at destination before t_{wait}; the number of stopped process counts the stops of concurrent processes due to the priority index.

The final values of the bus voltages at the PV buses are significantly improved with respect to the initial condition (e.g., for TF1 in case BLER0, BT0 and normal load the maximum deviation form 1 pu is equal to 1.1%). For BLER1, the number of compensation cycles reduces and the higher BLER causes both the interruption of incomplete processes and the start of concurrent processes (progressively stopped on the basis of their priority index) due to the loss of packets that carries critical information. Also for BT1, the additional transmissions cause a reduction of the number of compensation cycles and at the same time the increasing of the packets delay.

This is illustrated from Figure 3.35 to Figure 3.37. As an example, Figure 3.35 compares the power loss time evolution for TF1 with normal load with different BLER and BT conditions. For the BLER0 – BT0 and BLER0 – BT1, the OLTC operates a first tap change at 22 s and reaches a final tap equal to -1. The effects on the bus voltages due to the tap changes and to the reactive power compensations are shown in Figure 3.37. With BLER1 – BT0, the OLTC operates a first tap change to -1 at 22 s, a second tap change to -2 at 32 s and reaches a final tap equal to -1 at 62 s. With BLER1 – BT1, the OLTC operates a first tap change to -1 at 22 s, a second tap change to -2 at 33 s and reaches a final tap equal to -1 at 65 s. The increase of the power losses after each tap change is due to the increased consumption of voltage dependent loads. Thanks to the countermeasures described in Section 3.2.2.3, the final results with BLER1 and BT1 are similar to those relevant to BLER0 and BT1.

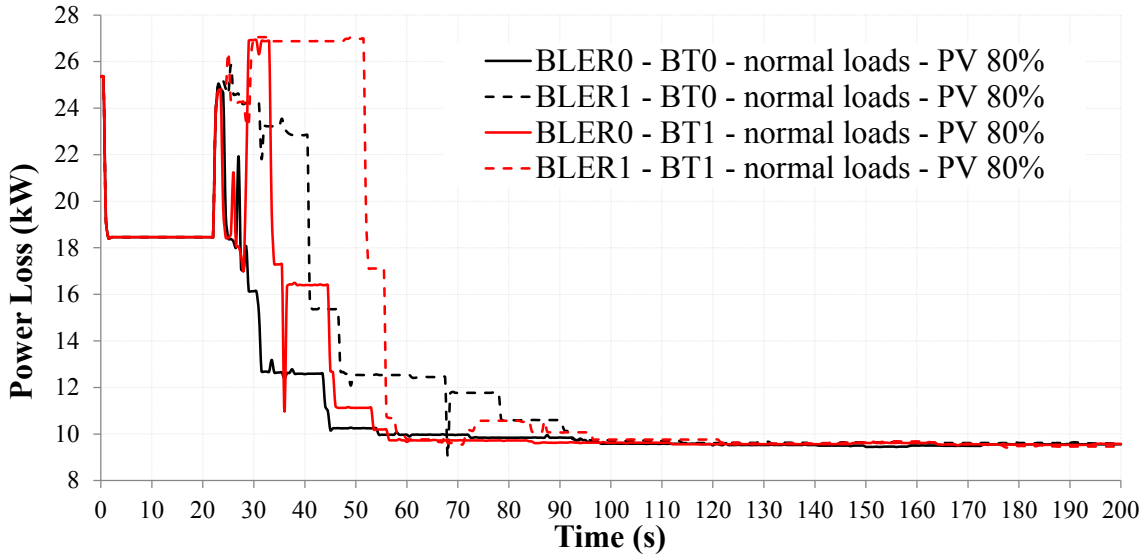

Figure 3.35 Power loss variation in TF1 for different BT and BLER levels

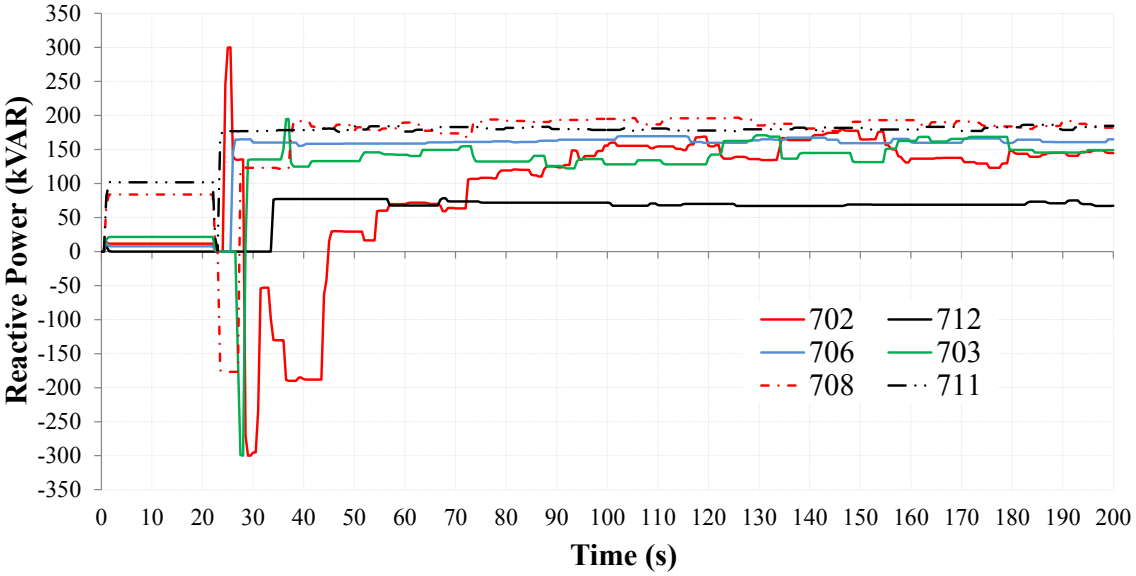

Figure 3.36 Variations of reactive power outputs of the PV inverters of TF1 for BLER0, BT0 and normal load levels

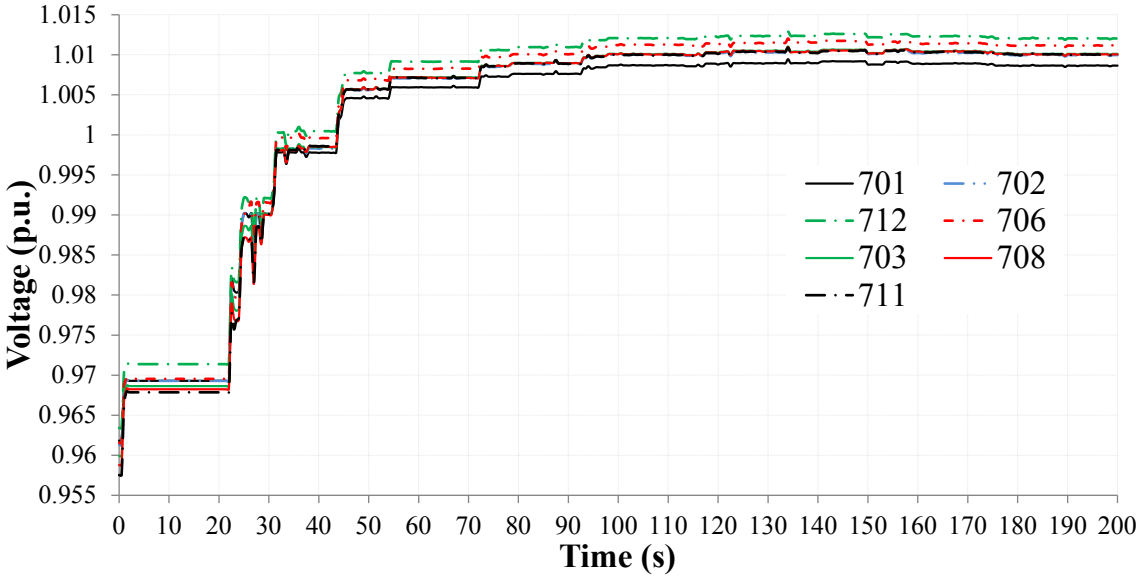

Figure 3.37 Voltage variations of the PV inverters of TF1 for BLER0, BT0 and normal load levels.

Chapter 4
INTEGRATION OF TRAFFIC AND GRID SIMULATOR FOR THE ANALYSIS OF E-MOBILITY IMPACT ON POWER DISTRIBUTION NETWORKS

4.1 Motivation and aim of the research

This chapter presents the development of a co-simulation platform composed by the open source framework for vehicular traffic simulations VeinS [75], adapted to represent the main characteristics of electric vehicles (EVs) and their charging requests and a power distribution network model implemented in the EMTP-rv (Electromagnetic transient program) simulation environment [76], which includes the aggregate representation of clusters of electric vehicles supply equipment (EVSE) units. Moreover the platform is interfaced with the communication network simulator Riverbed modeler (formerly called Opnet) [22], as described in [69] and [70]. A Semantic Information Broker (SIB) is introduced to allow information storing and sharing among the different actors [77].

The platform is useful to assess the effects of the transients caused by the concurrent charging of a large number of electric vehicles to the operating conditions of the MV network. Moreover, the platform is used to develop and test the performance of specific countermeasures against overload of power components, voltage variations and unbalances.

Several studies have been recently presented in the literature that analyze the foreseen impact of plug-in electrical vehicle charging on the electric power network, and present different approaches in order to limit the negative effects and optimize the operating conditions of the system (e.g. [78]–[87] and references therein). In this chapter we focus on parking lots that include fast public charging stations with power rating assumed equal to 50 kW. The EVSE units of each parking lot are fed through a MV/LV transformer. Following the hierarchical aggregation approach adopted in e.g. [81]–[83], we analyze a multi-agent system that is composed by the intelligent electronic devices (IEDs) installed at the HV/MV substation and in correspondence of critical branches of the network that may be overloaded due to EVs charging and by distributed agents, i.e. control units connected to the shared communication network, each associated to the cluster of EVSE units of a parking lot. The implemented distributed control algorithm allows the

congestion management of the network whilst a local regulation function of the agents reduces the charging effects on voltage variations. Each agent communicates also with each single EVSE of the cluster in order to allocate the maximum power that could be absorbed from the MV network among the various charging EVs taking into account their specific characteristics and requirements. In this chapter we assume that the multi-agent system (MAS) uses a third generation mobile cellular network, namely a Universal Mobile Telecommunication System (UMTS).

This framework has been developed through a collaboration with the research group of the Professor Luciano Bononi from the department of Computer Science and Professor Tullio Salmon Cinotti from the Advanced Research Center on Electronic Systems for Information and Communication Technologies (ARCES), of the University of Bologna.

The structure of the Chapter 4 is the following. Section 4.2 describes the architecture of the co-simulation platform and its components, namely the traffic simulator and the power system simulator integrated through a semantic middleware. Moreover the Section presents the main characteristics of the UMTS model adopted in this study. Section 4.3 describes the multi-agent system implemented in the simulator for the control of the EV charging stations. Section 4.4 presents extensive simulation results. Section 4.5 concludes the chapter.

4.2 Architecture of the co-simulation platform

As mentioned in the Section 4.1, the co-simulation platform integrates the traffic simulator, the power distribution simulator and the communication network simulator. The three simulation environments are described in the following subsections. Figure 4.1 illustrates the exchange of the data between the two environments, which is realized leveraging the semantic capabilities of the SIB, as described in Figure 4.2. Integration is carried out on 2 levels: time and data. Time integration is realized through a Web Server (WS) built in Python, with the role of a semaphore which regulates the synchronization of the simulation flow. Data integration is obtained using the SIB, a semantic middleware originated by the European Project SOFIA and improved during the subsequent project related to electric mobility Internet of Energy (IOE) [88]. The SIB stores shared data coming from the two simulation sides in an interoperable format, allowing a bidirectional information flow. The semantic format used for the data representation is regulated by an ontology developed in the context of the IOE project, and has been chosen because it allows future extensions in an incremental way [89],[90].

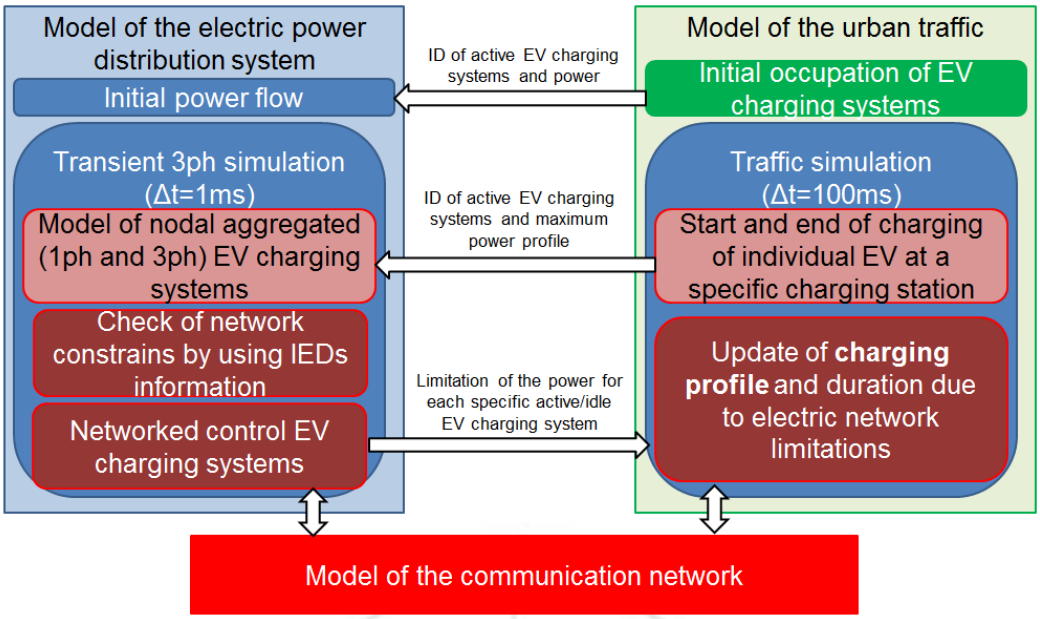

Figure 4.1 Data exchange between the traffic simulator, the power distribution simulator and communication network simulator.

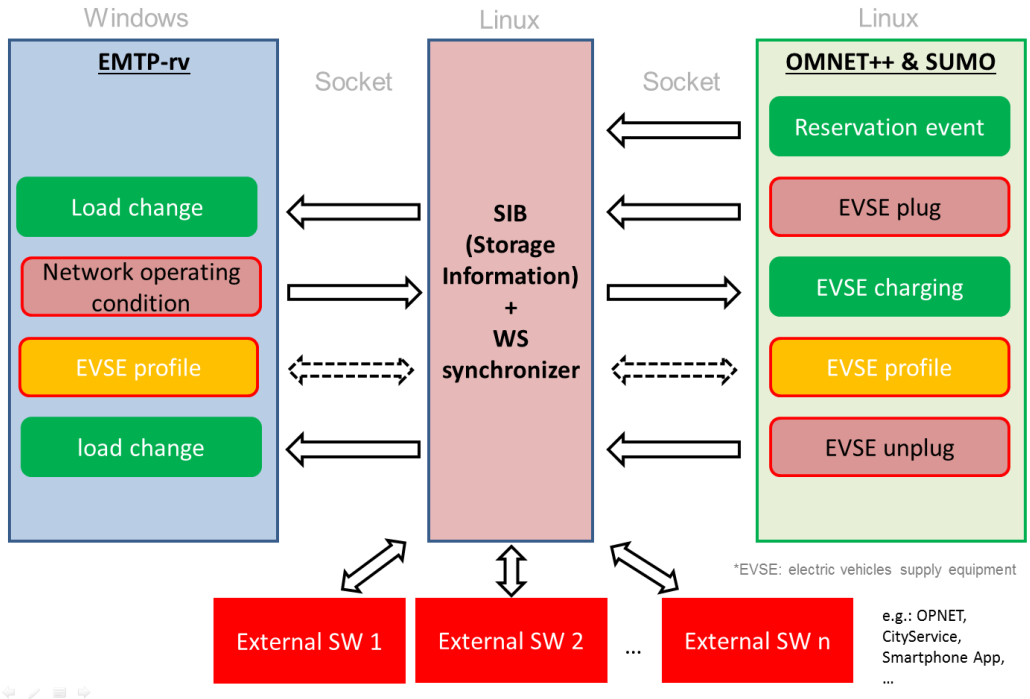

Figure 4.2 Use of the SIB for the exchange of information and the WS for platform synchronization.

4.2.1 Traffic simulator

The urban traffic is modelled using VeinS, which is an open source framework for vehicular network simulations based on two simulators: OMNeT++, a discrete event-based simulator, and SUMO, a road traffic simulator. It has been extended with the models of EVs and EVSE units (including the management of the EVs queues) and it has been integrated with the battery charging/discharging models described in [91]. For our analysis, we considered a large-scale

scenario (i.e. the downtown of Bologna), with a realistic street map (imported from the OpenStreetMap project).

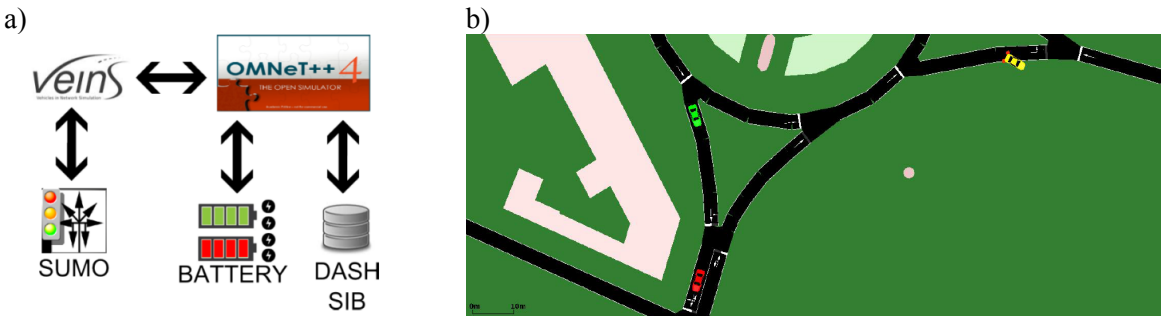

Figure 4.3 a) mobility simulator framework b) example of SUMO environment with correspondent electric vehicle (green), electric vehicle in charging (yellow) and fuel vehicle (red).

4.2.2 Power distribution system simulator

The Power distribution system simulator is based on the Electromagnetic Transient Program EMTP-rv. It is a time domain simulator, in which we have adopted a time step of Δt=1 ms in all the simulations. The model of the distribution feeders include the model of the three-phase unbalanced lines, three-phase HV/MV substation transformers equipped with an on-load tap changer (OLTC), and the models of the aggregated unbalanced loads (constant impedance / current / power) that includes the EVSE units.

The model of the aggregate EVSE (Figure 4.4) is an expanded model of the reactive power compensator represented in Section 3.3.2.2 (Figure 3.11). It is based on the control of a triplet of current sources, which is controlled by a feed-back regulator in order to inject or absorb the requested per-phase values of active and reactive power as described in [69],[70]. Each aggregate load is connected at the secondary side of a MV/LV transformer.

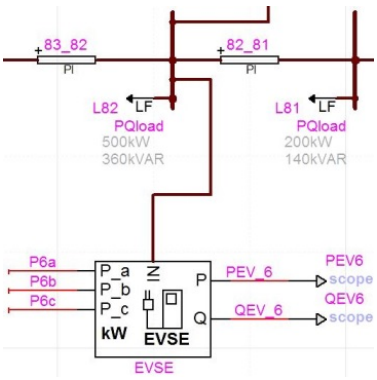

Figure 4.4 EMTP model of the aggregate EVSE

The EMTP model includes a DLL (Dynamic Link Library)-based interface that allows the communication with the SIB.

4.2.3 Communication network simulator

The simulator of the UMTS communication network is based on the OPNET-Riverbed Modeler Wireless suite v18.0 [3]. As can be seen from Figure 4.5, the Riverbed model represents the basic components of the UMTS network: the user equipment (UE), i.e. the UMTS module of each agent, the Node B, the Radio Network Controller (RNC), which manages the Node B logical resources and also the UE-Node B interface resources. The Serving GPRS support node (SGSN) maintains access controls, security functions and also keeps track of UE locations. Gateway GPRS support node (GGSN) encapsulates the packets and routes them to the SGSN that are received from the external network or Internet. The communication channels between each Node B and RNC are assumed wired with large data rate.

The implemented model accounts for a block error rate (BLER) i.e. the percentage of transport blocks with errors over the total number of transport blocks. The Riverbed software supports the UMTS four main types of quality of service (QoS): background, interactive, streaming and conversational. These types of QoS are characterized by the traffic class, maximum and guaranteed bit rates, delivery order, transfer delay, maximum size of the service data unit (SDU) and SDU error ratio. The UE radio link control (RLC) interface could operate in either unacknowledged mode (UM) or acknowledged mode (AM), which includes retransmissions that decrease the effects of the BLER but increase the communication delay.

In the simulations of this chapter, the information exchanged uses the interactive QoS class communication that has higher priority than background QoS although, as background, it does not guarantee a bit rate. We have chosen to operate in Acknowledge Mode (AM).

In order to test the robustness of the control procedure against delays in the communication network, some simulations includes a background traffic (BT) created by adding additional UEs, other than those associated with the agents. These new UEs and also the agents, generate the BT by using some default mobile user traffic profiles defined by Riverbed Modeler according to the 3GPP technical report TR 36.822. Since the analysis of the scheduling effects of the chosen QoS is out of the scope of this thesis, also the BT is assumed to use the interactive QoS.

4.3 Multi agent system for the distributed control of charging stations

As mentioned in the Introduction, we assume to associate an agent to each MV/LV transformer that feeds a cluster of EVSE units. Moreover intelligent electronic devices (IEDs) are assumed to be installed at the HV/MV substation and at the feeder branches that may reach their maximum current rate during the operation of the distribution network. In particular, we assume the presence of an IED at the beginning of each feeder connected to the secondary side of the HV/MV transformer. This IED measures the current and compares the value with the maximum operation current value of the line. We also assume the presence of an IED able to detect the overload state of the HV/MV transformer.

Each IED is able to communicate an index over UMTS cellular network that denotes whether and how much the corresponding power component is overloaded. In the literature this type of indexes are often called congestion prices (e.g., [79],[81]). The agent associated with each cluster of EVSEs is able to control the charging power according to the received congestion index.

The procedure implemented in the simulator is the following:

We assume that at time t, IEDj associated to the first branch of feeder j detect an overcurrent condition, i.e.

$e_t = \frac{i_{j,t} - i_{j,\max}}{i_{j,\max}}$ is greater than 1 where $i_{j,t}$ is the measured value of the current at time t and $i_{j,\max}$ is the maximum operating value. Then it calculates the variation of the congestion index Δprj as

$$\Delta pr_{j,t} = K_c \left[(e_t - e_{t-1}) + \frac{\Delta t}{\tau_I} \left(\frac{e_t + e_{t-1}}{2} \right) \right] \tag{4.1}$$

where K_c and τ_I are constants and in the simulations are chosen equal to 0.2 and 0.1 respectively. Equation (4.1) corresponds to the velocity algorithm of a digital PI controller. Through the communication network, value $\Delta pr_{j,t}$ is sent by IED_j to the agents associated to clusters of EVSE units connected to feeder j. IED_j continues to perform calculation (4.1) until $\Delta pr_{j,t}$ becomes and stay continuously negative for at least a predefined settling time T_{set} chosen equal to 10 seconds. After Tset, $\Delta pr_{j,t}$ is set equal to 0. With a selected time step Δt (chosen equal to 1 s or 3 s in the simulations), the updated value of $\Delta pr_{j,t}$ is sent to the agents.

Each agent i that receives $\Delta pr_{j,t}$ at time t updates its own congestion index as

$$pr_{i,t} = \max(1, pr_{i,t-1} + \Delta pr_{j,t}) \tag{4.2}$$

and fixes the maximum power that could be absorbed by the relevant cluster of EVSEs as

$$P_{EVSE_{i,t}} = \frac{\widehat{P}_{EVSE_{i,t}}}{pr_{i,t}} \tag{4.3}$$

where $\widehat{P}_{EVSE_{i,t}}$ is the maximum power requested by the EVSEs of the cluster associated to agent i at time t.

Compared with the broadcast of congestion indexes, the velocity form of the control mechanism provided by (4.1) avoids reset windup and, in (4.2), it permits to sum the contributions of various IEDs that detects the concurrent overload of different power components.

Each agent *i* also includes a local voltage regulator that proportionally reduces $P_{EVSE_{i,t}}$ if the local voltage at the MV side of the transformer is lower than a predefined value (e.g., 0.97 pu).

The allocation of power $P_{EVSE_{i,t}}$ made available by the agent among the various charging EVs taking into account their specific characteristics and requirements, such as the state of charge (SoC) and remaining charging time, is not dealt with in this chapter.

4.4 Simulation Results

In this section we describe the simulation results obtained with the presented framework. Figure 4.5 shows the locations of parking lots with EVSE units in Bologna. We focus here to two 15 kV feeders fed by 132/15 kV substation SB_A (indicated in red in Figure 4.5), to which four clusters of 50 kW EVSE units are assumed to be connected, namely EVSE_1 and EVSE_2 to feeder 1, EVSE_3 and EVSE_4 to feeder 2. Figure 4.5 also shows the main components of the implemented model of the UMTS communication network, assuming that all the four agents each associated to a cluster are served by the same Node B.

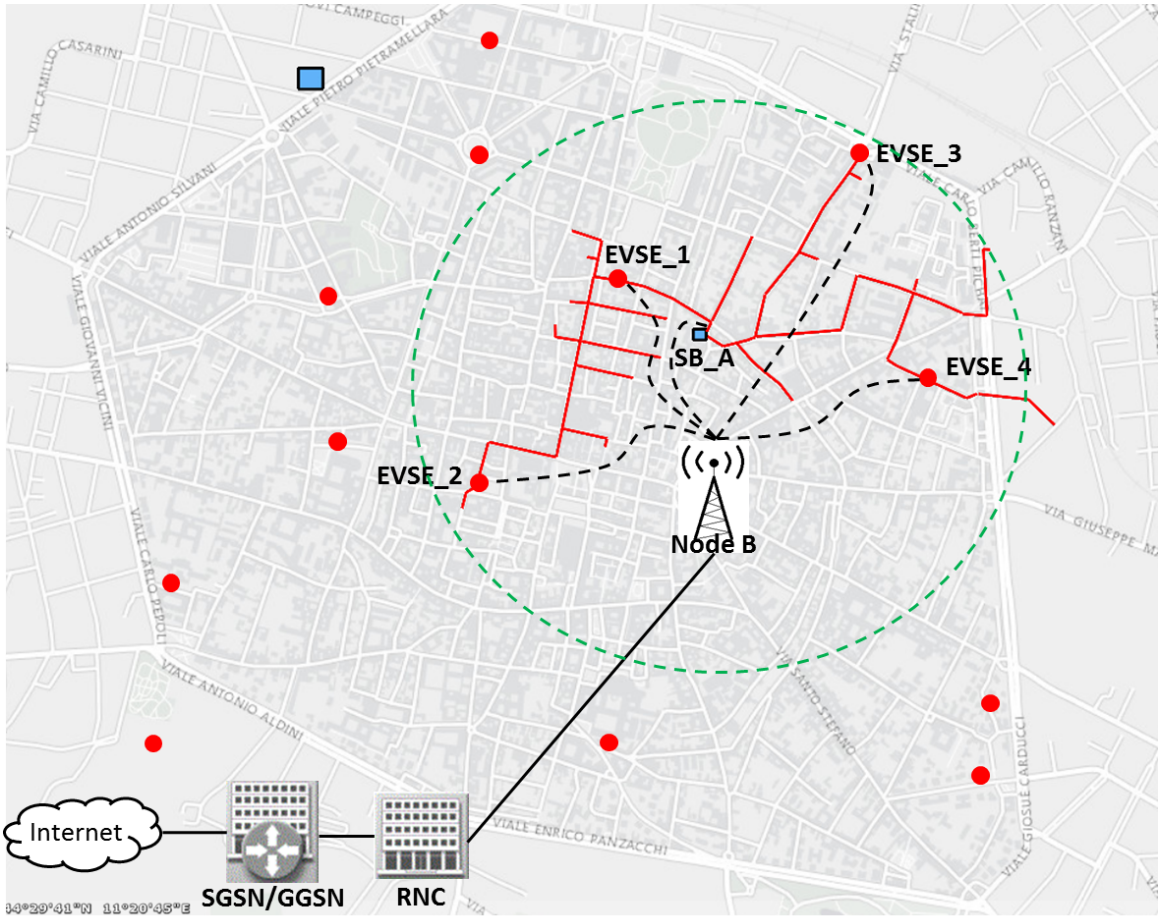

Figure 4.5 Top view of the map of Bologna with the indication of parking lots with EVSE clusters (red bullets), of HV/MV substations (blue rectangles), the two 15kV feeders of substation SB_A (in red) that connects the EVSE clusters denoted as EVSE_1, EVSE_2, EVSE_3, and EVSE_4 and the correspondent

UMTS communication network (dotted black lines represent wireless channels, solid black lines represent wired channel). The green circles indicate the estimated coverage areas of the Node B antennas.

The traffic simulator generates a flow of random events. Each event represents a specific trip of a vehicle in the city from a starting point to a destination. For the case of EVs, when the SoC of the corresponding battery is below a threshold set to 25%, the vehicle deviates from the planned journey and reaches the closest EVSE unit available.

The EMTP model represents the two 15 kV feeders of interests, the 132/15 kV transformer of the HV/MV substation and the equivalent impedance of the HV network. It includes also the model of three-phase loads (assumed constant for these simulations) and the aggregate EVSE models of clusters EVSE_1, EVSE_2, EVSE_3, and EVSE_4, each fed through a 15/0.4 kV transformer. Moreover the EMTP model represents both the IEDs and the agents that communicate between each other and the SIB through the DLL interface.

The results presented here refer to a simulation that starts with a random generation of 200 events, each one every 5 seconds. With a 50% uniform probability each event is associated with an EV, otherwise is represented by a fuel vehicle. Every time a vehicle leaves the simulation, i.e. reaches its destination, a new event is generated. For illustrative purpose, the EVs are generated with a SoC below the minimum threshold.

EMTP is linked and synchronized with VeinS after 400 s of traffic generation with the OLTC in tap position 0.

The simulations are repeated for two different BLER values: 1E-5 (case indicated as BLER0) and 0.1 (BLER1), which is a typical reference performance value (e.g. [21]).

Moreover the same simulations are repeated with BT (case indicated as BT1) and without the BT (BT0). BT is generated by the UEs associated to the agents and by seven additional UEs and two traffic receivers. The two adopted mobile users application models are characterized by a gamma distribution of the inter-arrival packet time (with parameters 0.0068, 5 s and 0.2, 0.5 s, respectively) and by an exponential distribution of packet size (with parameters 41.03 bytes and 62.97 bytes, respectively).

Note that, during both simulations, the OLTC operates a first tap change to -1 at 422 s and reaches a final tap equal to -2 at 439 s.

Figure 4.6 shows the dynamic change of the number of vehicles that are connected to an EVSE of each of the 4 considered clusters, whilst Figure 4.7 and Figure 4.8 show the requested power by each of the clusters and the current measured at the beginning of the two feeders. The current value of 1 pu indicates the maximum allowed operating value (in the considered feeders it is equal to 200 A)

As shown by Figure 4.8, after 420 s since the beginning of the EMTP simulation, the IEDs associated to the initial branch of the two feeders detect an overcurrent condition. They calculate the variation of the congestion indexes according to (4.1) and send them at each Δt=1 s to the agents of the relevant EVSE clusters. The sent values of the congestion index variations are

shown by Figure 4.9, whilst Figure 4.10 shows the congestion index values independently calculated by each of the agents of the four EVSE clusters by using (4.2). The congestion index is used by the agents in order to limit the EVSE power according to (4.3). Figure 4.7 shows the limitation of the absorbed power by each EVSE cluster, whilst Figure 4.8 shows the effectiveness of the control action that is able to promptly compensate the overloading conditions caused by each new connection of an EV to an EVSE.

As can be seen from Figure 4.7 and Figure 4.10, the control without communication interference and packet loss, the final power requested and congestion index by the clusters connected to the same feeder is equal. With delay and loss of information, this fairness condition is no longer verified and these values differ from each other by 9.3 kW for EVSE_1 and EVSE_2 (feeder 1) and by 4.8 kW for the EVSE_3 and EVSE_4 (feeder 2).

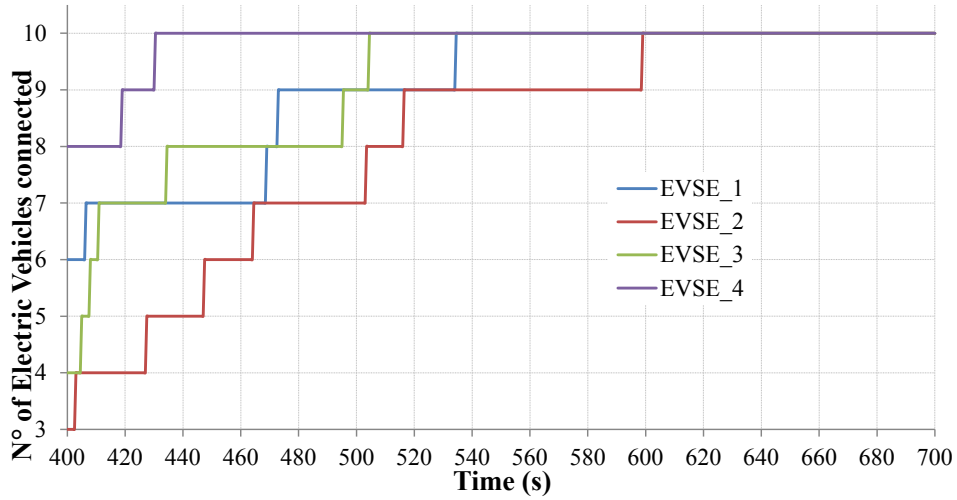

Figure 4.6 Number of EVs in charge in each of the considered clusters.

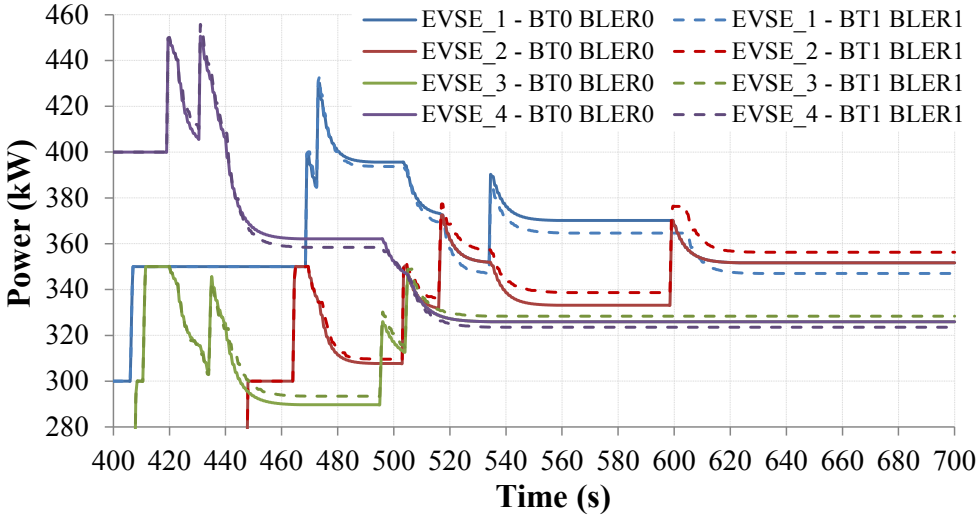

Figure 4.7 Power requested by each EVSE cluster. (Δt = 1 s).

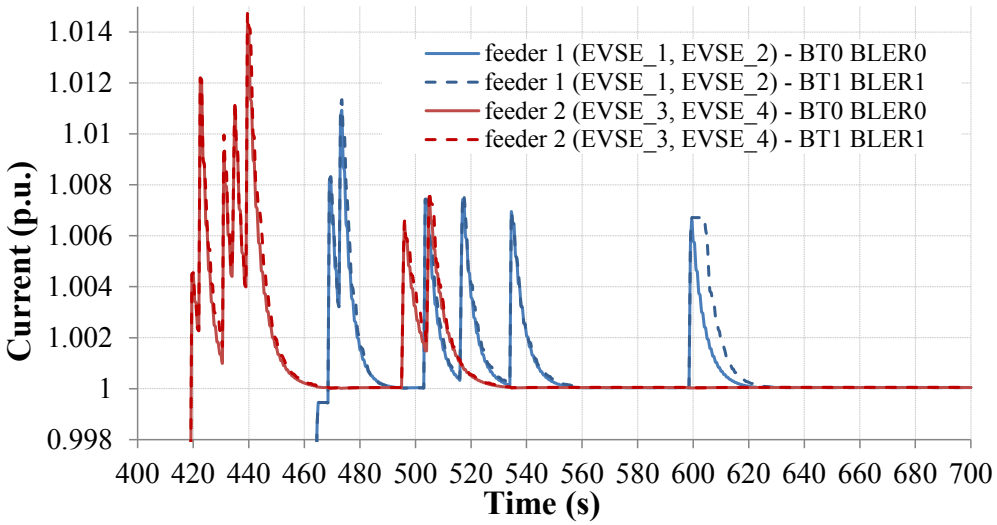

Figure 4.8 Current value measured by the IEDs associate to the first branch of the two considered feeders. (Δt = 1 s).

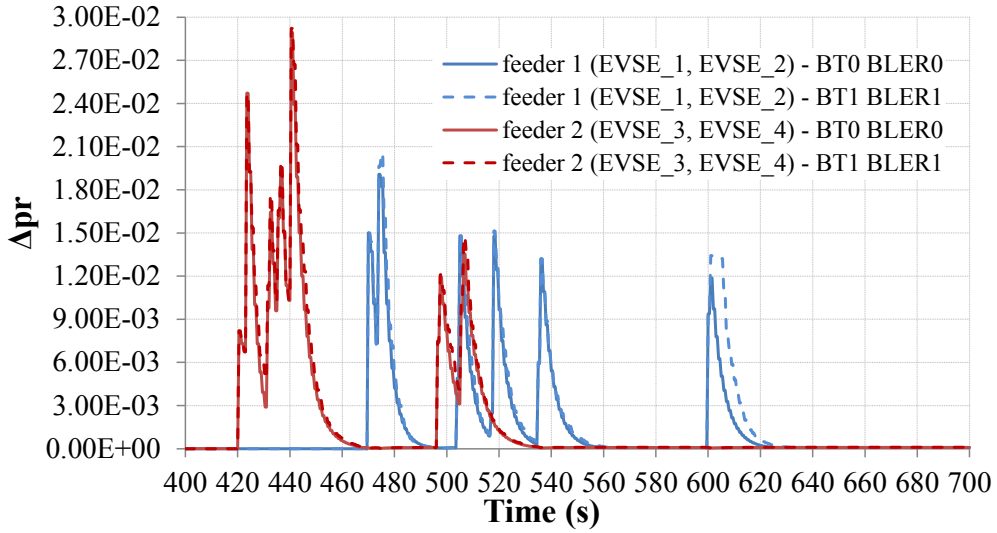

Figure 4.9 Congestion index variations sent by the two IEDs to the agents (Δt= 1 s).

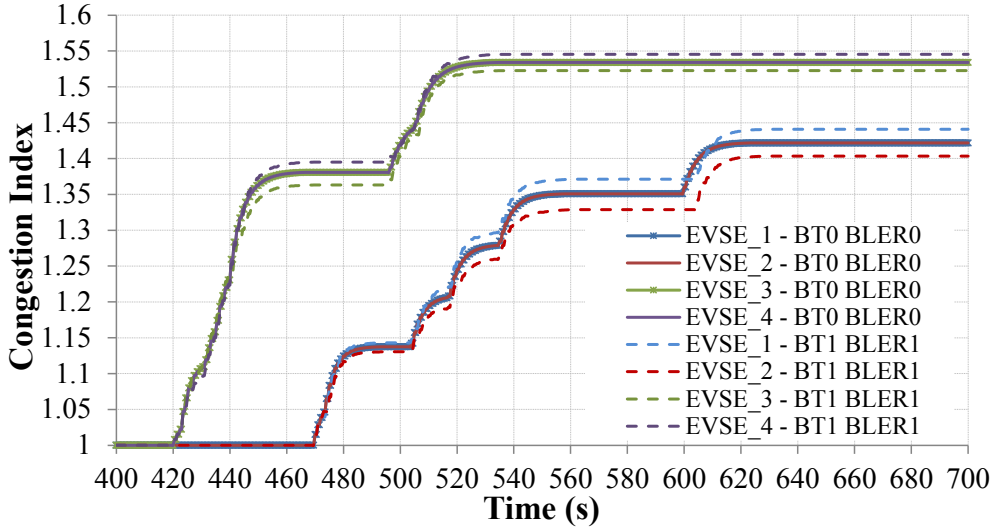

Figure 4.10 Congestion indexes independently calculated by each agent of an EVSE cluster. (Δt = 1 s).

The simulations have repeated for Δt = 3 s. Analogously to the previous figures, Figure 4.11, Figure 4.12, Figure 4.13 and Figure 4.14 show the power requested by each EVSE cluster, the measured currents, the congestion index variations and the congestion indexes calculated by each agents. The results refer to the same sequence of connection of EVs shown in Figure 4.6 and they are repeated for both the case of ideal communication and the case with both BLER and BT.

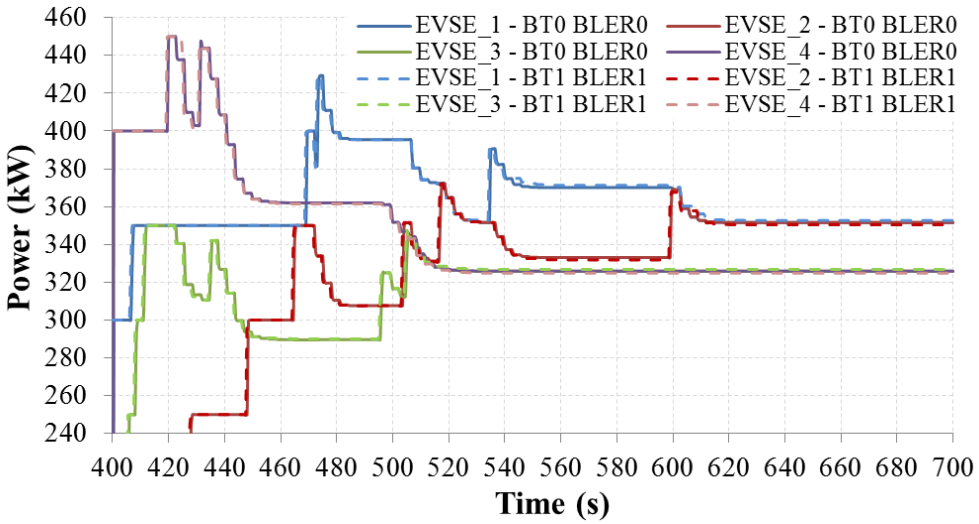

Figure 4.11 Power requested by each EVSE cluster (Δt = 3 s).

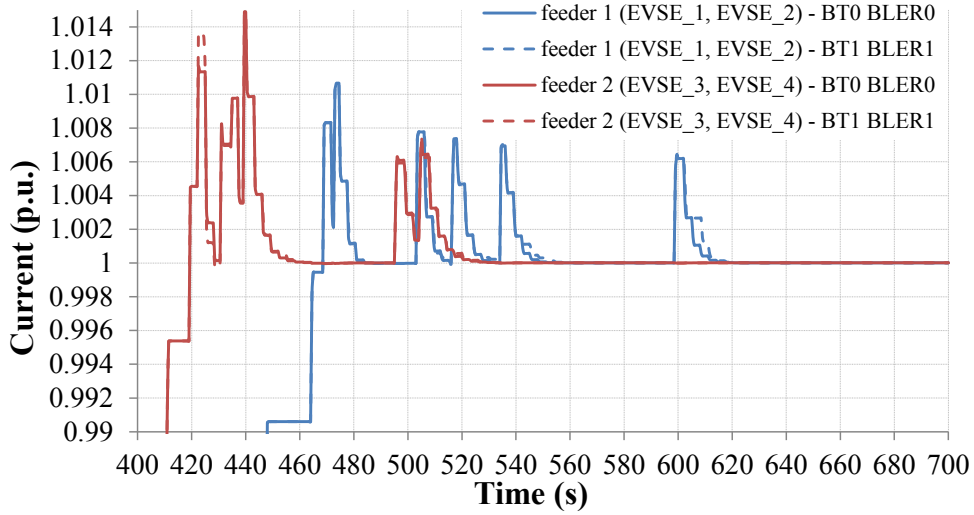

Figure 4.12 Current value measured by the IEDs associate to the first branch of the two considered feeders (Δt = 3 s).

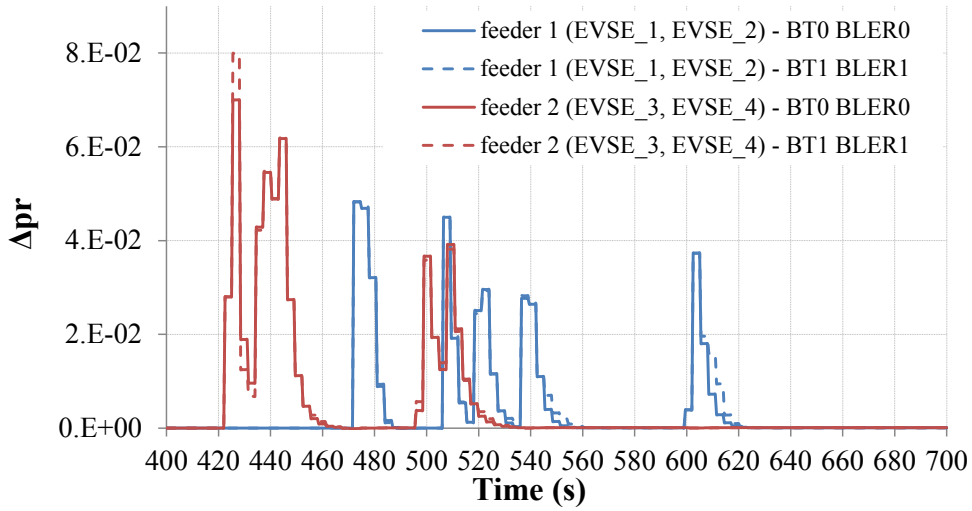

Figure 4.13 Congestion index variations sent by the two IEDs to the agents (Δt = 3 s).

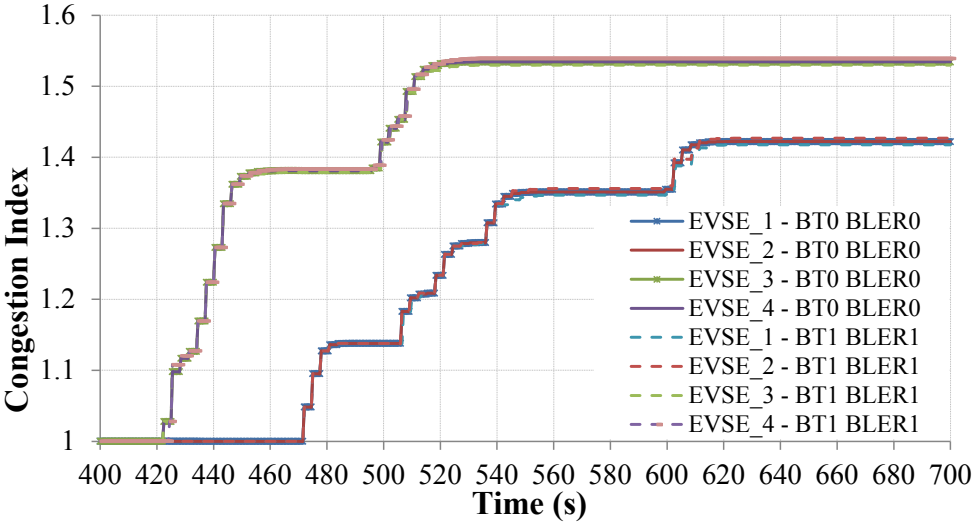

Figure 4.14 Congestion indexes independently calculated by each agent of an EVSE cluster (Δt = 3 s).

Table 4.I, shows additional details on the results: the total overloading duration during which the currents measured by the two IEDs, indicated as I_1 and I_2, exceed the maximum value, the maximum current measured by each IEDs, the mean and standard deviation of the delay of the communication packets and the correspondent number of packet transmitted and received. As expected, for the case of communication affected by BLER and BT, both the mean value and standard deviation of packet delays are larger than in the case of ideal communication. Moreover BLER causes the loss of some packets. The use of Δt = 3 s limits the number of packets and reduces the influence of both packet delay and packet loss.

Table 4.I Time above the current limit, packet delay and number of packets (tx: transmitted, rx: received)

BT BLER ΔT	TIME I_1>1P.U (S)	TIME I_2>1P.U (S)	I_1 MAX (P.U.)	I_2 MAX (P.U.)	PACKET DELAY (MS) MEAN (STDEV)	NUMBER OF PACKETS TX RX
BT0 BLER0 ΔT=1 S	93	79	1.010926	1.014279	142.6 (10.0)	378 378
BT1 BLER1 ΔT =1 S	101	81	1.011345	1.014691	231.3 (189.0)	406 363
BT0 BLER0 ΔT=3 S	71	69	1.0107	1.0149	149.7 (12.7)	122 122
BT1 BLER1 ΔT =3 S	81	69	1.0107	1.0149	235.3 (180.5)	128 120

As shown by figures and the Table, the overall performance of the implemented control strategy is not significantly affected by the presence of BLER and BT. The difference between the results obtained for Δt = 1 s and Δt = 3 s is not significant.

Chapter 5
CONCLUSIONS

The architecture of the developed ICT-Power Co-simulation platform has been described in Chapter 2. The platform appears to be useful in order to test different communication architectures and technologies as well as their impact on power system applications. The framework is based on the interface between Riverbed-OPNET v18.0 and EMTP-rv v3.0. The interface is based on the application of the HLA DLL standard.

As it is shown in Chapter 4, the developed platform has the capability to mutually exchanging information also with other components. The comparison between other co-simulation platform presented in literature shows that two main co-simulation approaches may be identified: one is an off-line approach and the other one is a real-time approach. The main difference between off-line approach and real-time approach is the way that information is exchanged between the simulators. The development of an off-line platform requires setting up and synchronizing different elements in the whole system (in the case of the simulator described in this thesis, using C++ programming language). Therefore, the off-line platform has a complex scalability but at the same time provides a considerable degrees of freedom, while it allow to modify, import and test different models, technologies, algorithms and protocols in the platform. However, the speed of communication interface and simulation is limited, because the control of the simulation and the synchronization is shared between the simulators (in the case of the simulator presented in this Thesis, the time-driven EMTP-rv simulation environment is and the event-driven Riverbed-OPNET simulator).

The platforms running in real time gives the important opportunity of Hardware In the Loop (HIL) experiments in order to directly test the performance and interoperability of the real components in the system, which is not the case in off-line platforms. However, the use of this kind of interaction needs some effort in order to create the relevant transaction functions for the representation of non-typical transport protocols. As the components of the co-simulation platform run in real time, there is no control on the simulation process or intervals and the synchronization is not necessarily needed. The scalability of the communication network model is limited by the performances of the adopted computer.

As a proof of functionality of the developed co-simulation platform, in the end of Chapter 2 a simple test case of an application scenario has been modelled and examined.

The Chapter 3 deals with the application of the developed ICT-power co-simulation platform to the analysis of a networked control system – NCS – scheme for the volt/var optimization –

VVO – of distribution feeders with several DGs with adjustable reactive power output and also on-load tap changers. The adopted NCS scheme is based on a leaderless gossip-like algorithm.

Section 3.2.2 presents the mechanisms introduced in the adopted gossip-like algorithm in order to improve its robustness against the limitations induced by background traffic and packed discard ratio in the communication channels. In particular, a mechanism based on a priority index has been implemented to allow for the start of multiple concurrent compensations processes whenever packet carrying critical information is lost. The processes with low priority indexes are progressively stopped by the agents in order to guarantee the convergence performances of the algorithm.

Although the algorithm is based on the use of the impedance matrix calculated assuming a balanced three-phase representation of the distribution feeder, the chapter presents its application to test systems characterized by unbalanced lines and loads. The obtained results show that the performances of the adopted approach appear reasonably good also for medium values of background data traffic and packet discard ratio taking into account the expected accuracy of phasor measurements units.

Moreover, a comparison between TCP and UDP is presented for different feeders and load conditions in order to analyze the effects on the control performances. As shown by the obtained results, due to the specific countermeasure implemented against packet loss and delayed, the performances of the adopted approach appear reasonably good even for the case of significant values of the background data traffic or packet discard ration. The statistical analysis of the results has allowed also to shows that the use of UDP allows reducing latency and a low percentage of incomplete cycles, so it is in general to be preferred for this application.

In Section 3.5 the distributed application has been extended supposing that the agents of the VVO are PV units which participate by using their reactive power capability. For this reason, the simulator implements a model that takes into account the reactive limits of the PV inverters, which dynamically vary according to the variation of the real power output set point determined by the maximum power point tracking (MPPT) algorithm. In addition, the communication has been tested over a third generation cellular network, namely a Universal Mobile Telecommunications System (UMTS).

In order to guarantee the convergence performances of the algorithm, the same countermeasures against communication latencies and packet loss has been adopted through the use of the UDP protocol. As it can be seen from simulation results of Section 3.5.4 the results appear reasonably good also taking into account the typical latencies of the UMTS network.

At last, Chapter 4 presents a further integration of the co-simulation platform presented in Chapter 2 for the application of a specifically developed framework to the analysis of a multi agent system scheme for the active power control of the EV charging station. The framework integrates a mobility simulator of the electric vehicles and their charging requests with a dynamic co-simulator of the power distribution network and its relative communication network. The tool appears useful in order to assess the effects of the transients caused by the concurrent charging of

a large number of electric vehicles to the operating conditions of the power network. The simulation results contains in the Section 4.4 shows the effectiveness of a congestion management approach based on the communication of congestion indexes variation between the agents that control the EVSE clusters and IEDs installed both at the HV/MV substation and the feeder branches that may reach their maximum current rate.

The analysis has been carried out taking care of communication network constraints. In particular the co-simulation platform incorporates a model of a mobile cellular network. Latency and communication errors do not appear to significantly affect the control scheme performance although equal allocation of the control effort among different EVSE clusters connected to the same feeder is reached only in the case of ideal communication.

REFERENCE

[1] S. Borlase, *Smart Grids: Infrastructure, Technology, and Solutions - CRC Press Book*. CRC Press, 2012, p. 607.

[2] S. D. J. McArthur, E. M. Davidson, V. M. Catterson, A. L. Dimeas, N. D. Hatziargyriou, F. Ponci, and T. Funabashi, "Multi-Agent Systems for Power Engineering Applications—Part II: Technologies, Standards, and Tools for Building Multi-agent Systems," *IEEE Trans. Power Syst.*, vol. 22, no. 4, pp. 1753–1759, Nov. 2007.

[3] Q. Yang, J. A. Barria, and T. C. Green, "Communication infrastructures for distributed control of power distribution networks," *IEEE Trans. Ind. Informatics*, vol. 7, no. 2, pp. 316–327, May 2011.

[4] Y. Chen, J. Lu, X. Yu, and D. J. Hill, "Multi-agent systems with dynamical topologies: consensus and applications," *IEEE Circuits Syst. Mag.*, vol. 13, no. 3, pp. 21–34, 2013.

[5] R. A. Gupta, "Networked control system: overview and research trends," *IEEE Trans. Ind. Electron.*, vol. 57, no. 7, pp. 2527–2535, Jul. 2010.

[6] "IEEE Guide for Smart Grid Interoperability of Energy Technology and Information Technology Operation with the Electric Power System (EPS), End-Use Applications, and Loads." pp. 1–126, 2011.

[7] S. P. Carullo and C. O. Nwankpa, "Experimental Validation of a Model for an Information-Embedded Power System," *IEEE Trans. Power Deliv.*, vol. 20, no. 3, pp. 1853–1863, Jul. 2005.

[8] Dong-qing Wang, Shi-hong Miao, Xiang-ning Lin, Pei Liu, Ying-Xin Wu, Dan Yang, D. Wang, S. Miao, X. Lin, P. Liu, Y.-X. Wu, D. Yang, and Dong-Qing, "Design of a novel wide-area backup protection system," in *2005 IEEE/PES Transmission & Distribution Conference & Exposition: Asia and Pacific*, 2005, pp. 1–6.

[9] K. Hopkinson, X. Wang, R. Giovanini, J. Thorp, K. Birman, D. Coury, L. Fellow, K. Birman, and D. Coury, "EPOCHS: A Platform for Agent-Based Electric Power and Communication Simulation Built From Commercial Off-the-Shelf Components," *IEEE Trans. Power Syst.*, vol. 21, no. 2, pp. 548–558, May 2006.

[10] J. Nutaro, P. T. Kuruganti, L. Miller, S. Mullen, and M. Shankar, "Integrated Hybrid-Simulation of Electric Power and Communications Systems," in *2007 IEEE Power Engineering Society General Meeting*, 2007, pp. 1–8.

[11] H. Lin, S. S. Veda, S. S. Shukla, L. Mili, and J. Thorp, "GECO: global event-driven co-simulation framework for interconnected power system and communication network," *IEEE Trans. Smart Grid*, vol. 3, no. 3, pp. 1444–1456, Sep. 2012.

[12] A. Monti, M. Colciago, P. Conti, M. Maglio, and R. Dougal, "A co-simulation approach for analysing the impact of the communication infrastructure in power system control," pp. 278–282, Jul. 2009.

[13] T. Godfrey, S. Mullen, R. C. Dugan, C. Rodine, D. W. Griffith, N. Golmie, R. C. Dugan, and C. Rodine, "Modeling Smart Grid Applications with Co-Simulation," in *2010 First IEEE International Conference on Smart Grid Communications*, 2010, pp. 291–296.

[14] F. Ponci, A. Monti, and A. Benigni, "Simulation for the design of Smart Grid controls," *2011 IEEE First Int. Work. Smart Grid Model. Simul.*, pp. 73–78, Oct. 2011.

[15] H. G. Molter and S. A. Huss, "The DEVS model of computation. A foundation for a novel embedded systems design methodology," in *The 2011 International Conference on Computer Engineering & Systems*, 2011, pp. xxi–xxvi.

[16] A. T. Al-Hammouri, "A comprehensive co-simulation platform for cyber-physical systems," *Comput. Commun.*, vol. 36, no. 1, pp. 8–19, 2012.

[17] D. Anderson, C. Hauser, V. Venkatasubramanian, D. Bakken, and A. Bose, "A virtual smart grid," *IEEE Power Energy Mag.*, vol. 10, no. 1, pp. 49–57, Jan. 2012.

[18] L. Vanfretti, M. Chenine, M. S. Almas, R. Leelaruji, L. Angquist, and L. Nordstrom, "SmarTS Lab — A laboratory for developing applications for WAMPAC Systems," in *2012 IEEE Power and Energy Society General Meeting*, 2012, pp. 1–8.

[19] D. E. Bakken, A. Bose, C. H. Hauser, D. E. Whitehead, and G. C. Zweigle, "Smart Generation and Transmission With Coherent, Real-Time Data," *Proc. IEEE*, vol. 99, no. 6, pp. 928–951, Jun. 2011.

[20] "OPAL-RT eMEGAsim." [Online]. Available: http://www.opal-rt.com/.

[21] R. Bottura, D. Babazadeh, K. Zhu, A. Borghetti, L. Nordstrom, and C. A. Nucci, "SITL and HLA co-simulation platforms: Tools for analysis of the integrated ICT and electric power system," in *Eurocon 2013*, 2013, pp. 918–925.

[22] "OPNET-Riverbed Modeler Wireless suite v18.0." [Online]. Available: http://www.riverbed.com/products/performance-management-control/opnet.html.

[23] "EMTP-RV v3.0." [Online]. Available: http://emtp.com/.

[24] J. Mahseredjian, "DLL programming in EMTP," in *EMTP User Manual*, EMTPWorks Inc., 2012, pp. 1–24.

[25] D. Z. Lu and H. Yang, *Unlocking the power of OPNET Modeler*. Cambridge University Press, 2012.

[26] J. Hošek, L. Růčka, and K. Molnár, "Mutual cooperation of external application and OPNET Modeler simulation environment," in *Proc. of the International WORKSHOP RTT 2009 Research in Telecommunication Technology*, 2009.

[27] Y. Yan, Y. Qian, H. Sharif, and D. Tipper, "A survey on smart grid communication infrastructures: motivations, requirements and challenges," *IEEE Commun. Surv. Tutorials*, vol. 15, no. 1, pp. 5–20, Jan. 2013.

[28] K. Mets, J. A. Ojea, and C. Develder, "Combining Power and Communication Network Simulation for Cost-Effective Smart Grid Analysis," *IEEE Commun. Surv. Tutorials*, pp. 1–26, 2014.

[29] S. D. J. McArthur, E. M. Davidson, V. M. Catterson, A. L. Dimeas, N. D. Hatziargyriou, F. Ponci, and T. Funabashi, "Multi-agent systems for power engineering applications—Part I: concepts, approaches, and technical challenges," *IEEE Trans. Power Syst.*, vol. 22, no. 4, pp. 1743–1752, Nov. 2007.

[30] L. Zhang, H. Gao, and O. Kaynak, “Network-induced constraints in networked control systems—A survey,” *IEEE Trans. Ind. Informatics*, vol. 9, no. 1, pp. 403–416, Feb. 2013.

[31] S. Deshmukh, B. Natarajan, and A. Pahwa, “Voltage/VAR Control in Distribution Networks via Reactive Power Injection Through Distributed Generators,” *IEEE Trans. Smart Grid*, vol. 3, no. 3, pp. 1226–1234, Sep. 2012.

[32] A. Borghetti, “Using mixed integer programming for the volt/var optimization in distribution feeders,” *Electr. Power Syst. Res.*, vol. 98, pp. 39–50, May 2013.

[33] L. Yu, D. Czarkowski, and F. de Leon, “Optimal Distributed Voltage Regulation for Secondary Networks With DGs,” *IEEE Trans. Smart Grid*, vol. 3, no. 2, pp. 959–967, Jun. 2012.

[34] A. Y. S. Lam, B. Zhang, and D. N. Tse, “Distributed algorithms for optimal power flow problem,” in *2012 IEEE 51st IEEE Conference on Decision and Control (CDC)*, 2012, pp. 430–437.

[35] P. Šulc, S. Backhaus, and M. Chertkov, “Optimal Distributed Control of Reactive Power via the Alternating Direction Method of Multipliers,” *arXiv:1310.5748v1*, p. 10, Oct. 2013.

[36] B. Zhang, A. Y. S. Lam, A. Dominguez-Garcia, and D. Tse, “Optimal Distributed Voltage Regulation in Power Distribution Networks,” *arXiv:1204.5226v3 [math.OC]*, Apr. 2012.

[37] S. Bolognani, R. Carli, G. Cavraro, and S. Zampieri, “A distributed control strategy for optimal reactive power flow with power constraints,” in *52nd IEEE Conference on Decision and Control*, 2013, pp. 4644–4649.

[38] M. E. Baran and I. M. El-Markabi, “A Multiagent-Based Dispatching Scheme for Distributed Generators for Voltage Support on Distribution Feeders,” *IEEE Trans. Power Syst.*, vol. 22, no. 1, pp. 52–59, Feb. 2007.

[39] A. A. Aquino-lugo, R. Klump, and T. J. Overbye, “A Control Framework for the Smart Grid for Voltage Support Using Agent-Based Technologies,” *IEEE Trans. Smart Grid*, vol. 2, no. 1, pp. 173–180, Mar. 2011.

[40] H. E. Z. Farag and E. F. El-Saadany, “A novel cooperative protocol for distributed voltage control in active distribution systems,” *IEEE Trans. Power Syst.*, vol. 28, no. 2, p. 1, 2012.

[41] S. Bolognani and S. Zampieri, “A gossip-like distributed optimization algorithm for reactive power flow control,” *Proc. IFAC World Congr.*, pp. 1–14, 2011.

[42] Saverio Bolognani and Sandro Zampieri, S. Bolognani, and S. Zampieri, “A distributed control strategy for reactive power compensation in smart microgrids,” *IEEE Trans. Automat. Contr.*, vol. in press, pp. 1–16, 2013.

[43] S. Bolognani, A. Carron, A. Di Vittorio, D. Romeres, L. Schenato, S. Zampieri, A. Di Vittorio, D. Romeres, L. Schenato, and S. Zampieri, “Distributed multi-hop reactive power compensation in smart micro-grids subject to saturation constraints,” in *51st IEEE Conference on Decision and Control (CDC 2012)*, 2012, no. 257462, pp. 1118–1123.

[44] P. Tenti, A. Costabeber, P. Mattavelli, and D. Trombetti, “Distribution loss minimization by token ring control of power electronic interfaces in residential microgrids,” *IEEE Trans. Ind. Electron.*, vol. 59, no. 10, pp. 3817–3826, Oct. 2012.

[45] V. Loia, A. Vaccaro, and K. Vaisakh, “A self-organizing architecture based on cooperative fuzzy agents for smart grid voltage control,” *IEEE Trans. Ind. Informatics*, vol. 9, no. 3, pp. 1415–1422, Aug. 2013.

[46] "IEEE PES distribution test feeders." [Online]. Available: http://ewh.ieee.org/soc/pes/dsacom/testfeeders/.

[47] A. G. Phadke and J. S. Thorp, *Synchronized Phasor Measurements and Their Applications (Power Electronics and Power Systems)*. Springer, 2008, p. 247.

[48] G. Sanchez-Ayala, J. R. Aguerc, D. Elizondo, and M. Lelic, "Current trends on applications of PMUs in distribution systems," in *2013 IEEE PES Innovative Smart Grid Technologies Conference (ISGT)*, 2013, pp. 1–6.

[49] A. Borghetti, C. A. Nucci, M. Paolone, G. Ciappi, and A. Solari, "Synchronized phasors monitoring during the islanding maneuver of an active distribution network," *IEEE Trans. Smart Grid*, vol. 2, pp. 70–79, 2011.

[50] M. Paolone, A. Borghetti, and C. A. Nucci, "A synchrophasor estimation algorithm for the monitoring of active distribution networks in steady state and transient conditions," in *17th Power Systems Computation Conference (PSCC'11) Stockholm, Sweden*, 2011, pp. 22–26.

[51] G. Kron, *Tensor Analysis of Networks*. New York: John Wiley & Sons, 1965.

[52] "Kron reduction of graphs with applications to electrical networks." [Online]. Available: http://arxiv.org/pdf/1102.2950v1.pdf. [Accessed: 23-Jan-2015].

[53] S. Boyd and A. Ghosh, "Randomized gossip algorithms," *Inf. Theory, IEEE ...*, vol. 52, no. 6, pp. 2508–2530, 2006.

[54] B. Khodabakhchian, "Modeling on-load tap changers in EMTP-RV," *EMTP-RV Newsletter*, vol. 1, no. 1, pp. 11–15, 2005.

[55] M. Larsson, "Coordination of cascaded tap changers using a fuzzy-rule-based controller," *Fuzzy Sets Syst.*, vol. 102, no. 1, pp. 113–123, Feb. 1999.

[56] T. Chen, M. Chen, T. Inoue, P. Kotas, and E. A. Chebli, "Three-phase cogenerator and transformer models for distribution system analysis," *IEEE Trans. Power Deliv.*, vol. 6, no. 4, pp. 1671–1681, 1991.

[57] M. Z. Kamh and R. Iravani, "Unbalanced model and power-flow analysis of microgrids and active distribution systems," *IEEE Trans. Power Deliv.*, vol. 25, no. 4, pp. 2851–2858, 2010.

[58] K. Turitsyn, P. Sulc, S. Backhaus, and M. Chertkov, "Options for Control of Reactive Power by Distributed Photovoltaic Generators," *Proc. IEEE*, vol. 99, no. 6, pp. 1063–1073, Jun. 2011.

[59] M. E. Baran, H. Hooshyar, Z. Shen, and A. Huang, "Accommodating High PV Penetration on Distribution Feeders," *IEEE Trans. Smart Grid*, vol. 3, no. 2, pp. 1039–1046, Jun. 2012.

[60] P. Jahangiri and D. C. Aliprantis, "Distributed Volt/VAr Control by PV Inverters," *IEEE Trans. Power Syst.*, vol. 28, no. 3, pp. 3429–3439, Aug. 2013.

[61] H.-G. Yeh, D. F. Gayme, and S. H. Low, "Adaptive VAR Control for Distribution Circuits With Photovoltaic Generators," *IEEE Trans. Power Syst.*, vol. 27, no. 3, pp. 1656–1663, Aug. 2012.

[62] R. Tonkoski, L. A. C. Lopes, and T. H. M. El-Fouly, "Coordinated Active Power Curtailment of Grid Connected PV Inverters for Overvoltage Prevention," *IEEE Trans. Sustain. Energy*, vol. 2, no. 2, pp. 139–147, Apr. 2011.

[63] A. Cagnano, E. De Tuglie, M. Liserre, and R. A. Mastromauro, “Online Optimal Reactive Power Control Strategy of PV Inverters,” *IEEE Trans. Ind. Electron.*, vol. 58, no. 10, pp. 4549–4558, Oct. 2011.

[64] V. Calderaro, G. Conio, V. Galdi, G. Massa, and A. Piccolo, “Optimal Decentralized Voltage Control for Distribution Systems With Inverter-Based Distributed Generators,” *IEEE Trans. Power Syst.*, vol. 29, no. 1, pp. 230–241, Jan. 2014.

[65] E. Dall’Anese, S. V. Dhople, and G. B. Giannakis, “Optimal dispatch of photovoltaic inverters in residential distribution systems,” in *2014 IEEE PES General Meeting | Conference & Exposition*, 2014, pp. 1–1.

[66] S. Jashfar and S. Esmaeili, “Volt/var/THD control in distribution networks considering reactive power capability of solar energy conversion,” *Int. J. Electr. Power Energy Syst.*, vol. 60, pp. 221–233, Sep. 2014.

[67] S. Weckx, C. Gonzalez, and J. Driesen, “Combined Central and Local Active and Reactive Power Control of PV Inverters,” *IEEE Trans. Sustain. Energy*, vol. 5, no. 3, pp. 776–784, Jul. 2014.

[68] M. E. Baran and I. M. El-Markabi, “A multiagent-based dispatching scheme for distributed generators for voltage support on distribution feeders,” *IEEE Trans. Power Syst.*, vol. 22, no. 1, pp. 52–59, Feb. 2007.

[69] R. Bottura, A. Borghetti, F. Napolitano, and C. A. Nucci, “ICT-power Co-simulation Platform for the Analysis of Communication-based Volt / Var Optimization in Distribution Feeders,” in *ISGT 2014*, 2014.

[70] R. Bottura and A. Borghetti, “Simulation of the Volt/Var Control in Distribution Feeders by Means of a Networked Multi-Agent System,” *IEEE Trans. Ind. Informatics*, vol. 10, no. 4, pp. 1–1, 2014.

[71] R. Albarracin and M. Alonso, “Photovoltaic reactive power limits,” in *2013 12th International Conference on Environment and Electrical Engineering*, 2013, pp. 13–18.

[72] F. Agharebparast and V. C. M. Leung, “Evaluation of UMTS QoS Support Using OPNET UMTS Model Suite *,” pp. 4–8.

[73] “3GPP Specification detail.” [Online]. Available: http://www.3gpp.org/dynareport/36822.htm.

[74] Mishra A.R., Ed., *Advanced Cellular Network Planning and Optimisation: 2G/2.5G/3G...Evolution to 4G*. John Wiley & Sons, 2007, p. 542.

[75] C. Sommer, R. German, and F. Dressler, “Bidirectionally Coupled Network and Road Traffic Simulation for Improved IVC Analysis,” *IEEE Trans. Mob. Comput.*, vol. 10, no. 1, pp. 3–15, Jan. 2011.

[76] J. Mahseredjian, S. Dennetière, L. Dubé, B. Khodabakhchian, and L. Gérin-Lajoie, “On a new approach for the simulation of transients in power systems,” *Electr. Power Syst. Res.*, vol. 77, no. 11, pp. 1514–1520, Sep. 2007.

[77] F. Morandi, L. Roffia, A. D’Elia, F. Vergari, and T. Salmon Cinotti, “RedSib: a Smart-M3 semantic information broker implementation,” in *Proc. 12th Conf. of Open Innovations Association FRUCT and Seminar on e-Tourism*, 2012, pp. 86–98.

[78] N. Rahbari-Asr and M.-Y. Chow, “Cooperative Distributed Demand Management for Community Charging of PHEV/PEVs Based on KKT Conditions and Consensus Networks,” *IEEE Trans. Ind. Informatics*, vol. 10, no. 3, pp. 1907–1916, Aug. 2014.

[79] O. Ardakanian, S. Keshav, and C. Rosenberg, “Real-Time Distributed Control for Smart Electric Vehicle Chargers: From a Static to a Dynamic Study,” *IEEE Trans. Smart Grid*, vol. 5, no. 5, pp. 2295–2305, Sep. 2014.

[80] Z. Ma, D. S. Callaway, and I. A. Hiskens, “Decentralized Charging Control of Large Populations of Plug-in Electric Vehicles,” *IEEE Trans. Control Syst. Technol.*, vol. 21, no. 1, pp. 67–78, Jan. 2013.

[81] M. D. Galus, R. A. Waraich, F. Noembrini, K. Steurs, G. Georges, K. Boulouchos, K. W. Axhausen, and G. Andersson, “Integrating Power Systems, Transport Systems and Vehicle Technology for Electric Mobility Impact Assessment and Efficient Control,” *IEEE Trans. Smart Grid*, vol. 3, no. 2, pp. 934–949, Jun. 2012.

[82] E. L. Karfopoulos and N. D. Hatziargyriou, “A Multi-Agent System for Controlled Charging of a Large Population of Electric Vehicles,” *IEEE Trans. Power Syst.*, vol. 28, no. 2, p. 1, 2012.

[83] C.-K. Wen, J.-C. Chen, J.-H. Teng, and P. Ting, “Decentralized Plug-in Electric Vehicle Charging Selection Algorithm in Power Systems,” *IEEE Trans. Smart Grid*, vol. 3, no. 4, pp. 1779–1789, Dec. 2012.

[84] S. Deilami, A. S. Masoum, P. S. Moses, and M. A. S. Masoum, “Real-Time Coordination of Plug-In Electric Vehicle Charging in Smart Grids to Minimize Power Losses and Improve Voltage Profile,” *IEEE Trans. Smart Grid*, vol. 2, no. 3, pp. 456–467, Sep. 2011.

[85] L. Pieltain Fernandez, T. Gomez San Roman, R. Cossent, C. Mateo Domingo, and P. Frias, “Assessment of the Impact of Plug-in Electric Vehicles on Distribution Networks,” *IEEE Trans. Power Syst.*, vol. 26, no. 1, pp. 206–213, Feb. 2011.

[86] E. Sortomme, M. M. Hindi, S. D. J. MacPherson, and S. S. Venkata, “Coordinated Charging of Plug-In Hybrid Electric Vehicles to Minimize Distribution System Losses,” *IEEE Trans. Smart Grid*, vol. 2, no. 1, pp. 198–205, Mar. 2011.

[87] K. Clement-Nyns, E. Haesen, and J. Driesen, “The Impact of Charging Plug-In Hybrid Electric Vehicles on a Residential Distribution Grid,” *IEEE Trans. Power Syst.*, vol. 25, no. 1, pp. 371–380, Feb. 2010.

[88] “Internet of Energy (IOE) for Electric Mobility.” [Online]. Available: http://www.artemis-ioe.eu/.

[89] J. Honkola, H. Laine, R. Brown, and O. Tyrkko, “Smart-M3 information sharing platform,” in *The IEEE symposium on Computers and Communications*, 2010, pp. 1041–1046.

[90] E. Ovaska, T. Salmon Cinotti, and A. Toninelli, “The design principles and practices of interoperable smart spaces,” in *Advanced design approaches to emerging software systems*, X. Liu and Y. Li, Eds. Hershey PA: IGI Global, 2011, pp. 18–47.

[91] L. Bedogni, L. Bononi, M. Di Felice, A. D. Elia, R. Mock, F. Montori, F. Morandi, L. Roffia, S. Rondelli, T. S. Cinotti, and F. Vergari, “An Interoperable Architecture for Mobile Smart Services over the Internet of Energy,” pp. 1–14, 2013.